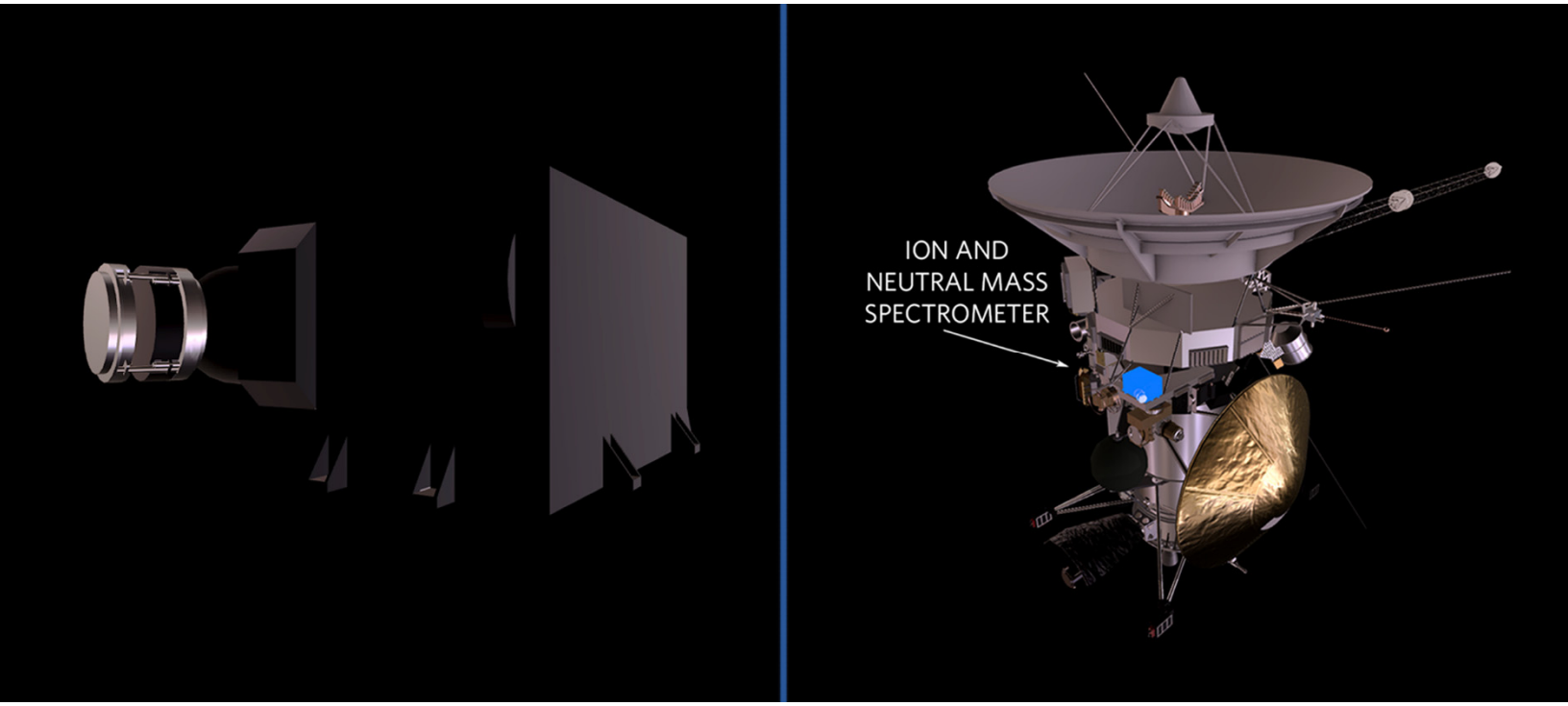

Ion and Neutral Mass Spectrometer

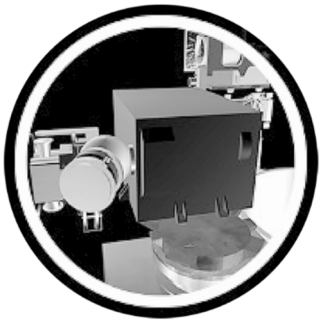

The Ion and Neutral Mass Spectrometer (INMS) was designed to determine the chemical, elemental and isotopic composition of the gaseous and volatile components of the neutral particles and the low energy ions in the Saturn system. The **science objectives** of INMS were to determine the composition and structure of Titan's ionosphere and upper atmosphere, to investigate the neutral and plasma environments of the rings and icy satellites and the interaction with the magnetosphere of Saturn. INMS directly sampled the gas in the Enceladus plume.

The instrument was a quadrupole mass spectrometer with two ion source inlets, a closed ion source for measurement of non-reactive neutral gas and an open ion source for the measurement of ions and reactive neutrals.

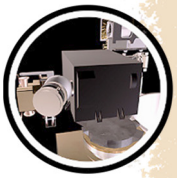

CONTENTS

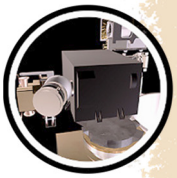

Figures

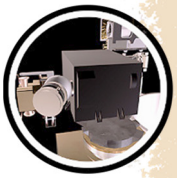

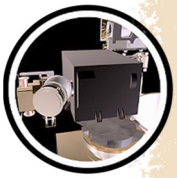

Tables

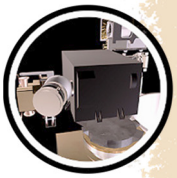

EXECUTIVE SUMMARY

The two primary scientific objectives of the Cassini Ion Neutral Mass Spectrometer (INMS) investigation were: 1) to characterize the composition, structure, and chemical behavior of Titan's upper atmosphere and its interaction with Saturn's magnetosphere; and 2) to investigate the neutral and plasma environments of the rings and icy satellites and their magnetospheric interactions [Waite et al. 2004]. Careful determination of the gas densities of the environment is necessary for the proper execution of these objectives. The ion density extraction process has been discussed in detail by Mandt et al. [2012b] for ram pointed flybys, and many other aspects of the INMS calibration and instrument response to ions and neutrals have been addressed in literature [Teolis et al. 2015; Cui et al. 2009a; Magee et al. 2009; Perry et al. 2010; Teolis et al. 2010b; Vuitton et al. 2008; Waite et al. 2004]. These include compositional extraction from mass spectra, wall adsorption of sticky gases such as H_2O and NH_3, thruster firing contamination, radiation background, high-pressure background effects, residual gas tails, high-sensitivity detector saturation, and on-going work to refine the instrument calibration with the ground-based refurbished engineering unit.

INMS produced results beyond expectation for all objects examined: Titan, Enceladus, Dione, Rhea, the inner magnetosphere, the rings, and the ring/atmosphere interaction in Saturn's equatorial atmosphere. The expectations at Titan were the measurement of the principal components of the atmosphere (nitrogen and methane) and their primary photochemical products (acetylene, ethane, hydrogen cyanide, and their ion counterparts). What emerged was the measurement of a plethora of organic compounds across the whole mass range of INMS that provided a window on a novel way to produce organics through ion neutral chemistry, perhaps an insight into the world of interstellar molecular clouds. There were no expectations for Enceladus, but in reality, this became the most compelling satellite in the system with INMS working in tandem with cosmic dust analyzer (CDA) to demonstrate the habitability of an internal ocean that no one even knew existed before the mission began. The crowning achievement was INMS measurements of molecular hydrogen in the plume that allowed the team to demonstrate that the interior ocean had the latent chemical energy to support methanogenic archea. Dione, Rhea, and the inner magnetosphere provided examples of sputtering of icy satellites, the first time this had been quantitatively investigated in the space environment. The Grand Finale proved *grand* indeed by providing the most complex spectra of the mission (Figure INMS-1) and uncovering a complex chemical interaction between the Saturn atmosphere and rings involving methane, water, carbon dioxide, and ammonia and a host of nanograin organic material—a truly amazing finish to an extraordinary mission.

INMS produced results beyond expectation for all objects examined: Titan, Enceladus, Dione, Rhea, the inner magnetosphere, the rings, and the ring/atmosphere interaction in Saturn's equatorial atmosphere.

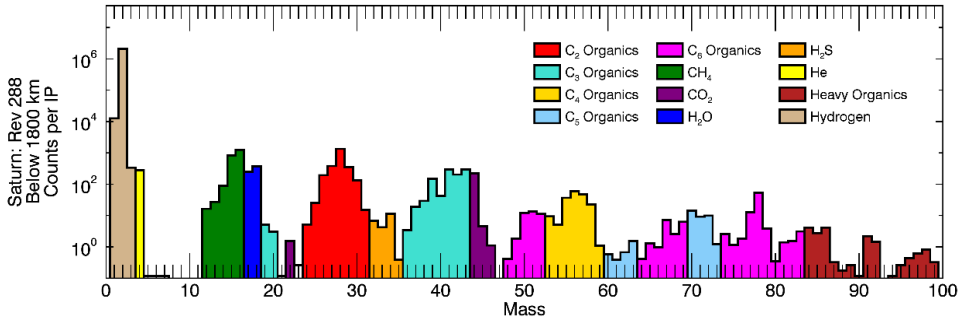

Figure INMS-1. INMS mass spectra of Saturn's upper atmosphere from the Grand Finale. Preliminary mass deconvolution of compounds measured by INMS on the last six orbits of the mission between 1700 and 1800 km at latitudes within 10° of the equator. The spectrum shown here is from the first of these orbits. The axis is in units of mass (u) and extends over the full mass range of INMS (1–99 u).

Instrument Summary

The INMS (Figure INMS-2) is a mass spectrometer described in detail by Waite et al. [2004]. The instrument is a quadrupole mass spectrometer (Figure INMS-3) with two source inlets: 1) a closed ion source (CS) for measurement of non-reactive neutral gas; and 2) an open ion source (OS) for the measurement of ions and reactive neutrals without wall collisions within the instrument interior (Figure INMS-4). The sources are housed in an Ion Source Enclosure (ISE). In flight, measurements alternate in a programmable fashion between the two sources. Gas enters the CS inlet through the entrance aperture as a well collimated molecular beam since the relative gas-spacecraft speed is typically much greater than the molecule thermal speeds. Molecule velocities are isotropized and slowed (thermally accommodated) by colliding (roughly 120 times) with the walls of the inlet's antechamber and antechamber-to-CS transfer tube [Teolis et al. 2015] before passing through the tube to the CS ionization region (Figure INMS-4, labeled with density n_s). The resulting density enhancement in the antechamber and CS is a function of the ram angle between the spacecraft velocity vector and the entrance aperture normal. A typical Titan flyby at 6 km/s produces a ram factor of ~71 for nitrogen relative to the density for a spacecraft at rest if one neglects the leakage paths out of the CS. Scaling the ram factor by $\sqrt{T_a/T_s}$ yields the CS to ambient density ratio at the CS and ambient gas temperatures T_s and T_a (see Teolis et al. [2015], Eq. A17). The side vent (Figure INMS-3 and Figure INMS-4) limits the accumulation of residual gas inside the instrument, and constitutes a major leakage pathway out of the instrument. Neutral gas is ionized in the CS using an electron beam (commandable to ~25 or 70 eV) generated by one of two redundant hot filaments. The OS inlet is located below the CS inlet, and consists of an entrance aperture and ion beam collimator. In-flight measurement of ambient ion densities is described by Mandt et al. [2012b]. In-flight measurement of ambient neutral densities is described by Teolis et al. [2015]. Positive ions from the CS or OS are extracted into the electrostatic quadrupole lens (Figure INMS-4), which is used as a deflector to switch ion trajectories between the two sources [Mahhafy and Lai 1990]. The quadrupole lens voltages are set to transfer the ions into the analyzer ion focus lenses and in turn into the quadrupole mass analyzer (QMA). The voltage setting on the ion focus lenses can increase or reduce the sensitivity by affecting how well the beam of ionized neutrals is focused into the mass analyzer.

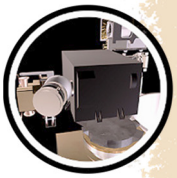

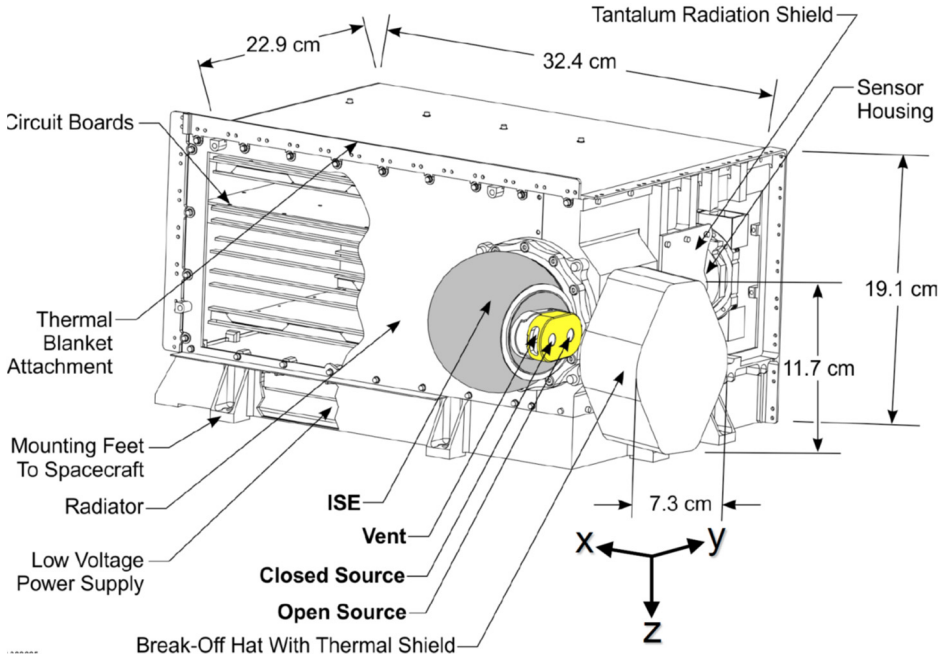

Figure INMS-2. Drawing of the INMS. Showing (*gray*) the ISE and CS and OS inlet apertures, and vent, in relation to (no color) the instrument and electronics housing. The Break-Off Hat was jettisoned after the launch of Cassini.

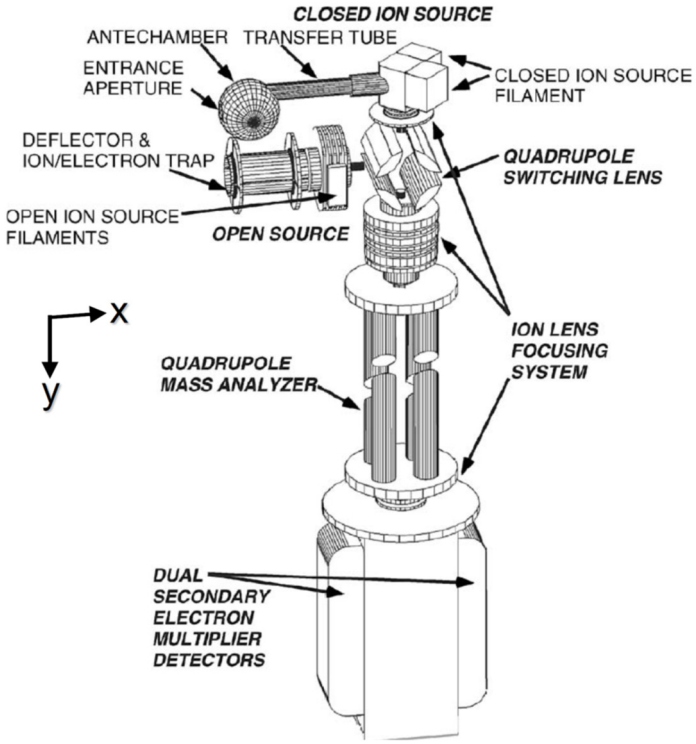

Figure INMS-3. Schematic showing the main components of the INMS. The ram factor model considers the sections above the quadrupole mass analyzer within the ISE (not shown).

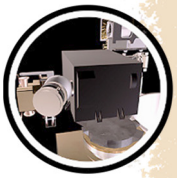

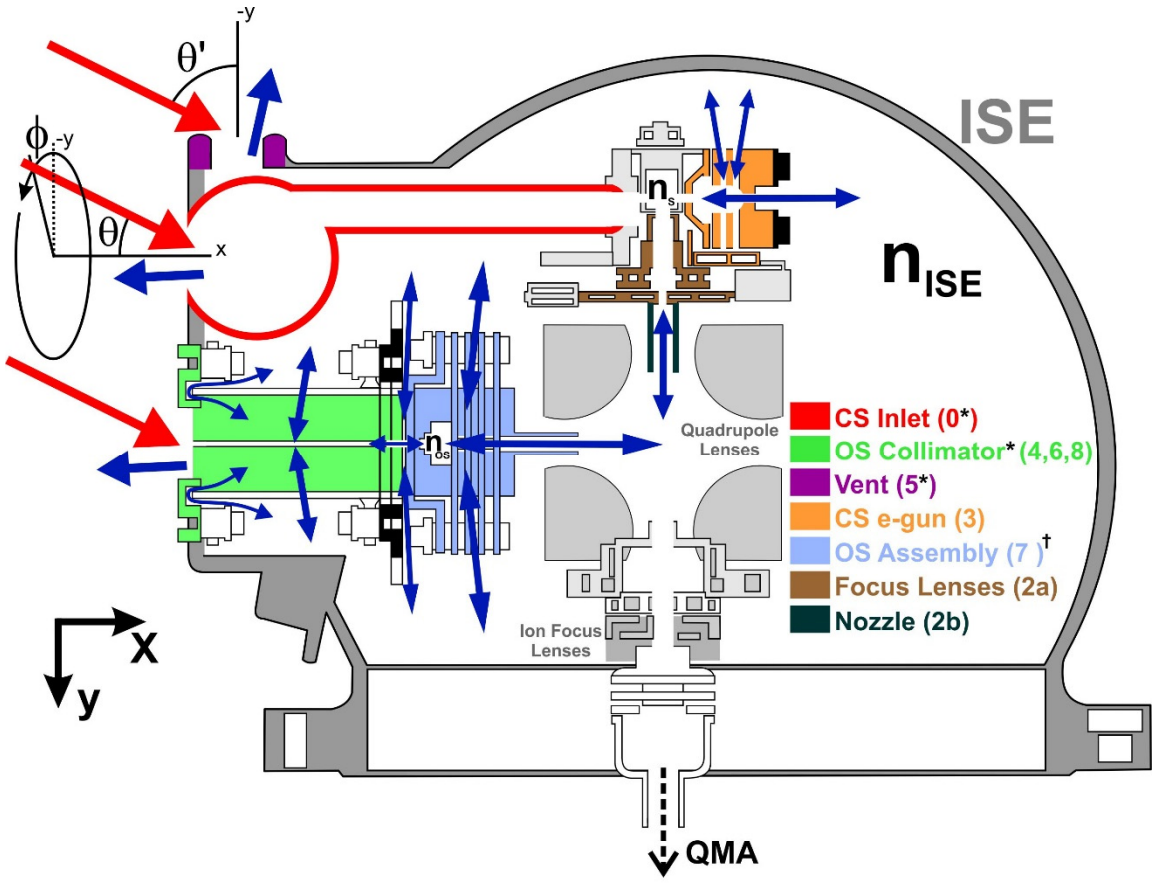

Figure INMS-4. Cross-section diagram (to scale) of the INMS ISE (shown in yellow in Figure INMS-2) with ion sources and gas inlet system shown, together with the azimuthal (ϕ), ram (θ) and vent ram (θ′) angles, spacecraft coordinates axes, gas flows (*Red arrows:* ram flux; *Blue arrows:* thermalized flows), and the approximate locations of densities n_s, n_{os}, and n_{ISE}. Conduction paths considered in the ram factor model are colored as indicated by the legend, with number-letter notation (detailed in Teolis et al. [2015], Appendix A) in parentheses. *Asterisks:* effective area estimated by Monte Carlo simulations. *Dagger:* effective area estimated by fit to Cassini T85 and T88 data. For remaining pathways, we estimated the effective areas analytically. For clarity, leakage through both CS electron guns is shown here as a single conduction pathway. See Teolis et al. [2015], Figure 4 for multiple pathways considered in the CS e-gun conductance calculation. *Grey components*: are neglected in the model, since these sections are treated as having either negligible (e.g., CS enclosure around n_s, ion focus lenses and QMA) or maximum (quadrupole lenses) conductance.

The QMA selects the mass-per-charge ratio (m/q) in the range of 0.5 to 8.5 and 11.5 to 99.5 u per charge, by way of a quadrupole radio frequency mass filter. The detector fore optics consists of three lenses: 1) the Einzel; 2) the Mask I; and 3) the Mask II, which together focus the ions into the detectors. The lens voltage settings can modify the INMS sensitivity depending on how well they focus the beam exiting the QMA into the detectors. Two secondary electron multipliers detect the resulting ion beam operating in a pulse counting mode. These detectors differ in effective sensitivity, with the lower sensitivity detector operating off of secondary electrons produced from the adjacent higher sensitivity detector [Waite et al. 2004]. INMS neutral species-dependent sensitivity factors s_f (for species f) are calibrated on the ground by seven factors: 1) the electron

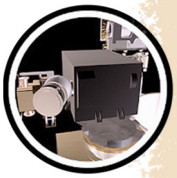

impact efficiency in the sources as determined by the ionization cross-sections of each neutral species; 2) the efficiency for extraction of ions from the CS or OS into the quadrupole lens; 3) the transmission band-pass of the quadrupole switching lens; 4) the degree of focusing in the ion focus lenses into the mass analyzer; 5) the QMA transmission; 6) the detector fore optics transmission; and 7) the detector efficiency.

The OS has three modes of operation: open source ion (OSI), open source neutral beam (OSNB), and open source neutral thermal (OSNT). In the OSI and OSNB modes the OS is used to analyze the ram flux (or molecular beam) of ambient ions and neutrals entering the OS at spacecraft speed, respectively. For more details on the OSNT, see Teolis et al. [2015]; for the OSI see, Mandt et al. [2012]; and for the OSNB, see Waite et al. [2004, 2017].

Over the course of the mission the INMS measurements of Titan's atmospheric neutral mass density were found to be systematically lower than that measured by the Cassini Attitude and Articulation Control System (AACS) and by Navigation (NAV), both of which use spacecraft drag data and aerodynamic models of the spacecraft to derive mass density, as reported by the Titan Atmospheric Working Group (TAMWG); Lee and Hanover [2005]. RPWS Langmuir probe (LP) electron densities can serve as a proxy for total ion densities, while ion densities can be retrieved from Cassini Plasma Spectrometer-Ion Beam Spectrometer (CAPS-IBS) data [Crary et al. 2009]. Comparisons of these sources of ion densities also show systematic differences with the ion densities measured by INMS. Teolis et al. [2015] traced the differences between INMS neutral density measurements and other spacecraft systems in part to gas escape from the CS through leakage pathways not accounted for in the original INMS calibration model. The escape competes with the ram dynamic pressure entering the INMS, yielding lower CS gas densities than indicated by the original calibration, and resulting in a lower INMS neutral gas sensitivity estimate. Therefore, the INMS original calibration model that assumed a sealed CS, used until 2015 to relate the CS density to the ambient density was replaced by a more accurate approach. Teolis et al. [2015] also re-analyzed the INMS detector gain, and found that the gain reduction that occurred during pre-launch characterization testing [Waite et al. 2004], had not been accounted for in the original calibration model. This gain reduction contributes to the reduced INMS sensitivity estimate in the model of Teolis et al. [2015]. The new calibration model brought Cassini INMS results into agreement within expected errors (30%) with the other Cassini systems on the Titan ion and neutral atmospheric densities, and enabled the extraction of Titan neutral density profiles from several previous flybys that yielded unusual and unreasonable densities using the original calibration model.

KEY OBJECTIVES FOR INMS

The Announcement of Opportunity (AO) and Cassini Solstice Mission (CSM) objectives listed below have been drawn from the original documents and filtered for relevance to INMS. The objectives are given by key target or working group. Under each key target the AO objectives are first listed followed by the CSM objectives. The AO objectives are fairly general and, in most cases, apply to the overall mission. On the other hand, the CSM objectives largely pertain to new discoveries during the first half of the mission or to seasonal variation objectives during the CSM.

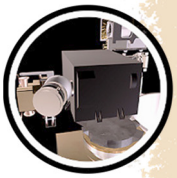

Saturn

The Grand Finale phase of the Cassini mission provided a unique opportunity to study the Saturn Ionosphere Magnetosphere interaction as anticipated. However, what was not expected was information on the equatorial composition and thermal structure (**S_AO1**), the variability of trace gases (**SN1c**), unique H/D and He/H_2 ratio measurements (**S_AO5**), and information on short time scale variations between the rings and the atmosphere (**SC2a**).

Saturn AO objectives

- **Saturn Temperature, Clouds, Composition (S_AO1)** - Determine temperature field, cloud properties, and composition of the atmosphere of Saturn.
- **Saturn Ionosphere-Magnetosphere Interaction (S_AO4)** - Study the diurnal variations and magnetic control of the ionosphere of Saturn.
- **Saturn Formation and Evolution (S_AO5)** - Provide observational constraints (gas composition, isotope ratios, heat flux …) on scenarios for the formation and the evolution of Saturn.

CSM objectives

- *Priority 1* **SN1c** - Measure the spatial and temporal variability of trace gases and isotopes.
- *Priority 2* **SC2a** - Observe the magnetosphere, ionosphere, and aurora as they change on all time scales—minutes to years—and are affected by seasonal and solar cycle forcing.

Rings

Once again, the Grand Finale phase of the mission allowed unique opportunities to address the rings composition (**R_AO2**) and the magnetosphere ring interaction (**R_AO5**) as anticipated, but also allowed unanticipated contributions in understanding ring structure and dynamics (**R_AO1, RN1a, RN1c,** and **RC1b**).

Rings AO objectives

- **Ring Structure and Dynamics (R_AO1)** - Study configuration of the rings and dynamical processes (gravitational, viscous, erosional, and electromagnetic) responsible for ring structure.
- **Ring Particle Composition and Size (R_AO2)** - Map composition and size distribution of ring material.

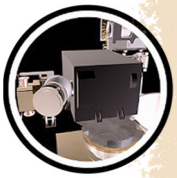

- **Ring Magnetosphere-Ionosphere Interactions (R_AO5)** - Study interactions between the rings and Saturn's magnetosphere, ionosphere, and atmosphere.

CSM objectives

- *Priority 1* **RN1a** - Constrain the origin and age of the rings by direct determination of the ring mass, and of the composition of ring ejecta trapped on field lines.
- *Priority 1* **RC1b** - Determine the temporal variability of ring structure on all timescales up to decadal for regions including Encke gap, D-ring, F-ring, and ring edges by substantially increasing the cadence and time baseline of observations.
- *Priority 1* **RN1c** - Determine structural and compositional variations at high resolution across selected ring features of greatest interest, using remote and in situ observations.

MAPS

INMS was generally expected to address the MAPS AO and CSM objectives listed below (**M_AO2, M_AO4, M_AO5, MC1a, MN1b, MC2a,** and **MN2a**) and did indeed contribute in a meaningful way to all of the listed objectives.

MAPS AO objectives

- **Magnetosphere Charged Particles (M_AO2)** - Determine current systems, composition, sources, and sinks of magnetosphere charged particles.
- **Magnetosphere and Solar Interactions with Titan (M_AO4)** - Study the effect of Titan's interaction with the solar wind and magnetospheric plasma.
- **Plasma Interactions with Titan’s Atmosphere and Ionosphere (M_AO5)** - Investigate interactions of Titan's atmosphere and exosphere with the surrounding plasma.

CSM objectives

- *Priority 1* **MC1a** - Determine the temporal variability of Enceladus’ plumes.
- *Priority 1* **MN1b** - Conduct in situ and remote sensing studies of Saturn’s ionosphere and inner radiation belt.
- *Priority 2* **MC2a** - Observe seasonal variation of Titan’s ionosphere, from one Solstice to the next.
- *Priority 2* **MN2a** - Determine the coupling between Saturn’s rings and ionosphere.

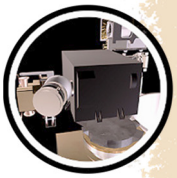

Icy Satellites

INMS was anticipated to contribute to AO objectives (**I_AO5** and **IN1c**). However, the plumes of Enceladus were not anticipated and thrust INMS into a fundamental role in addressing objectives (**I_AO1, I_AO3, I_AO4, IN1a,** and **IC1a**). INMS was unable to contribute to objectives (**IN2b** and **IN2e**) as a result of low satellite outgassing, proximity to the body, or a combination of both, which led to a very low signal to noise ratio in the measurements.

Icy Satellites AO objectives

- **Icy Satellite Geology and History (I_AO1)** - Determine the general characteristics and geological histories of the satellites.
- **Icy Satellite Surface Composition (I_AO3**) - Investigate the compositions and distributions of surface materials, particularly dark, organic rich materials and low melting point condensed volatiles.
- **Icy Satellite Interior Properties (I_AO4)** - Constrain models of the satellites' bulk compositions and internal structures.
- **Icy Satellite Magnetosphere and Ring Interactions (I_AO5)** - Investigate interactions with the magnetosphere and ring systems and possible gas injections into the magnetosphere.

CSM objectives

- *Priority 1* **IN1a** - Determine the presence of an ocean at Enceladus as inferred from induced magnetic field and plume composition, search for possible anomalies in the internal structure of Enceladus as associated with plume sources, and constrain the mechanisms driving the endogenic activity by in situ observations and remote sensing.
- *Priority 1* **IC1a** - Identify long-term secular and seasonal changes at Enceladus, through observations of the South Polar Region, jets, and plumes.
- *Priority 1* **IN1c** - Determine whether Dione exhibits evidence for low-level activity, now or in recent geological time.
- *Priority 2* **IN2b** - Determine whether Tethys contributes to the E-ring and the magnetospheric ion and neutral population.
- *Priority 2* **IN2e** - Understand the unusual appearance of Hyperion with remote sensing observations of the highest resolution possible.

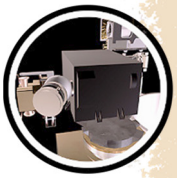

Titan

Titan was always a primary objective of interest for INMS (**T_AO1** and **T_AO5**). However, the importance of ion neutral chemistry in producing organic compounds that are connected to the aerosols and surface deposits (**T_AO2, TC1a, TC1b,** and **TN1c**) was an unanticipated objective. An unfortunate oversight of these processes in Phase B led to descoping the mass range of INMS during development, which in hindsight was a significant impediment in understanding the full extent of the ion neutral chemistry (**T_AO2** and **T_AO5**). Objective **TN2a** on resolving atmospheric density discrepancies between INMS, AACS, and NAV was discovered during the mission and was a direct result of descoping the calibration system for INMS during development.

Titan AO objectives

- **Titan Atmospheric Formation and Evolution (T_AO1)** - Determine abundances of atmospheric constituents (including any noble gases), establish isotope ratios for abundant elements, constrain scenarios of formation and evolution of Titan and its atmosphere.
- **Titan Atmospheric Composition and Distribution (T_AO2)** - Observe vertical and horizontal distributions of trace gases, search for more complex organic molecules, investigate energy sources for atmospheric chemistry, model the photochemistry of the stratosphere, study formation and composition of aerosols.
- **Titan Upper Atmosphere (T_AO5)** - Investigate the upper atmosphere, its ionization, and its role as a source of neutral and ionized material for the magnetosphere of Saturn.

CSM objectives

- *Priority 1* **TC1a** - Determine seasonal changes in the methane-hydrocarbon hydrological cycle: of lakes, clouds, aerosols, and their seasonal transport.
- *Priority 1* **TC1b** - Determine seasonal changes in the high-latitude atmosphere, specifically the temperature structure and formation and breakup of the winter polar vortex.
- *Priority 1* **TN1c** - Measure aerosol and heavy molecule layers and properties.
- *Priority 2* **TN2a** - Resolve current inconsistencies in atmospheric density measurements (critical to a future Flagship mission).

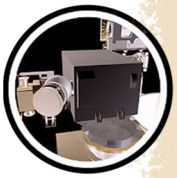

INMS Science Assessment

Rating of Relevant Cassini AO and Solstice Objectives

The Key Objectives for INMS detailed above provide some rationale for the color-coded ratings given in Table INMS-1 for summary purposes.

Table INMS-1. Science Assessment. Note: This table is an Assessment of Data collected to satisfy an objective. It is not an assessment of the status of data analysis/publications.

Fully/Mostly Accomplished: **Partially Accomplished:** **Not Accomplished:**

INMS Science Objectives	AO and TM Science Objectives	INMS Science Assessment	Comments if yellow (partially fulfilled)
Saturn			
Saturn Temperature, Clouds, Composition	S_AO1		Measured temperatures and composition in the exosphere of Saturn near the equator.
Saturn Ionosphere-Magnetosphere Interaction	S_AO4		
Saturn Formation and Evolution	S_AO5		
Measure the spatial and temporal variability of trace gases and isotopes. *(Priority 1)*	SN1c		
Observe the magnetosphere, ionosphere, and aurora as they change on all time scales - minutes to years - and are affected by seasonal and solar cycle forcing. *(Priority 2)*	SC2a		Observed inner magnetospheric composition throughout the mission. Unable to sample in the auroral region close enough to the planet to see any atmospheric or ionospheric effects associated with the aurora.
Rings			
Ring Structure and Dynamics	R_AO1		Positively contributed to understanding the exchange of material between the C-ring and D-ring during the proximal orbits.
Ring Particle Composition and Size	R_AO2		
Ring Magnetosphere-Ionosphere Interactions	R_AO5		
Determine the temporal variability of ring structure on all timescales up to decadal for regions including Encke gap, D-ring, F-ring, and ring edges by substantially increasing the cadence and time baseline of observations. *(Priority 1)*	RC1b		Positively contributed to understanding the exchange of material between the C-ring and D-ring during the proximal orbits.
Constrain the origin and age of the rings by direct determination of the ring mass, and of the composition of ring ejecta trapped on field lines. *(Priority 1)*	RN1a		Positively contributed to understanding the exchange of material between the C-ring and D-ring during the proximal orbits. Also observed material infalling from the D-ring into the atmosphere and determined it to be an important source of ring decay.
Determine structural and compositional variations at high resolution across selected ring features of greatest interest, using remote and in situ observations. *(Priority 1)*	RN1c		INMS contributions limited to comparisons of material infall to Imaging Science Subsystem (ISS) brightness measurements of D68 ringlet during the proximal orbits.

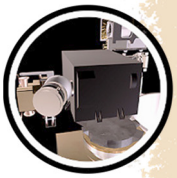

Table INMS-1. Science Assessment. Note: This table is an Assessment of Data collected to satisfy an objective. It is not an assessment of the status of data analysis/publications.

Fully/Mostly Accomplished: **Partially Accomplished:** **Not Accomplished:**

INMS Science Objectives	AO and TM Science Objectives	INMS Science Assessment	Comments if yellow (partially fulfilled)
MAPS			
Magnetosphere Charged Particles	M_AO2		The INMS contribution to the magnetospheres studies was very limited due to the energy range covered by the open source ions.
Magnetosphere and Solar Interactions with Titan	M_AO4		
Plasma Interactions with Titan's Atmosphere and Ionosphere	M_AO5		
Determine the temporal variability of Enceladus' plumes. *(Priority 1)*	MC1a		
Conduct in situ and remote sensing studies of Saturn's ionosphere and inner radiation belt. *(Priority 1)*	MN1b		
Observe seasonal variation of Titan's ionosphere, from one Solstice to the next. *(Priority 2)*	MC2a		
Determine the coupling between Saturn's rings and ionosphere. *(Priority 2)*	MN2a		
Icy Satellites			
Icy Satellite Geology and History	I_AO1		Measured evolutional implications for Enceladus.
Icy Satellite Surface Composition	I_AO3		
Icy Satellite Interior Properties	I_AO4		
Icy Satellite Magnetosphere and Ring Interactions	I_AO5		
Identify long-term secular and seasonal changes at Enceladus, through observations of the south polar region, jets, and plumes.	IC1a		Measured variability but were unable to distinguish secular versus seasonal changes.
Determine the presence of an ocean at Enceladus as inferred from induced magnetic field and plume composition, search for possible anomalies in the internal structure of Enceladus as associated with plume sources, and constrain the mechanisms driving the endogenic activity by in situ observations and remote sensing. *(Priority 1)*	IN1a		
Determine whether Dione exhibits evidence for low-level activity, now or in recent geological time. *(Priority 1)*	IN1c		
Determine whether Tethys contributes to the E-ring and the magnetospheric ion and neutral population. *(Priority 2)*	IN2b		INMS was unable to contribute as a result of low outgassing, proximity to the body, or a combination of both, which led to a very low signal to noise ratio in the measurements.

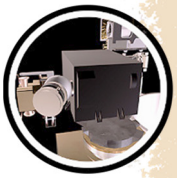

Table INMS-1. Science Assessment. Note: This table is an Assessment of Data collected to satisfy an objective. It is not an assessment of the status of data analysis/publications.

Fully/Mostly Accomplished: **Partially Accomplished:** **Not Accomplished:**

INMS Science Objectives	AO and TM Science Objectives	INMS Science Assessment	Comments if yellow (partially fulfilled)
Understand the unusual appearance of Hyperion with remote sensing observations of the highest resolution possible. *(Priority 2)*	IN2e		INMS was unable to contribute as a result of low outgassing, proximity to the body, or a combination of both, which led to a very low signal to noise ratio in the measurements.
Titan			
Titan Atmospheric Formation and Evolution	T_AO1		
Titan Atmospheric Composition and Distribution	T_AO2		
Titan Upper Atmosphere	T_AO5		
Determine seasonal changes in the methane-hydrocarbon hydrological cycle: of lakes, clouds, aerosols, and their seasonal transport. *(Priority 1)*	TC1a		
Determine seasonal changes in the high-latitude atmosphere, specifically the temperature structure and formation and breakup of the winter polar vortex. *(Priority 1)*	TC1b		Measurements at INMS in situ altitudes provided little information on processes in the stratosphere.
Measure aerosol and heavy molecule layers and properties. *(Priority 1)*	TN1c		
Resolve current inconsistencies in atmospheric density measurements (critical to a future Flagship mission). *(Priority 2)*	TN2a		

Alternative Science Performance Assessment – Mapping of Refereed Publications

An alternative way to assess INMS science performance is to take the science performance requirements compiled prelaunch and match them with the complete list of INMS refereed publications. A relationship between the science performance and functional requirements for INMS was spelled out in the Cassini Orbiter Functional Requirements Book Ion and Neutral Mass Spectrometer (INMS), Rev. A, CAS-4-2074, dated July 4, 1997 prepared just before launch. The performance is encapsulated in a series of science objectives spelled out in Section 3.3.1 of Functional Requirements Book and repeated below in summary assessment form with references of related published INMS papers.

Titan – atmospheric structure

1. What gases (and isotopes) are present besides the N_2, CH_4, and C_2H_2 detected by the Voyager UltraViolet Spectrometer (UVS)?

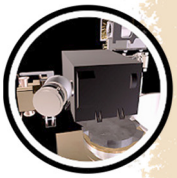

2. What is the extent of diffusive separation (or, where is the homopause)? This may require a comparison with Cassini Probe data.

RELEVANT PAPERS

There are 31 refereed papers listed below that discuss the bulk structure and composition of Titan's atmosphere. The methane homopause was located at ~1100 km above the surface. The papers range in topics from major species structure to isotope and minor species structure in altitude, longitude, and latitude. The quality and quantity of papers far exceeds performance expectations. Solar cycle variability was also examined.

Bell, J. M., J. H. Waite, J. H. Westlake, S. W. Bougher, A. J. Ridley, R. Perryman, K. Mandt, (2014), Developing a self-consistent description of Titan's upper atmosphere without hydrodynamic escape, Journal of Geophysical Research, 119, 4957–4972.

Bell, J. M., J. Westlake, J. H. Waite Jr., (2011a), Simulating the time-dependent response of Titan's upper atmosphere to periods of magnetospheric forcing, Geophysical Research Letters, 38, L06202.

Bell, J., S. W. Bougher, J. H. Waite Jr., A. J. Ridley, B. Magee, K. Mandt, J. Westlake, A. D. DeJong, A. Bar-Nun, R. Jacovi, G. Toth, V. de la Haye, (2011b), Simulating the one-dimensional structure of Titan's upper atmosphere, Part III: Mechanisms determining methane escape, Journal of Geophysical Research, 116, E11002.

Bell, J., S. W. Bougher, J. H. Waite Jr., A .J. Ridley, B. Magee, K. Mandt, J. Westlake, A. D. DeJong, A. Bar-Nun, R. Jacovi, G. Toth, V. de la Haye, (2010a), Simulating the one-dimensional structure of Titan's upper atmosphere, Part I: Formulation of the Titan global ionosphere-thermosphere model and benchmark simulations, Journal of Geophysical Research, 115, E12002.

Bell, J., S. W. Bougher, J. H. Waite Jr., A.J. Ridley, B. Magee, K. Mandt, J. Westlake, A. D. DeJong, V. de la Haye, D. Gell, G. Fletcher, A. Bar-Nun, R. Jacovi, G. Toth, (2010b), Simulating the one-dimensional structure of Titan's upper atmosphere, Part II: Alternative scenarios for methane escape, Journal of Geophysical Research, 115, E12018.

Cui, J., Y. Lian, I. C. F. Müller-Wodarg, (2013), Compositional effects in Titan's thermospheric gravity waves, Geophysical Research Letters, 40, 43–47, doi: 1 0.1029/2012GL054621.

Cui, J., R. V. Yelle, D. F. Strobel, I. C. F. Müller-Wodarg, D. S. Snowden, T. T. Koskinen, M. Galand, (2012), The CH4 structure in Titan's upper atmosphere revisited, Journal of Geophysical Research, 117, E11006, doi: 10.1029/2012JE004222.

Cui, J., R. V. Yelle, I. C. F. Müller-Wodarg, P. P. Lavvas, M. Galand, (2011), The implications of the H2 variability in Titan's exosphere, Journal of Geophysical Research, 116, A11324.

Cui, J., R. V. Yelle, V. Vuitton, J. H. Waite, W. T. Kasprzak, D. A. Gell, H. B. Niemann, I. C. F. Müller-Wodarg, N. Borggren, G. G. Fletcher, E. L. Patrick, E. Raaen, B. A. Magee, (2009a),

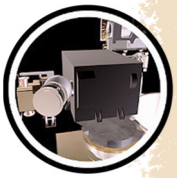

Analysis of Titan's neutral upper atmosphere from Cassini ion neutral mass spectrometer measurements, Icarus, 200, 581–615, doi: 10.1016/j.icarus.2008.12.005.

Cui, J., R. V. Yelle, K. Volk, (2008), Distribution and escape of molecular hydrogen in Titan's thermosphere and exosphere, Journal of Geophysical Research, 113, E10004, doi: 10.1029/2007JE003032.

De La Haye, V., J. H. Waite Jr., T. E. Cravens, I. P. Robertson, S. Lebonnois, (2008a), Coupled ion and neutral rotating model of Titan's upper atmosphere, Icarus, 197, 110–136, doi: 10.1016/j.icarus.2008.03.022.

De La Haye, V., J. H. Waite, R. E. Johnson, R. V. Yelle, et al., (2007a), Cassini Ion and Neutral Mass Spectometer data in Titan's upper atmosphere and exosphere: Observation of a suprathermal corona, Journal of Geophysical Research, 12, A07309.

Magee, B. A., J. H. Waite, K. E. Mandt, J. Bell, J. Westlake, D. A. Gell, V. De la Haye, (2009), INMS derived composition of Titan's upper atmosphere: Analysis methods and model comparison, Planetary and Space Science, 57, 1895–1916.

Mandt, K. E., J. H. Waite Jr., B. Teolis, B. A. Magee, J. Bell, J. Westlake, C. Nixon, O. Mousis, J. Lunine, (2012a), The 12C/13C ratio on Titan from Cassini INMS measurements and implications for the evolution of methane, Astrophysical Journal, 749, 160, doi: 10.1088/0004-637X/749/2/160.

Mandt, K. E., J. H. Waite Jr., W. Lewis, J. I. Lunine, O. Mousis, J. Bell, B. A. Magee, D. Cordier, (2009), Isotopic evolution of the major constituents of Titan's atmosphere based on Cassini data, Planetary and Space Science, 57, 1917–1930.

Mousis, O., J. I. Lunine, S. Picaud, D. Cordier, J. H. Waite, Jr., K. E. Mandt, (2011), Removal of Titan's atmospheric noble gases by their sequestration in surface clathrates, The Astrophysical Journal, 740, L9.

Mousis, O., J. I. Lunine, M. Pasek, D. Cordier, J. H. Waite Jr., K. E. Mandt, W. S. Lewis, M.-J. Nguyen, (2009b), A primordial origin for the atmospheric methane of Saturn's moon Titan, Icarus, 204, 749–751.

Müller-Wodarg, I. C. F., R. V. Yelle, J. Cui, J. H. Waite, (2008), Horizontal structures and dynamics of Titan's thermosphere, Journal of Geophysical Research, 113, E10003, doi: 10.1029/2007JE003031.

Müller-Wodarg, I. C. F., R. V. Yelle, N. Borggren, J. H. Waite, (2006a), Waves and horizontal structures in Titan's thermosphere, Journal of Geophysical Research, 111, A12315.

Müller-Wodarg, I. C. F., R. V. Yelle, M. J. Mendillo, A. D. Aylward, (2003), On the global distribution of neutral gases in Titan's upper atmosphere and its effect on the thermal structure, Journal of Geophysical Research: Space Physics, vol. 108, issue A12, doi: 10.1029/2003JA010054.

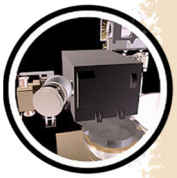

Müller-Wodarg, I. C. F. and R. V. Yelle, (2002a), The effect of dynamics on the composition of Titan's upper atmosphere, Geophysical Research Letters, vol. 29, issue 23, 54-1–54-4, doi: 10.1029/2002GL016100.

Müller-Wodarg, I. C. F., (2002b), The application of general circulation models to the atmospheres of terrestrial-type moons of the giant planets, In Atmoshperes in the Solar System: Comparative Aeronomy, Volume 120, Part IV: Models of Aeronomic Systems, (eds.) M. Mendillo, A. Nagy, J. H. Waite, American Geophysical Union, Geophysical Monograph Series, pp. 307–318, doi: 10.1029/GM130.

Müller-Wodarg, I. C. F., R. V. Yelle, M. Mendillo, L. A. Young, A. D. Aylward, (2000), The thermosphere of Titan simulated by a global three-dimensional time-dependent model, Journal of Geophysical Research, 105, pp. 20833–20856, doi: 10.1029/2000JA000053.

Shematovich, V. I., R. E. Johnson, M. Michael, J. G. Luhmann, (2003), Nitrogen loss from Titan, Journal of Geophysical Research, 108, E8, id. 5087, doi: 10.1029/2003JE002094.

Strobel, D. F., S. K. Atreya, B. Bézard, F. Ferri, F. M. Flasar, M. Fulchignoni, E. Lellouch, I. C. F. Müller-Wodarg, (2009), Atmospheric structure and composition, In Titan from Cassini-Huygens, (eds.) R. Brown, J.-P. Lebreton, J. H. Waite, Springer Dordrecht, pp. 235–257, doi: 10.1007/978-1-4020-9215-2_10.

Vuitton, V., R. V. Yelle, J. Cui, (2008), Formation and distribution of benzene on Titan, Journal of Geophysical Research, doi: 1 0.1029/2007JE002997.

Waite, J. H., J. Bell, R. Lorenz, R. Achterberg, F. M. Flasar, (2013), A model of variability in Titan's atmospheric structure, Planetary and Space Science, 86, 45–56, doi: 10.1016/j.pss.2013.05.018.

Waite, J. H., H. Niemann, R. V. Yelle, W. T. Kasprzak, T. E. Cravens, J. G. Luhmann, R. L. McNutt, W.-H. Ip, D. Gell, V. de la Haye, I. Müller-Wordag, B. McGee, N. Borggren, S. Ledvina, G. Fletcher, E. Walter, R. Miller, S. Scherer, R. Thorpe, J. Xu, B. Block, K. Arnett, (2005a), Ion Neutral Mass Spectrometer (INMS) results from the first flyby of Titan, Science, 308 (5724), 982–986.

Westlake, J. H., J. H. Waite, J. M. Bell, R. Perryman, (2014a), Observed decline in Titan's thermospheric methane due to solar cycle drivers, Journal of Geophysical Research, 119, 8586–8599, doi: 10.1002/2014JA020394.

Yelle, R.V., J. Cui, and I.C.F. Müller-Wodarg, (2008), Methane Escape from Titan's Atmosphere, Journal of Geophysical Research, 113, E10003, doi: 10.1029/2007JE003031.

Yelle, R. V., N. Borggren, V. De La Haye, W. T. Kasprzak, H. B. Niemann, I. Müller-Wodarg, J. H. Waite Jr., (2006), The vertical structure of Titan's upper atmosphere from Cassini ion neutral mass spectrometer measurements, Icarus, 182, 567–576.

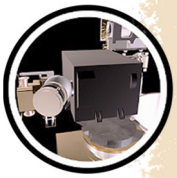

Titan – thermal structure and energetics

1. What is the exospheric temperature and how does it vary (diurnally, spatial, or long term)?

2. What energy sources and sinks determine the heat balance of the exosphere and lower thermosphere?

3. What role do radiatively active species play in the upper atmospheric heat balance and the coupling of the lower and upper atmosphere thermal processes?

RELEVANT PAPERS

There are 10 papers listed below that report the thermal structure of the atmosphere including solar heating, particle precipitation, and gravity wave forcing. Solar heating was found to be the primary energy source and hydrogen cyanide rovibrational emissions the major cooling process. The papers met expectations for the performance noted prior to the mission.

Cui, J., R. V. Yelle, T. Li, D. S. Snowden, I. C. F. Müller-Wodarg, (2014), Density waves in Titan's upper atmosphere, Journal of Geophysical Research, 119, 490–518, doi: 10.1001/2013JA019113.

Cravens T. E., I. P. Robertson, S. A. Ledvina, D. Mitchell, S. M. Krimigis, J. H. Waite Jr., (2008a), Energetic ion precipitation at Titan, Geophys. Res. Lett., 35, L03103, doi: 10.1029/2007GL032451.

De La Haye, V., J. H. Waite, Jr., T. E. Cravens, S. W. Bougher, I. P. Robertson, J. M. Bell, (2008b), Heating Titan's upper atmosphere, Journal of Geophysical Research, 113, A11314.

De La Haye, V., J. H. Waite Jr., T. E. Cravens, A. F. Nagy, R. E. Johnson, S. Lebonnois, I. P. Robertson, (2007b), Titan's Corona: The contribution of exothermic chemistry, Icarus, 191, 236–250.

Snowden, D. and R. V. Yelle, (2014a), The global precipitation of magnetospheric electrons into Titan's upper atmosphere, Icarus, 243, 1–15, doi: 10.1016/j.icarus.2014.08.027.

Snowden, D. and R. V. Yelle, (2014b), The thermal structure of Titan's upper atmosphere, II: Energetics, Icarus, vol. 228, pp. 64–77, doi: 10.1016/j.icarus.2013.08.027.

Snowden, D., R. Yelle, J. Cui, J.-E. Wahlund, N. J. T. Edberg, K. Ågren, (2013a), The thermal structure of Titan's upper atmosphere, I: Temperature profiles from Cassini INMS observations, Icarus, vol. 226, pp. 552–582, doi: 10.1016/j.icarus.2013.06.006.

Snowden, D., R. V. Yelle, M. Galand, A. J. Coates, A. Wellbrock, G. H. Jones, and P. Lavvas, (2013b), Auroral electron precipitation and flux tube erosion in Titan's upper atmosphere, Icarus, 226, 186-204, doi: 10.1016/j.icarus.2013.05.021.

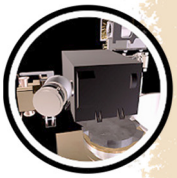

Vigren, E., M. Galand, R. V. Yelle, J. Cui, J.-E. Wahlund, K. Ågren, P. P. Lavvas, I. C. F. Müller-Wodarg, D. F. Strobel, V. Vuitton, A. Bazin, (2013), On the thermal electron balance in Titan's sunlit upper atmosphere, Icarus, vol. 223, pp. 234–251, doi: 10.1016/j.icarus.2012.12.010.

Westlake, J. H., J. Bell, J. H. Waite, Jr., R. E. Johnson, J. G. Luhmann, K. E. Mandt, B. A. Magee, A. M. Rymer, (2011), Titan's thermospheric response to various plasma and solar environments, Journal of Geophysical Research, 116, A03318.

Titan – ionospheric structure

1. What are the sources of ionization? What is the chemistry of positive ions? How important are vertical and horizontal transports of ions and electrons?

2. What are the energy sources and sinks for ions and electrons? What ions and neutrals are escaping from Titan? What is the environment in which the intense airglow (aurora?) is produced?

RELEVANT PAPERS

There are 51 papers listed below that deal with the ionosphere—its formation and chemistry, especially the complex ion neutral chemistry that forms the heavy organic compounds found on the Titan surface. This work far exceeds the pre-flight expectations.

Ågren, K., J. E. Wahlund. R. Modolo, D. Lummerzheim, M. Galand, I. Müller-Wodarg, P. Canu, W. S. Kurth, T. E. Cravens, R. V. Yelle, J. H. Waite Jr., A. J. Coates, G. R. Lewis, D. T. Young, C. Bertucci, M. K. Dougherty, (2007), On magnetospheric electron impact ionisation and dynamics in Titan's ram-side & polar ionosphere-a Cassini case study, Annales Geophysicae, 25.

Brecht, S. H., J. G. Luhmann, D. J. Larson, (2000), Simulation of the Saturnian magnetospheric interaction with Titan, Journal of Geophysical Research, vol. 105, issue A6, 13119–13130, doi: 10.1029/1999JA900490.

Coates, A. J., A. Wellbrock, G. R. Lewis, G. H. Jones, D. T. Young, F. J. Crary, J. H. Waite Jr., (2009), Heavy negative ions in Titan's ionosphere: Altitude and latitude dependence, Planetary and Space Science, 57, 1866–1871.

Crary, F. J., B. A. Magee, K. E. Mandt, J. H. Waite, J. Westlake, D. T. Young, (2009), Heavy ions, temperatures and winds in Titan's ionosphere: Combined Cassini CAPS and INMS observations, Planetary and Space Science, 57, 1847–1856.

Cravens, T. E., M. Richard, Y.-J. Ma, C. Bertucci, J. G. Luhmann, S. Ledvina, I. P. Robertson, J.-E. Wahlund, K. Ågren, J. Cui, I. Müller-Wodarg, J. H. Waite, M. Dougherty, J. Bell, D. Ulusen, (2010), Dynamical and Magnetic Field Time Constants for Titan's Ionosphere - Empirical Estimates, Journal of Geophysical Research, 115, A08319.

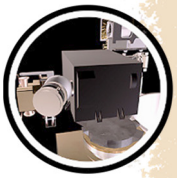

Cravens, T. E., R. V. Yelle, J.-E. Wahlund, D. E. Shemansky, A. F. Nagy, (2009a), Composition and structure of the ionosphere and thermosphere, In Titan from Cassini-Huygens, Chapter 11, (eds.) R. H. Brown, J. P. Lebreton, J. H. Waite, Springer, Dordrecht, pp. 259–295, doi: 10.1007/978-1-4020-9215-2_11.

Cravens, T. E., I. P. Robertson, J. H. Waite Jr., R. V. Yelle, V. Vuitton, A. J. Coates, J.-E. Wahlund, K. Ågren, M. S. Richard, V. De La Haye, A. Wellbrock, F. N. Neubauer, (2009b), Model-data comparisons for Titan's nightside ionosphere, Icarus, 199, 174–188, doi: 10.1016/j.icarus.2008.09.005.

Cravens, T. E., I. P. Robertson, J. H. Waite Jr., R. V. Yelle, V. Vuitton, A. J. Coates, J.-E. Wahlund, K. Ågren, M. S. Richard, V. De La Haye, A. Wellbrock, F. N. Neubauer, (2008b), Model-data comparisons for Titan’s nightside ionosphere, Icarus, doi: 10.1016/j.icarus.2008.09.005.

Cravens, T. E., I. P. Robertson, J. H. Waite Jr., R. V. Yelle, W. T. Kasprzak, C. N. Keller, S. A. Ledvina, H. B. Niemann, J. G. Luhmann, R. L. McNutt, W.-H. Ip, V. De La Haye, I. Müller-Wodarg, J.-E. Wahlund, V. G. Anicich, V. Vuitton, (2006), The composition of Titan's ionosphere, Geophysical Research Letters, 33, L07105.

Cravens, T. E., I. P. Robertson, J. Clark, J.-E. Wahlund, J. H. Waite Jr., S. A. Ledvina, H. B. Niemann, R. V. Yelle, W. T. Kasprzak, J. G. Luhmann, R. L. McNutt, W.-H. Ip, V. De La Haye, I. Müller-Wodarg, D. T. Young, A. J. Coates, (2005), Titan's ionosphere: Model comparisons with Cassini Ta data, Geophysical Research Letters, vol. 32, issue 12, doi: 10.1029/2005GL023249.

Cravens, T. E., J. Vann, J. Clark, J. Wu, C. N. Keller, C. Brull, (2004), The ionosphere of Titan: An updated theoretical model, Advances in Space Research, 33, 212.

Cravens, T. E., C. N. Keller, B. Ray, (1997), Photochemical sources of non-thermal neutrals for the exosphere of Titan, Planetary and Space Science, 45, 889.

Cui, J., M. Galand, R. V. Yelle, J.-E. Wahlund, K. Ågren, J. H. Waite Jr., M. K. Dougherty, (2010), Ion transport in Titan's upper atmosphere, Journal of Geophysical Research, 115, A06314.

Cui, J., M. Galand, R. V. Yelle, V. Vuitton, I. C. F. Müller-Wodarg, J. -E. Wahlund, P. P. Lavvas, T. E. Cravens, W. T. Kasprzak, J. H. Waite Jr., (2009b), Diurnal variations of Titan's ionosphere, Journal of Geophysical Research, 114, A06310.

Edberg, N. J. T., D. J. Andrews, O. Shebanits, K. Ågren, J.-E. Wahlund, H. J. Opgenoorth, T. E. Cravens, Z. Girazian, (2013a), Solar cycle modulation of Titan’s ionosphere, Journal of Geophysical Research, 118, 5255–5264, doi: 10.1002/jgra.50463.

Edberg, N. J. T., D. J. Andrews, O. Shebanits, K. Ögren, J.-E. Wahlund, H. J. Opgenoorth, E. Roussos, P. Garnier, T. E. Cravens, S. V. Badman, R. Modolo, C. Bertucci, M. K. Dougherty, (2013b), Extreme densities in Titan’s ionosphere during the T85 magnetosheath encounter, Geophysical Research Letters, 40, 2879–2883, doi: 10.1002/grl.50579.

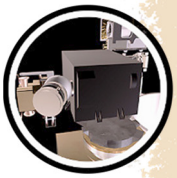

Galand, M., A. J. Coates, T. E. Cravens, J.-E. Wahlund, (2014), Titan's ionosphere, In Titan: Interior, Surface, Atmosphere, and Space Environment, Chapter 11, (eds.) I. Müller-Wodarg, C. A. Griffith, E. Lellouch, T. E. Cravens, Cambridge University Press, pp. 376–419.

Garnier, P., J.-E. Wahlund, L. Resnqvist, R. Modolo, K. Ågren, N. Sergis, P. Canu, M. Andre, D. A. Gurnett, W. S. Kurth, S. M. Krimgis, A. Coates, M. Dougherty, J. H. Waite Jr., (2009), Titan's ionosphere in the magnetosheath: Cassini RPWS results during the T32 flyby, Annales Geophysicae, 27, 4257–4272.

Keller, C. N., V. G. Anicich, T. E. Cravens, (1998), Model of Titan's ionosphere with detailed hydrocarbon ion chemistry, Planetary and Space Science, 46, 1157.

Ledvina, S. A. and S. H. Brecht, (2012a), Consequences of negative ions for Titan's plasma interaction, Geophysical Research Letters, 39, L20103, doi: 10.1029/2012GL053835.

Ledvina, S. A., S. H. Brecht, T. E. Cravens, (2012b), The orientation of Titan's dayside ionosphere and its effects on Titan's plasma interaction, Earth Planets Space, 64, 207–230.

Ledvina, S. A., Y. Ma, E. Kallio, (2008), Modeling and simulating flowing plasmas and related phenomena, Space Science Reviews, doi: 10.1007/s11214-008-9384-6.

Ledvina, S. A., T. E. Cravens, K. Kecskemety, (2005), Ion distributions in Saturn's magnetosphere near Titan, Journal of Geophysical Research, 110, A06211, doi: 10.1029/2004JA010771.

Ledvina, S. A., J. G. Luhmann, S. H. Brecht, T. E. Cravens, (2004a), Titan's induced magnetosphere, Advances in Space Research, 33, 2092.

Ledvina, S. A., J. G. Luhmann, T. E. Cravens, (2004b), Ambient ion distributions in Saturn's magnetosphere near Titan during a non-Voyager type interaction, Advances in Space Research, 33, 221.

Ledvina, S. A., S. H. Brecht, J. G. Luhmann, (2004c), Ion distributions of 14 amu pickup ions associated with Titan's plasma interaction, Geophysical Research Letters, 31, L17S10, doi: 10.1029/2004GL019861.

Luhmann, J. G., D. Ulusen, S. A. Ledvina, K. Mandt, B. Magee, J. H. Waite, J. Westlake, T. E. Cravens, I. Robertson, N. Edberg, K. Ågren, J.-E. Wahlund, Y.-J. Ma, H. Wei, C. T. Russell, M. K. Dougherty, (2012), Investigating magnetospheric interaction effects of Titan's ionosphere with the Cassini orbiter ion neutral mass spectrometer, Langmuir Probe and magnetometer observations during targeted flybys, Icarus, 219, 534–555, doi: 10.1016/j.icarus.2012.03.015.

Luhmann, J. G., S. A. Ledvina, C. T. Russell, (2004), Induced magnetospheres, Advances in Space Research, 33, 1905.

Luhmann, J. G., (1996), Titan's ion exosphere wake: A natural ion mass spectrometer? Journal of Geophysical Research, 101, E12, pp. 29387–29393, doi: 10.1029/96JE03307.

Ma, Y., K. Altwegg, T. Breus, M. R. Combi, et al., (2008), Plasma flow and related phenomena in planetary aeronomy, Space Science Reviews, 139, no. 1–4, 311–353, doi: 10.1007/s11214-008-9389-1.

- - - - - - - - - - - - - -

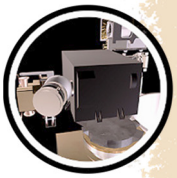

Ma, Y., A. F. Nagy, T. E. Cravens, I. V. Sokolov, K. C. Hansen, J.-E. Wahlund, F. J. Crary, A. J. Coates, M. K. Dougherty, (2006), Comparisons Between MHD Model Calculations and Observations of Cassini Flybys of Titan, Journal of Geophysical Research, 111, A05207, doi: 10.1029/2005JA011481.

Ma, Y.-J., A. F. Nagy, T. E. Cravens, I. G. Sokolov, J. Clark, K. C. Hansen, (2004), 3-D global MHD model prediction of the first close flyby of Titan by Cassini, Geophysical Research Letters, 31, doi: 10.1029/2004GL021215.

Madanian, H., T. E. Cravens, M. S. Richard, J. H. Waite, N. J. T. Edberg, J. H. Westlake, J.-E. Wahlund, (2016), Solar cycle variations in ion composition in the dayside ionosphere of Titan, Journal of Geophysical Research, 121, 8013–8037, doi: 10.1002/2015JA022274.

Mandt, K. E. , D. A. Gell, M. Perry, J. H. Waite Jr., F. A. Crary, D. Young, B. A. Magee, J. H. Westlake, T. Cravens, W. Kasprzak, G. Miller, J.-E. Wahlund, K. Ågren, N. J. T. Edberg, A. N. Heays, B. R. Lewis, S. T. Gibson, V. de la Haye, M.-C. Liang, (2012b), Ion densities and composition of Titan's upper atmosphere derived from the Cassini ion neutral mass spectrometer: Analysis methods and comparison of measured ion densities to photochemical model simulations, Journal of Geophysical Research, 117, E10006, doi: 10.1029/2012JE004139.

Michael, M., R. E. Johnson, F. Leblanc, M. Liu, J. G. Luhmann, V. I. Shematovich, (2005), Ejection of nitrogen from Titan's atmosphere by magnetospheric ions and pick-up ions, Icarus, vol. 175, Issue 1, pp. 263–267, doi: 10.1016/j.icarus.2004.11.004.

Nagy, A. F. and T. E. Cravens, (1998), Titan's ionosphere: A review, Planetary and Space Science, 46, 1149, doi: 10.1016/S0032-0633(98)00049-X.

Richard, M. S., T. E. Cravens, C. Wylie, D. Webb, Q. Chediak, R. Perryman, K. Mandt, J. Westlake, J. H. Waite, I. Robertson, B. A. Magee, N. J. T. Edberg, (2015a), An empirical approach to modeling ion production rates in Titan’s ionosphere I: Ion production rates on the dayside and globally, Journal of Geophysical Research, 120, 1264–1280, doi: 10.1002/2013JA019706.

Richard, M. S., T. E. Cravens, C. Wylie, D. Webb, Q. Chediak, K. Mandt, J. H. Waite, A. Rymer, C. Bertucci, A. Wellbrock, A. Windsor, A. J. Coates, (2015b), An empirical approach to modeling ion production rates in Titan’s ionosphere II: Ion production rates on the nightside, Journal of Geophysical Research, 120, 1281–1298, doi: 10.1002/2014JA020343.

Richard, M. S., T. E. Cravens, I. P. Robertson, J. H. Waite, J.-E. Wahlund, F. J. Crary, A. J. Coates, (2011), Energetics of Titan's ionosphere: model comparisons with Cassini data, Journal of Geophysical Research, 116, A09310.

Robertson, I. P., T. E. Cravens, J. H. Waite Jr., R. V. Yelle, V. Vuitton, A. J. Coates, J. E. Wahlund, K. Ågren, B. Magee, K. Mandt, M. S. Richard, (2009), Structure of Titan's ionosphere: model comparisons with Cassini data, Planetary and Space Science, 57, 1834–1846.

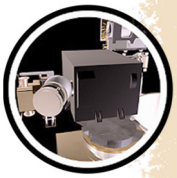

Rosenqvist, L., J.-E. Wahlund, K. Ågren, R. Modolo, H. J. Opgenoorth, D. Strobel, I. Müller-Wodarg, P. Garnier, C. Bertucci, (2009), Titan ionospheric conductivities from Cassini measurements, Planetary and Space Science, 57, 1828–1833, doi: 10.1016/j.pss.2009.01.007.

Sagnières, L. B. M., M. Galand, J. Cui, P. P. Lavvas, E. Vigren, V. Vuitton, R. V. Yelle, A. Wellbrock, A. J. Coates, (2015), Influence of local ionization on ionospheric densities in Titan's upper atmosphere, Journal of Geophysical Research, 120, 5899–5921, doi: 10.1002/2014JA020890.

Shebanits, O., J.-E. Wahlund, N. J. T. Edberg, F. J. Crary, A. Wellbrock, D. J. Andrews, E. Vigren, R. T. Desai, A. J. Coates, K. E. Mandt, J. H. Waite, (2016), Ion and aerosol precursor densities in Titan's ionosphere: A multi-instrument case study, Journal of Geophysical Research, 121, 10075–10090, doi: 10.1002/2016JA022980.

Ulusen, D., J. G. Luhmann, Y. J. Ma, K. Mandt, J. H. Waite, M. K. Dougherty, J.-E. Wahlund, C. T. Russell, T. A. Craven, N. Edberg, K. Agren, (2012), Comparisons of Cassini flybys of the Titan magnetospheric interaction with an MHD model: Evidence for organized behavior at high altitudes, Icarus, 217, 43–54, doi: 10.1016/j.icarus.2011.10.009.

Ulusen, D., J. Luhmann, Y. Ma, S. Ledvina, T. Cravens, K. Mandt, J. H. Waite Jr., J.-E. Wahlund, (2010), Investigation of the force balance in the Titan ionosphere: Cassini T5 flyby model/data comparisons, Icarus, 210, 867–880.

Vigren, E., M. Galand, R. V. Yelle, A. Wellbrock, A. J. Coates, D. Snowden, J. Cui, P. Lavvas, N. J. T. Edberg, O. Shebanits, J.-E. Wahlund, V. Vuitton, K. Mandt, (2015), Ionization balance in Titan's nightside ionosphere, Icarus, 248, 539–546, doi: 10.1016/j.icarus.2014.11.012.

Vuitton, V., P. Lavvas, R. V. Yelle, M. Galand, A. Wellbrock, G. R. Lewis, A. J. Coates, J.-E. Wahlund, (2009), Negative ion chemistry in Titan's upper atmosphere, Planetary and Space Science, 57, 1558–1572.

Wahlund, J.-E., M. Galand, I. Meuller-Wodarg, J. Cui, R. V. Yelle, F. J. Crary, K. Mandt, B. Magee, J. H. Waite, Jr., D. T. Young, A. J. Coates, P. Garnier, K. Ågren, M. Andre, A. I. Eriksson, T. E. Cravens, V. Vuitton, D. A. Gurnett, W. S. Kurth, (2009), On the amount of heavy molecular ions in Titan's ionosphere, Planetary and Space Science, 57, 1857–1865.

Westlake, J. H., J. H. Waite, N. Carrasco, M. Richard, T. Cravens, (2014b), The role of ion-molecule reactions in the growth of heavy ions in Titan's ionosphere, Journal of Geophysical Research, 119, 5951–5963, doi: 10.1002/2014JA0202008.

Westlake, J. H., C. P. Paranicas, T. E. Cravens, J. G. Luhmann, K. E. Mandt, H. T. Smith, D. G. Mitchell, A. M. Rymer, M. E. Perry, J. H. Waite Jr., J.-E. Wahlund, (2012a), The observed composition of ions outflowing from Titan, Geophysical Research Letters, 39, L19104, doi: 10.1029/2012GL053079.

Westlake, J. H., J. H. Waite Jr., K. E. Mandt, N. Carrasco, J. M. Bell, B. A. Magee, J.-E. Wahlund, (2012b), Titan's ionospheric composition and structure: Photochemical modeling of Cassini INMS data, Journal of Geophysical Research, 117, E01003, 21, doi: 10.1029/2011JE003883.

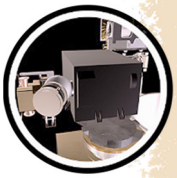

Titan – unanticipated findings

There are five papers listed below that detail unanticipated findings by INMS. The complex nature and complexity of the ion neutral chemistry was totally unanticipated, as was our overall characterization of the formation of the Saturn system through compositional measurements.

RELEVANT PAPERS

Carrasco, N., J. Westlake, P. Pernot, J. H. Waite Jr., (2013), Nitrogen in Titan's Atmospheric Aerosol Factory, The Early Evolution of the Atmospheres of Terrestrial Planets, 35, doi: 10.1007/978-1-4614-5191-4_11.

Glein, C. R., (2017), A whiff of nebular gas in Titan's atmosphere – Potential implications for the conditions and timing of Titan's formation, Icarus, 293, 231–242.

Vuitton, V., R. V. Yelle, M. J. McEwan, (2007), Ion Chemistry and N-containing Molecules in Titan's Upper Atmosphere, Icarus, doi: 10.1016/j.carus.2007.06.023.

Waite, J. H., D. T. Young, A. J. Coates, F. J. Crary, B. A. Magee, K. E. Mandt, J. H. Westlake, (2008), The source of heavy organics and aerosols in Titan's atmosphere, Proceedings of the International Astronomical Union, vol. 4, issue S251 (Organic Matter in Space), pp. 321-326, doi: 10.1017/S1743921308021844.

Waite Jr., J. H., D. T. Young, T. E. Cravens, A. J. Coates, F. J. Crary, B. Magee, J. Westlake, (2007), The process of tholin formation in Titan's upper atmosphere, Science, 316, 870–875.

Rings and icy satellites

There are 11 papers listed below that discuss Saturn's rings and icy satellites. INMS allowed a characterization of the E-ring and F-ring as expected. The sputtered atmospheres of Dione and Rhea were well characterized, including the unexpected seasonal variations associated with those atmospheres. The D-ring interaction with Saturn's atmosphere during the Grand Finale exceeded all expectations.

RELEVANT PAPERS

Ip W.-H., (2006), On a ring origin of the equatorial ridge of Iapetus, Geophysical Research Letters, 33, L16203.

Ip, W.-H., (2005), An update on the ring exosphere and plasma disc of Saturn, Geophysical Research Letters, doi: 10.1029/2004GL022217.

Johnson, R. E., J. G. Luhmann, R. L. Tokar, M. Bouhram, J. J. Berthelier, E. C. Sittler, J. F. Cooper, T. W. Hill, H. T. Smith, M. Michael, M. Liu, F. J. Crary, D. T. Young, (2006), Production, ionization and redistribution of O2 in Saturn's ring atmosphere, Icarus, 180, 393.

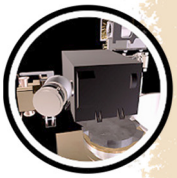

Luhmann, J. G., R. E. Johnson, R. L. Tokar, S. A. Ledvina, T. E. Cravens, (2006), A model of the ionosphere of Saturn's rings and its implications, Icarus, 181 (2), 465–474.

Perry, M. E., B. Teolis, H. T. Smith, R. L. McNutt, G. Fletcher, W. Kasprzak, B. Magee, D. G. Mitchell, J. H. Waite Jr., (2010), Cassini INMS observations of neutral molecules in Saturn's E-ring. Journal of Geophysical Research, 115, A10206.

Teolis, B. D. and J. H. Waite, (2016), Dione and Rhea seasonal exospheres, revealed by Cassini CAPS and INMS, Icarus, 272, 277–289, doi: 10.1016/j.icarus.2016.02.031.

Teolis, B. D., I. Sillanpää, J. H. Waite, K. K. Khurana, (2014), Surface current balance and thermoelectric whistler wings at airless astrophysical bodies: Cassini at Rhea, Journal of Geophysical Research, 119, 8881–8901, doi: 10.1002/2014JA020094.

Teolis, B., G. H. Jones, P. F. Miles, R. L. Takar, B. A. Magee, J. H. Waite, E. Roussos, D. T. Young, F. J. Crary, A. J. Coates, R. E. Johnson, W.-L. Tseng, R. A. Baragiola, (2010a), Cassini Finds an Oxygen-Carbon Dioxide Atmosphere at Saturn's Icy Moon Rhea, Science, 330, 24.

Waite Jr., J. H., R. Perryman, M. Perry, K. Miller, J. Bell, T. E. Cravens, C. R. Glein, J. Grimes, M. Hedman, J. Cuzzi, T. Brockwell, B. Teolis, L. Moore, D. Mitchell, A. Persoon, W. S. Kurth, J-E. Wahlund, M. Morooka, L. Z. Hadid, S. Chocron, J. Walker, A. Nagy, R. Yelle, S. Ledvina, R. Johnson, W. Tseng, O. J. Tucker, W.-H. Ip, (2018), Chemical Interactions between Saturn’s Atmosphere and its Rings, Science, doi: 10.1126/science.aat2382.

Waite Jr., J. H., M. Combi, W.-H. Ip, T. E. Cravens, R. L. McNutt, Jr., W. Kasprzak, R. Yelle, J. Luhmann, H. Niemann, D. Gell, B. Magee, G. Fletcher, J. Lunine, W.-L. Tseng, (2006), Cassini Ion and Neutral Mass Spectrometer: Enceladus plume composition and structure, Science, 311, 1419–1422.

Waite, J. H., T. E. Cravens, W.-H. Ip, W. T. Kasprzak, J. G. Luhmann, R. L. McNutt, H. B. Niemann, R. V. Yelle, I. Müller-Wodarg, S. A. Ledvina, S. Scherer, (2005b), Oxygen ions observed near Saturn’s A Ring, Science, 307 (5713), 1260–1262.

Magnetosphere

There is one paper listed below that discusses the magnetosphere. The INMS contribution to the magnetospheres studies was limited due to the energy range covered by the open source ions.

RELEVANT PAPERS

Blanc, M., S. Bolton, J. Bradley, M. Burton, T. E. Cravens, I. Dandouras, M. K. Dougherty, M. C. Festou, J. Feynman, R. E. Johnson, T. G. Gombosi, W. S. Kurth, P. C. Liewer, B. H. Mauk, S. Maurice, D. Mitchell, F. M. Neubauer, J. D. Richardson, D. E. Shemansky, E. C. Sittler, B. T. Tsurutani, P. Zarka, L. W. Esposito, E. Grün, D. A. Gurnett, A. J. Kliore, S. M. Krimigis, D. Southwood, J. H. Waite Jr., D. T. Young, (2002), Magnetospheric and plasma science with Cassini-Huygens, Space Science Reviews, 104, 1, 253–346.

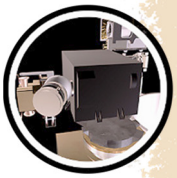

Enceladus

The most startling and unanticipated contribution from INMS was the characterization of the gas composition of the Enceladus plume. The 18 papers listed below discuss the composition, structure, and dynamics of the plume. Most noteworthy were the discovery that the water in the plumes has the same D/H ratio of some Oort cloud comets, and that the plume contained molecular hydrogen that showed a positive chemical affinity to the reaction for methanogenesis $[4\ H_2 + CO_2 \rightarrow CH_4 + 2\ H_2O]$. There is food for microbes in the global ocean.

RELEVANT PAPERS

Bouquet, A., C. R. Glein, D. Wyrick, J. H. Waite Jr., (2017), Alternative energy: Production of H_2 by radiolysis of water in the rocky cores of icy bodies, The Astrophysical Journal Letters, 840, L8, doi:10.3847/2041-8213/aa6d56.

Cravens, T. E., R. L. McNutt Jr., J. H. Waite Jr., I. P. Robertson, J. G. Luhmann, R. V. Yelle, W. Kasprzak, W.-H. Ip, (2009c), Plume ionosphere of Enceladus as seen by the Cassini Ion and Neutral Mass Spectrometer, Geophysical Research Letters, 36, L08106, doi: 10.1029/2009GL037811.

Dong, Y., T. W. Hill, B. D. Teolis, B. A. Magee, J. H. Waite Jr., (2011), The water vapor plumes of Enceladus, Journal of Geophysical Research, 116, A10204.

Farrell, W. M., W. S. Kurth, D. A. Gurnett, R. E. Johnson, M. L. Kaiser, J.-E. Wahlund, J. H. Waite Jr., (2009), Electron density dropout near Enceladus in the context of water-vapor and water-ice, Geophysical Research Letters, 36, L10203.

Glein, C. R., J. A. Baross, J. H. Waite Jr., (2015), The pH of Enceladus' ocean, Geochimica et Cosmochimica Acta, 162, 202–219, doi: 10.1016/j.gca.2015.04.017.

Hansen, C. J., D. E. Shemansky, L. W. Esposito, A. I. F. Stewart, B. R. Lewis, J. E. Colwell, A. R. Hendrix, R. A. West, J. H. Waite Jr., B. Teolis, B. A. Magee, (2011), The composition and structure of the Enceladus plume, Geophysical Research Letters, 38, L11202.

Hurley, D. M., M. E. Perry, H. J. Waite Jr., (2015), Modeling insights into the locations of density enhancements from the Enceladus water vapor jets, Journal of Geophysical Research, 120, 1763–1773, doi: 10.1002/21015JE004872.

Jones, G. H., C. S. Arridge, A. J. Coates, G. R. Lewis, S. Kanani, A. Wellbrock, D. T. Young, F. J. Crary, R. L. Tokar, R. J. Wilson, R. E. Johnson, D. G. Mitchell, J. Schmidt, S. Kempf, U. Beckmann, C. T. Russell, Y. D. Jia, M. K. Dougherty, J. H. Waite Jr., B. A. Magee, (2009), Fine jet structure of electrically charged grains in Enceladus' plume, Geophysical Research Letters, 36, L16204.

Magee, B. A. and J. H. Waite, (2017), Neutral gas composition of Enceladus' plume - Model parameter insights from Cassini-INMS, 48th Lunar and Planetary Science Conference, 20–24 March 2017, The Woodlands, TX, LPI Contribution No. 1964, id. 2974.

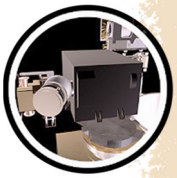

Mousis, O., J. I. Lunine, J. H. Waite Jr., B. Magee, W. S. Lewis, K. E. Mandt, D. Marquer, D. Cordier, (2009a), Formation conditions of Enceladus and origin of its methane reservoir, The Astrophysical Journal Letters, 701, L39-L42.

Ozak, N., T. E. Cravens, G. H. Jones, A. J. Coates, I. P. Robertson, (2012), Modeling of electron fluxes in the Enceladus plume, Journal of Geophysical Research, 117, A06220, doi: 10.1029/2011JA017497.

Perry, M. E., B. D. Teolis, D. M. Hurley, B. A. Magee, J. H. Waite, T. G. Brockwell, R. S. Perryman, R. L. McNutt, (2015), Cassini INMS measurements of Enceladus plume density, Icarus, 257, 139–162, doi: 10.1016/j.icarus.2015.04.037.

Sakai, S., T. E. Cravens, N. Omidi, M. E. Perry, J. H. Waite Jr.,(2016) Ion energy distributions and densities in the plume of Enceladus, Planetary and Space Science, 130, 60–79, doi: 10.1016/j.oss.2016.05.007.

Tenishev, V., D. C. S. Öztürk, M. R. Combi, M. Rubin, J. H. Waite Jr., M. Perry, (2014), Effect of the Tiger Stripes on the water vapor distribution in Enceladus' exosphere, Journal of Geophysical Research, 119, 2658–2667, doi: 10.1002/2014JE004700.

Tenishev, V., M. R. Combi, B. D. Teolis, J. H. Waite Jr., (2010). An approach to numerical simulation of the gas distribution in the atmosphere of Enceladus, Journal of Geophysical Research, 115, A09302.

Teolis, B., M. E. Perry, B. A. Magee, J. Westlake, J. H. Waite Jr., (2010b), Detection and measurements of ice grains and gas distribution in the Enceladus plume by Cassini's ion neutral mass spectrometer, Journal of Geophysical Research, 115, A09222.

Waite Jr., J. H., C. R. Glein, R. S. Perryman, B. D. Teolis, B. A. Magee, G. Miller, J. Grimes, M. E. Perry, K. E. Miller, A. Bouquet, J. L. Lunine, T. Brockwell, S. J. Bolton, (2017), Cassini finds molecular hydrogen in the Enceladus plume: Evidence for hydrothermal processes, Science, 356, 155–159.

Waite Jr., J. H., W. S. Lewis, B. A. Magee, J. I. Lunine, W. B. McKinnon, C. R. Glein, O. Mousis, D. T. Young, T. Brockwell, J. Westlake, M.-J. Nguyen, B. D. Teolis H. B. Niemann, R. L. McNutt, M. Perry, W.-H. Ip, (2009), Liquid water on Enceladus from observations of ammonia and 40Ar in the plume, Nature, 460, 487–490.

Instrument

The four papers listed below describe the INMS instrument, including instrument operations, calibrations, and lab activities.

Kasprzak, W. T., H. Niemann, D. Harpold, J. Richards, H. Manning, E. Patrick, P. Mahaffy, (1996), Cassini orbiter ion neutral mass spectrometer instrument, Proceedings SPIE, vol. 2803, Cassini-Huygens: A Mission to the Saturnian Systems, International Symposium on Optical Science, Engineering, and Instrumentation, Denver, CO, doi: 10.1117/12.253413.

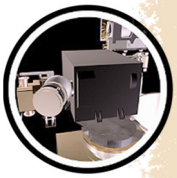

Patrick, E. L. , (2006), Silicon carbide nozzle for producing molecular beams, Review of Scientific Instruments, 77, 043301, doi:10.1063/1.2188907.

Teolis, B. D., H. B. Niemann, J. H. Waite, D. A. Gell, R. S. Perryman, W. T. Kasprzak, K. E. Mandt, R. V. Yelle, A. Y. Lee, F. J. Pelletier, G. P. Miller, D. T. Young, J. M. Bell, B. A. Magee, E. L. Patrick, J. Grimes, G. G. Fletcher, and V. Vuitton, (2015), A revised sensitivity model for Cassini INMS: Results at Titan, Space Science Reviews, doi: 10.1007/s11214-014-0133-8.

Waite Jr., J. H., W. S. Lewis, W. T. Kasprzak, V. G. Anicich, B. P. Block, T. C. Cravens, G. G. Fletcher, W.-H. Ip, J. G. Luhmann, R. L. McNutt, H. B. Niemann, J. K. Parejko, J. E. Richards, R. L. Thorpe, E. M. Walter, R. V. Yelle, (2004), The Cassini Ion and Neutral Mass Spectrometer (INMS) investigation, Space Science Reviews, 114, 113–231.

INMS Saturn System Science Results

Titan Science

Titan highlights

- **Complex Ion Neutral Chemistry:** Existence demonstrated of a complex ionospheric chemistry on Titan dominated by hydrocarbon and nitrogen-bearing species.
- **Solar Radiation as the Primary Ionospheric Source:** Demonstration that solar radiation dominates as the global source of Titan's ionosphere but that locally on the nightside particle precipitation from Saturn's magnetosphere is an important source.
- **Atmospheric Escape:** Early studies by Yelle et al. [2006, 2008] and Strobel [2008, 2010] demonstrated possible need for enhanced methane escape from Titan to explain the data. Later studies by Bell et al. [2014] and Tucker et al. [2013] that combined thermal balance, dynamical, and chemical calculations reproduced INMS without hydrodynamic escape of methane. The New Horizons mission also demonstrated that hydrodynamic escape is not likely at Pluto and by extension, Titan. However, the possibility remains that high escape rates could be possible due to other non-thermal mechanisms. Definite implications for evolution of Titan [Mandt et al. 2012a].
- **Thermosphere Temperatures:** Rapid changes in upper atmosphere temperatures could be due to a combined effect of upward propagating gravity waves (see Müller-Wodarg et al. [2006a, 2008]; Strobel [2006]; Snowden et al. [2013a, 2013b]) and downwelling plasma from Saturn's co-rotating magnetosphere [Westlake et al. 2011; Bell et al. 2011a]. Thus, this is a thermosphere driven from above and below in unique ways in the solar system.

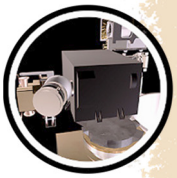

Summary of Titan science

Instruments on the Cassini Orbiter carried out extensive measurements of the upper atmosphere and ionosphere of Titan over a 12-year period of time, starting in 2005. The first INMS neutral measurements were made during the TA pass and the first ion composition were made on Titan's nightside during the T5 pass. The INMS measured densities of ion species up to a mass number of 99 throughout the main and topside ionosphere, on the dayside and nightside, the ramside and wakeside (with respect to the external flow of magnetospheric plasma), and when Titan was in different regions of Saturn's magnetosphere. The measured ion composition and densities provided insight into several aspects of Titan's ionosphere and its linkage between the neutral atmosphere and the external environment including the Sun (solar ionizing radiation), Saturn's magnetosphere, and the solar wind. In particular, ionospheric processes were shown to play a critical role in how external particles and radiation, combined with a nitrogen and methane neutral atmosphere, in driving photochemistry in the upper atmosphere that leads to complex organic composition and also to aerosol growth.

TITAN UPPER ATMOSPHERE/IONOSPHERE MAJOR FINDINGS (NEUTRAL)

- INMS made first in situ measurements of the major constituents of Titan's upper atmosphere and ionosphere, discovering an unexpectedly complex and rich ion and neutral chemistry occurring above 1000 km. **(T_AO2, T_AO1,** and **T_AO5)**.
- The INMS measurements of the $^{12}C/^{13}C$ and $^{14}N/^{15}N$ isotopic ratios have allowed for assessments of Titan's evolutionary history. **(T_AO1)**.
- INMS observations have revealed significant variations in thermal structures that suggest a combination of magnetospheric and wave/tide energy deposition. **(T_AO5)**.
- INMS observations over time have revealed that the atmospheric content of methane above 1000 km is sensitive to the solar cycle.
- INMS measurements over time demonstrated that solar ionizing radiation is the dominant source of the ionosphere and correlated with solar activity, although ionization by energetic particle precipitation from Saturn's magnetosphere is important on the nightside **(T_AO5)**.

Table INMS-2 shows the INMS Titan objective, the AO and TM/CSM science objective, and the color-coded rating assessment.

Figure INMS-5 shows the inferred neutral temperatures from INMS nitrogen density measurements.

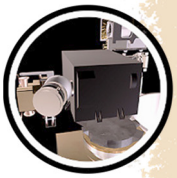

Table INMS-2. Final Report INMS – Titan Science.

Fully/Mostly Accomplished: Partially Accomplished: Not Accomplished:

INMS Objectives	AO and TM/CSM Science Objectives	Assessment
Titan Objectives		
Titan Atmospheric Formation and Evolution	T_AO1	
Titan Atmospheric Composition and Distribution	T_AO2	
Titan Upper Atmosphere	T_AO5	

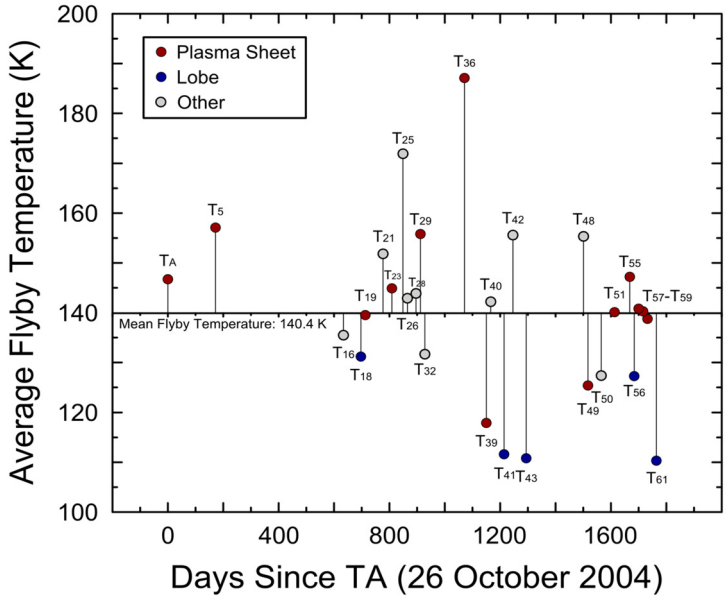

Figure INMS-5. Inferred neutral temperatures (vertical axis) from INMS nitrogen density measurements over time since the TA.

Titan's neutral atmosphere

Observations of neutral densities (mainly N_2), have allowed us to make inferences into the thermal structure of Titan's upper atmosphere [cf. Müller-Wodarg et al. 2006a, 2008; Cui et al. 2008, 2009a; Magee et al. 2009; Westlake et al. 2011; Snowden et al. 2013a]. The average thermospheric temperature derived from INMS data is around 150 K, which is in good agreement with pre-Cassini estimates [Müller-Wodarg et al. 2000, 2003; Müller-Wodarg and Velle 2002a]. However, the temperature of Titan's thermosphere exhibits a high degree of variability that was not predicted prior to Cassini—see, for example, Müller-Wodarg et al. [2000, 2003]; Müller-Wodarg and Velle [2002a]. Pre-Cassini models calculated day-night variations on the order of 10–15 K. Cassini has observed temperature variations much larger than this over the course of a single Titan day, even when observing the same region of atmosphere at a similar local time. The variations in

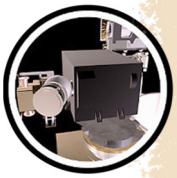

temperature are not correlated with solar input, indicating there are additional heating/cooling mechanisms with magnitudes that are similar to solar insulation. The short-timescales associated with the large variations in temperature has led some to postulate that the magnetosphere may provide sporadic and localized inputs [Westlake et al. 2011] or internal gravity waves may be depositing significant energy into the upper atmosphere [Müller-Wodarg et al. 2006a; Snowden et al. 2013a]. Atmospheric escape may also significantly alter the temperature of the upper thermosphere [Tucker et al. 2013] as can spatial and temporal variation of minor species that are strong sources of radiative cooling such as HCN and CH_4.

INMS data indicates that, similar to other atmospheres, waves are a persistent feature in Titan's thermosphere. Wave characteristics derived by fitting INMS data (Figure INMS-6) indicates vertical wavelengths are the order of several hundred kilometers, amplitudes are on the order of 10%, and wave periods are on the order of several hours [Müller-Wodarg et al. 2006a; Snowden et al. 2013a; Cui et al. 2013]. The persistence of waves in Titan's thermosphere indicates that the zonal wind speed must exceed 100 m/s [Snowden et al. 2013a]. Super rotating winds around 100 m/s have also been employed to explain day-night variation in short and long-lived ions observed by INMS in Titan's upper atmosphere [Cui et al. 2009b].

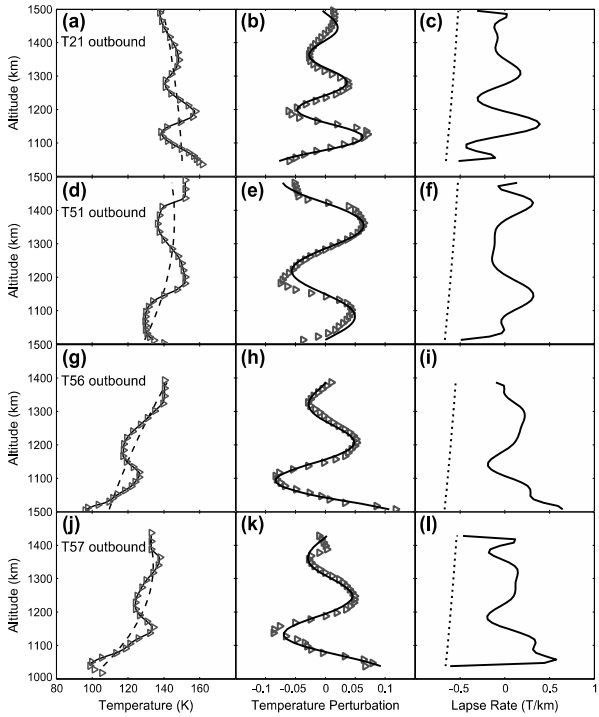

Figure INMS-6. The panels show how wave properties are determined by fitting the vertical temperature profiles derived from INMS data from four flybys. Panels on the right compare the vertical gradient in temperature to the adiabatic lapse rate to show that waves of this scale can be stable in Titan's thermosphere. [Snowden et al. 2013a].

Not only has INMS revealed the nature of Titan's upper atmospheric thermal structure, but it has also shown that the methane in the upper atmosphere can exhibit significant solar cycle

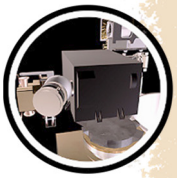

variations. As seen in Figure INMS-7, the methane densities (abundances) during the extended solar minimum remained relatively stable and consistent relative to the major background species N_2. However, as the solar activity levels increased (Figure INMS-7, panels 4 and 5), methane was significantly reduced relative to N_2. This occurred despite the fact that, as shown by the panel 3 in Figure INMS-7, Titan was moving farther away from the Sun, and all things being equal, should have experienced reduced solar insolation. These observations demonstrated that methane is a chemically active species, responding relatively quickly to increases in solar insolation, again highlighting the surprisingly dynamic nature of Titan's upper atmosphere.

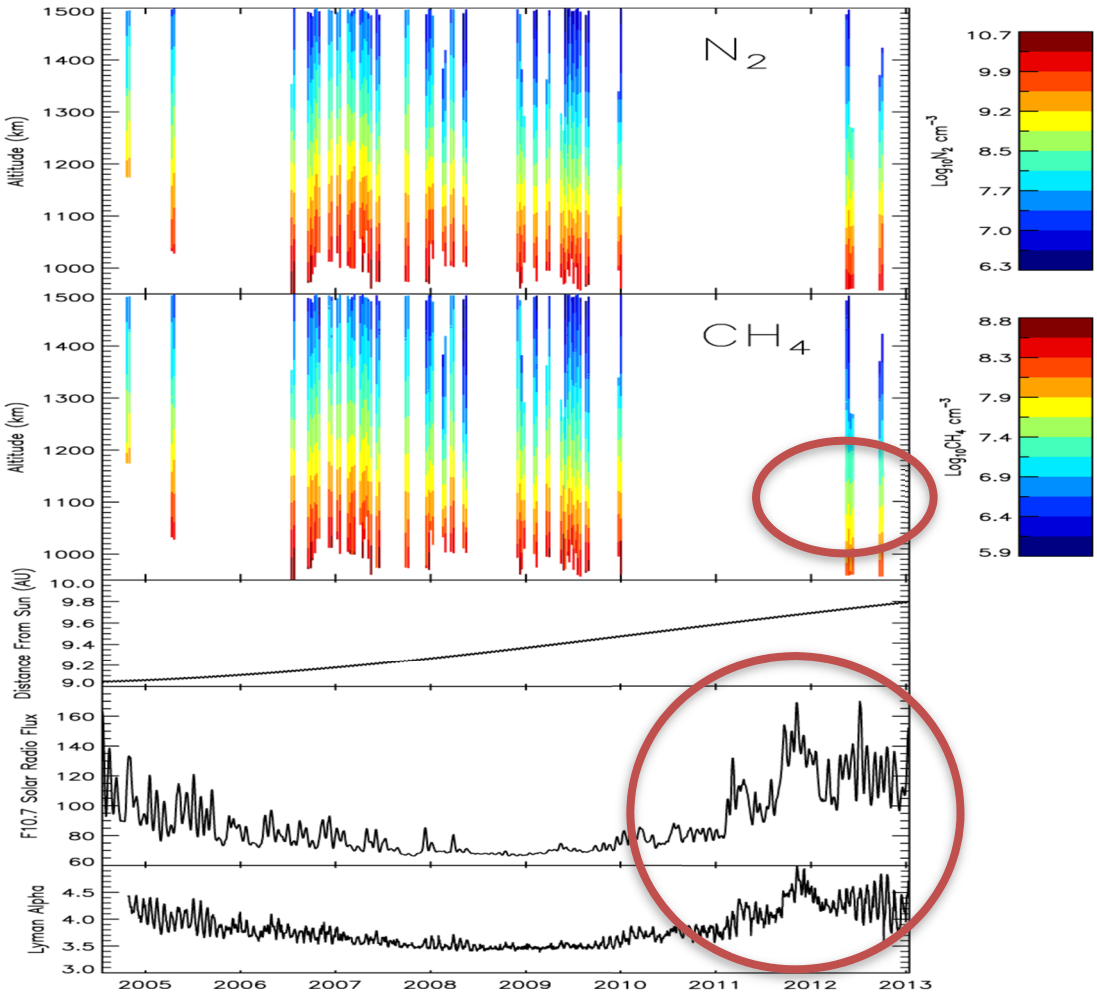

Figure INMS-7. Titan's upper atmospheric thermal structure shows that the methane in the upper atmosphere can exhibit significant solar cycle variations. Multipanel plot showing N_2 densities (*panel 1*), CH_4 densities (*panel 2*), Titan-Saturn orbital distance (*panel 3*), Solar $F_{10.7\text{-cm}}$ radio flux (*panel 4*), and Lyman-alpha fluxes at Titan's orbit (*panel 5*) as a function of time (horizontal axis). The circles point to the time periods of significantly reduced methane measured by INMS that correlates with high solar activity [Westlake et al. 2012a].

While no direct thermosphere wind measurements could be made with the INMS or any other Cassini or Earth based instrumentation, the horizontal density variations in the thermosphere as

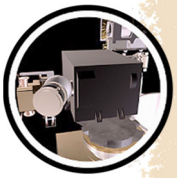

measured by the INMS were used in conjunction with balance of forces calculations as well as more sophisticated General Circulation Model (GCM) simulations to infer horizontal wind speeds reaching around 150 m/s [Müller-Wodarg et al. 2008]. These calculations also determined the important influence of thermospheric winds on the distribution of atmospheric gases such as CH_4. More recent calculations with the Titan thermosphere GMC [Müller-Wodarg et al. 2003] demonstrated that much of the significant variability in densities and temperatures observed by the INMS [Snowden et al. 2013a] could be explained by variability in the stratosphere which strongly affected the thermosphere.

Titan's ionosphere

Voyager measurements, both in situ of the magnetotail and radio occultation of the main ionosphere, showed the existence of an ionosphere at Titan [Neubauer et al. 1984; Bird et al. 1997]. Subsequent theoretical modeling suggested that the ionospheric composition could be quite complex, largely due to the presence of hydrocarbons associated with dissociation and ionization of methane [Nagy and Cravens 1998; Keller et al. 1992, 1998; Fox and Yelle 1997]. But the series of Cassini measurements by INMS, CAPS, and the Radio and Plasma Wave Science (RPWS) LP quantified the ionospheric densities and the extent of the ionosphere. The INMS science of Titan's ionosphere is organized into 3 sub-sections: 1) sources, 2) chemistry, and 3) dynamics.

Sources of Titan's ionosphere

The major ion species produced is N_2^+, since N_2 is the major neutral species. However, chemical considerations told us that the main ion species at mass 28 is not N_2^+ but $HCNH^+$, so another ion species, CH_3^+, was used to almost directly deduce ion production rates [Richard et al. 2015a, 2015b; Vigren et al. 2015; Sagnières et al. 2015]. The rapid chemical reaction of N_2^+ with CH_4 produces CH_3^+ (mass 15). The ionization rate of CH_4 can be deduced by the measured CH_4^+ ions at mass 16 [Richard et al. 2015a, 2015b].

It was found that solar ionizing radiation is the dominant source of the dayside ionosphere, not surprisingly, and the quantification of the source rate was largely as expected given the solar flux and the relevant photoionization cross-sections for N_2 and CH_4. Given that Cassini spanned a large part of a solar cycle, the INMS-deduced ion production rates were shown to increase with increasing solar activity [Madanian et al. 2016].

Sources of ionization deep on the nightside were also studied by Cassini and INMS. Globally, solar radiation accounts for 90% of total ionization, but precipitation of energetic electrons and ions leading to ionization is obviously locally important on the nightside [Ågren et al. 2007; Cravens et al. 2008a, 2008b; Cravens et al. 2009b; Vigren et al. 2015; Snowden and Yelle 2014a, 2014b; Edberg et al. 2013a, 2013b; Robertson et al. 2009; Galand et al. 2014]. As on Venus and Mars, the two possible sources of the nightside ionosphere are local/direct ionization from precipitation (i.e., a diffuse aurora) and transport of plasma from the dayside. Evidence for the precipitation source was provided by INMS by measurements of primary or almost primary ion species (CH_3^+,

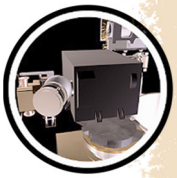

CH_4^+, CH_5^+…), which have short chemical lifetimes and could only be produced locally. On T5 a correlation between secondary auroral electron fluxes measured by CAPS ELS correlated with the CH_5^+ densities [Cravens et al. 2008a]. Longer-lived ion species (e.g., $HCNH^+$) can also be transported from day to night and both sources can operate [Cui et al. 2009a]. Modeling combined with INMS, CAPS, and RPWS data determined that the precipitation ionization source depend on magnetic topology and on the location of Titan in Saturn's magnetosphere. Incident magnetospheric electron fluxes, and the associated nightside ionosphere, were more robust when Titan was located in the plasmasheet region as opposed to the magnetic lobes of Saturn's magnetosphere [Richard et al. 2015a; Rymer et al. 2009].

Chemistry of the Upper Atmosphere and Ionosphere

The chemistry of Titan's upper atmosphere and ionosphere is complex due to the presence of a large number of organic species extending up to high mass numbers. The neutral and ion chemistry is linked together [Waite et al. 2007]. The INMS has played a key role in improving our understanding of this chemistry. Photodissociation and photoionization of N_2 and CH_4 form ion and neutral species that are very reactive and that initiate a series of reactions producing increasing larger species, up to aerosol-sized particles [Waite et al. 2007]. Primary N_2^+ ions react with CH_4 to produce CH_3^+, which again reacts with CH_4 to produce $C_2H_5^+$. $C_2H_5^+$ reacts with HCN to produce the very abundant species $HCNH^+$. Reactions of $C_2H_5^+$ and $HCNH^+$ with C_2H_2, C_2H_4, and C_4H_2 drive a chain of reactions leading to families of $C_nH_m^+$ species, including protonated benzene ($C_6H_7^+$), and up to masses exceeding 99 Da [Anicich and McEwan 1997; Cravens et al. 2006; Vuitton et al. 2006, 2007, 2009; Westlake et al. 2014b; Cui et al. 2009a; Mandt et al. 2012a] (Figure INMS-8 and Figure INMS-9). Figure INMS-10 shows INMS ion density profiles versus neutral density (i.e., altitude). CAPS measurements, albeit at low mass resolution, indicated the presence of species up to at least 1100 Da [Crary et al. 2009; Coates et al. 2010]. For example, CH_2NH_2, CH_3CN, and other nitrogen-bearing species react with lower mass ion species to produce protonated ion species [Vuitton et al. 2007].

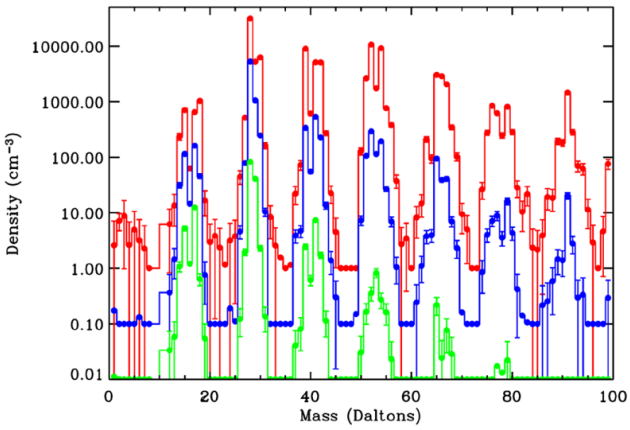

Figure INMS-8. Shown are the first INMS measurements of ion densities versus mass number at three different altitudes for the T5 nightside ionosphere [Cravens et al. 2006]. *Red:* 1027–1200 km. *Blue:* 1200–1400 km. *Green:* 1400–1600 km. Chemical complexity increases with decreasing altitude.

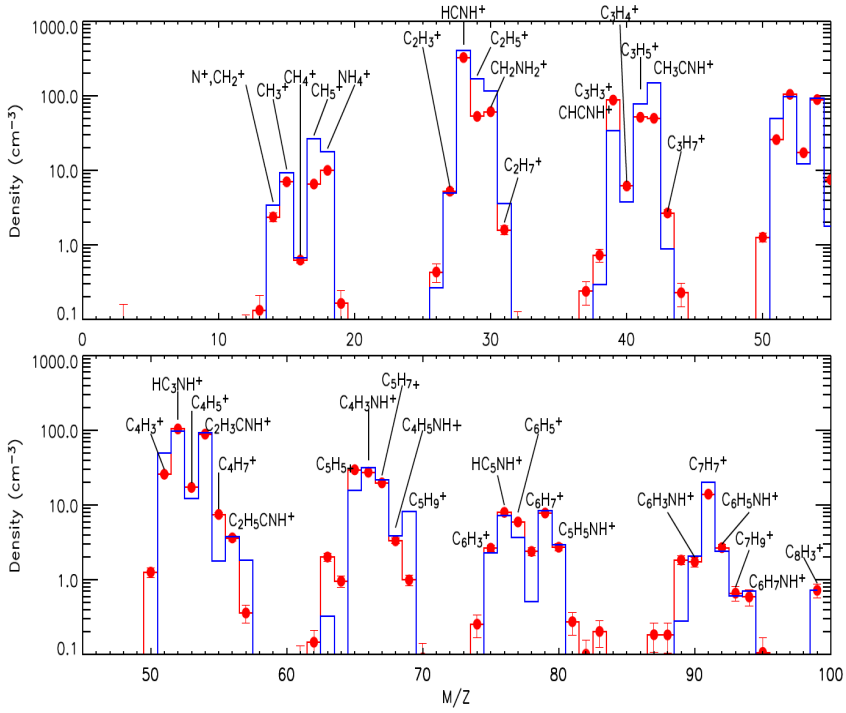

Figure INMS-9. INMS T5 data compared with a photochemical model which put forward the presence of protonated nitrogen ion species. The *blue line* is the modeled mass spectrum [Vuitton et al. 2007].

INMS data for 4 ion species. *Ion Density vs. neutral density*.

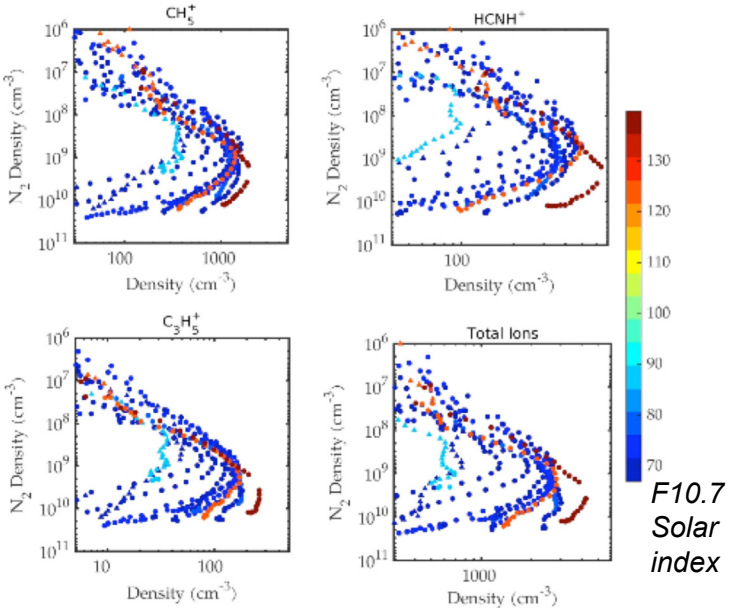

Figure INMS-10. INMS ion density profiles versus neutral density measured throughout the mission with different solar activity levels (as given by the solar extreme ultraviolet (EUV) proxy F10.7—*color bar*). Total ions denote the total INMS ion density. In general, higher solar activity correlates with higher density. [Madanian et al. 2016].

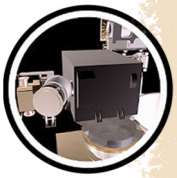

Titan's ionosphere consists of positive and negative ions, some of which have masses of up to and possibly beyond 1000s u [Waite et al. 2007; Coates et al. 2007]. The study of Vuitton et al. [2007] identified over 100 ions in the INMS spectrum including several N-bearing species such as protonated ammonia (NH_4^+), $CH_2NH_2^+$, and CH_3CNH^+. Titan's atmosphere is a reducing atmosphere (little or no oxygen species are present) and as such the ionization will flow from species whose parent neutral molecules have low proton affinities (PA) to those whose parent neutral molecules have greater PAs. The proton affinity of a molecule is a measure of the gas-phase basicity or its propensity to undergo a reaction in which a proton is gained. In general, molecules containing unsaturated carbon bonds (those which have double or triple covalent bonds between adjacent molecules) have larger proton affinities.

The hydrocarbon chemistry at Titan has been shown to lead to the production of benzene [Waite et al. 2007; De La Haye et al. 2008b; Vuitton et al. 2008]. There have been several attempts by the modeling community to reproduce the INMS observed benzene abundances including those based solely on radical neutral and termolecular processes [Lebonnois 2005], some ion-molecule reactions coupled with neutral processes [Wilson et al. 2003], and intricately coupled ion-molecule chemical schemes [De La Haye et al. 2008b; Vuitton et al. 2008]. The INMS measured molar fraction of benzene was found to be about 2×10^{-6} at 1050 km altitude [Magee et al. 2009]. The study of Vuitton et al. [2008] argues that most of the observed benzene is a product of reactions between phenyl radicals (C_6H_5) and hydrogen within the INMS instrument's antechamber yielding a benzene abundance that contributes one-third of the total observed peak level. This implies significant amounts of the phenyl radical are present in Titan's upper atmosphere. Further analysis of the INMS data revealed that it is difficult to disentangle heterogeneous surface chemistry of radicals from adsorption/desorption of the parent molecule [Cui et al. 2009b]. Regardless of interpretation, the Cassini INMS data shows that the mixing ratio of benzene or benzene and phenyl is a few times 10^{-6} indicating that the chemistry is efficient in producing not only unsaturated hydrocarbons but also aromatic hydrocarbons.

Although NH_3 and CH_2NH were not directly detected on Titan, we have shown that the mass spectra obtained by Cassini indicate the presence of NH_4^+ and $CH_2NH_2^+$. This implies quantities of NH_3 and CH_2NH close to 10 ppm in the upper atmosphere, because the NH_4^+/NH_3 and $CH_2NH_2^+/CH_2NH$ couples are connected to each other by proton exchange and electron recombination reactions. However, the presence of such an amount of NH_3 in the upper atmosphere of Titan was not predicted by photochemical models.

In order to tackle this problem, we have proposed a new way for the formation of NH_3, by reaction of the radical NH_2 with H_2CN, the latter being also the precursor of HCN. To confirm this hypothesis, we calculated the kinetic constant and showed that it is indeed fast (7.5×10^{-11} cm^3 s^{-1} at 150 K). The calculated NH_4^+ and $CH_2NH_2^+$ densities are then in agreement with the densities measured for the entire altitude range for which observations are available, which leads to the conclusion that the main mechanisms of production and loss of NH_3 and CH_2NH have been properly identified. More generally, we have shown that ammonia and methanimine are formed from a complex network of reactions involving both neutral and charged species, which, as for

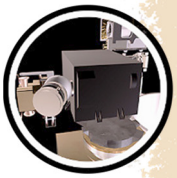

C_6H_6, shows the importance of ion chemistry for the composition of the neutral atmosphere [Yelle et al. 2010].

Below about 1200 km in Titan's atmosphere positive ions with masses greater than 100 u have been found [Waite et al. 2007; Crary et al. 2009]. A sample spectrum obtained by the CAPS-IBS instrument during the T26 flyby is shown in Figure INMS-11. The composition of the high mass ions has been suggested to primarily consist of polycyclic aromatic hydrocarbon (PAH) that are multi-ringed molecules built from benzene [Crary et al. 2009]. PAH ions are likely the precursors to the tholins observed in the haze layer at about 500 km [Waite et al. 2007; Lavvas et al. 2008a, 2008b]. Models have shown that the most efficient pathway for production of the haze layer is through PAHs [Wilson et al. 2003]. Several theoretical models have also been developed to describe the process of producing PAHs from benzene through neutral chemistry in the context of flame chemistry [Wang and Frenklach 1997; Richter and Howard 2000], and interstellar environments [Bohme 1992; Snow et al. 1998]. Computational models have been developed to describe the energy required to build PAHs through neutral chemistry [Bauschlicher and Ricca 2000], cation chemistry [Bauschlicher et al. 2002], as well as, the efficiency for incorporating nitrogen into PAHs [Ricca et al. 2001a, 2001b].

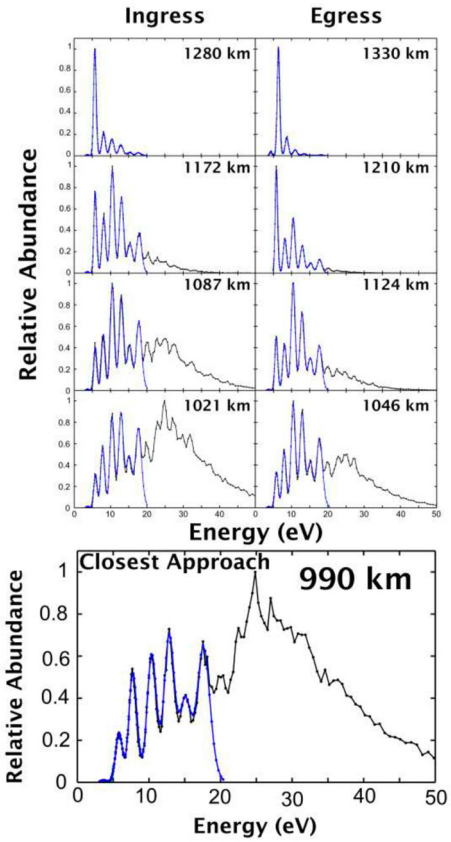

Figure INMS-11. Shown are nine ion mass spectra obtained by the CAPS-IBS instrument at various altitudes during the T26 flyby. The *blue lines* show the INMS data converted using the CAPS-IBS instrument response model.

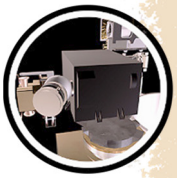

The Cassini INMS measures positive ions with masses up to 100 u. The CAPS-IBS can be used to measure positive ions with much larger masses at lower resolution. The CAPS-IBS measures the energy per charge of incident ions with an energy resolution of 1.4% [Young et al. 2004]. The energy per charge spectrum can be converted to a mass per charge spectrum by fitting the CAPS-IBS and INMS measurements using the spacecraft potential, ion temperature, and crosstrack winds as free parameters [Crary et al. 2009]. The high mass ion densities were found to increase exponentially with altitude down to the lowest observed Cassini altitudes [Crary et al. 2009]. An analysis of the chemical production mechanisms studied by Wilson et al. [2003] was compared to the peak spectrum, and it was found that the most likely compounds were aromatic in character. This further supports that aromatic chemistry is efficient in Titan's ionosphere, and that it is likely to proceed past benzene.

Westlake et al. [2014b] analyzed the T57 flyby in detail between the CAPS and INMS observations to determine the characteristics of the processes responsible for the production and loss of the large hydrocarbons observed at Titan. Altitude profiles (Figure INMS-12) of heavy ions

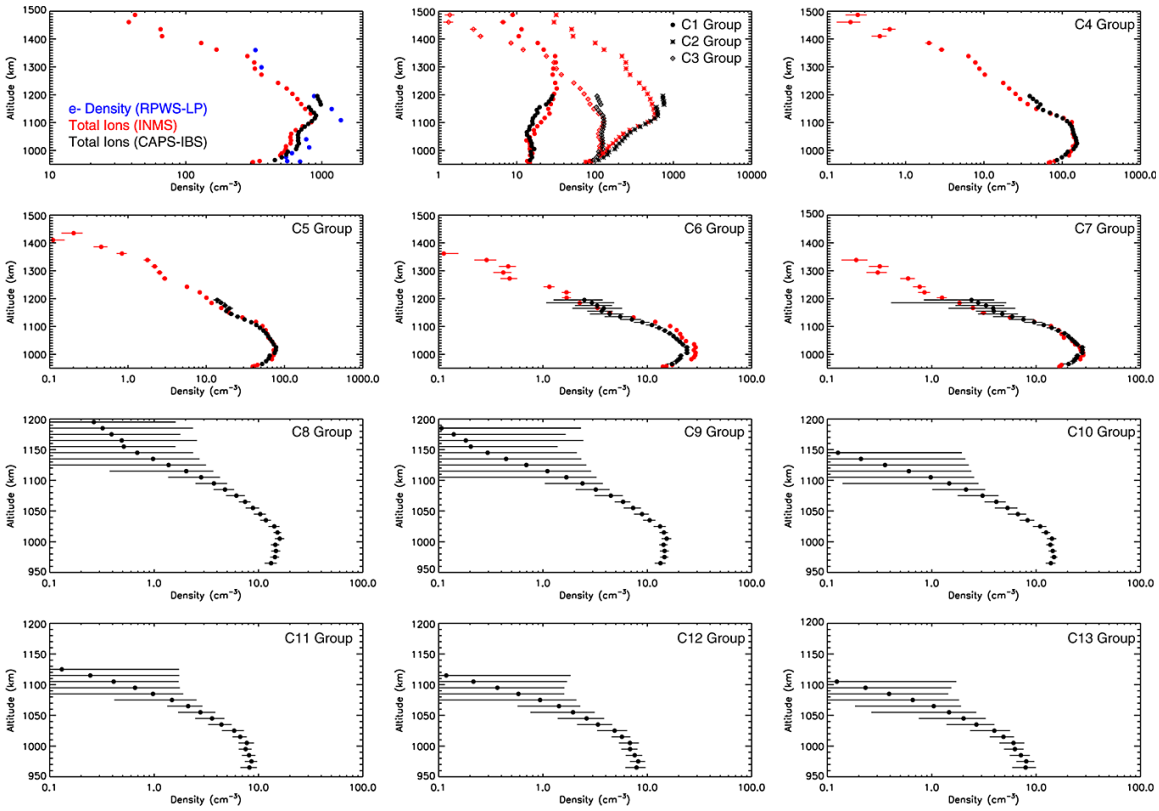

Figure INMS-12. Hydrocarbon group densities from the C1 to the C13 groups for the T57 flyby. A group density is simply the integrated density between the minima in the mass spectrum. The labeling using carbon number (C_i) indicates the number of heavy atoms (carbon, nitrogen, oxygen, etc.) expected within this mass grouping. The *black points* represent CAPS-IBS data, the *red points* give the INMS data, and the *blue points* give the RPWS-LP total electron density. The CAPS-IBS data are both summed within carbon groups and 10 km height bins. The *error bars* in the CAPS-IBS and INMS data represent the statistical counting errors.

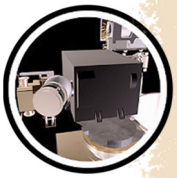

from the C6–C13 group (C_i indicates the number, i, of heavy atoms in the molecule) using a CAPS-IBS/INMS cross calibration reveal structure that indicates a region of initial formation and growth at altitudes below 1200 km followed by a stagnation and dropoff at the lowest altitudes (1050 km). Westlake et al. [2014b] suggested that an ion-molecule reaction pathway could be responsible for the production of the heavy ions, namely reactions that utilize abundant building blocks such as C_2H_2 and C_2H_4, which have been shown to be energetically favorable and that have already been identified as ion growth patterns for the lighter ions detected by the INMS. This growth scenario, in contrast with alternative growth scenarios, has implications for the densities of the source heavy neutrals in each scenario. Westlake et al. (2014b) showed that the high-mass ion density profiles are consistent with ion-molecule reactions as the primary mechanism for large ion growth and derived a production rate for benzene from electron recombination of $C_6H_7^+$ of 2.4×10^{-16} g cm^{-2} s^{-1} and a total production rate for large molecules of 7.1×10^{-16} g cm^{-2} s^{-1}.

Magnetosphere – Titan Interactions Science

The INMS and other Cassini instruments including RPWS, Magnetospheric Imaging Instrument (MIMI), CAPS, and Magnetometer (MAG) provided data, that with associated modeling (including global magneto-hydrodynamic (MHD) and hybrid models) has increased our understanding of Titan's plasma interaction with Saturn's magnetosphere and, rarely, with the solar wind plasma [Ledvina et al. 2012a, 2012b; Ulusen et al. 2010, 2012]. As alluded to earlier, the precipitation of energetic particles can lead to the ionization and heating of the neutral atmosphere. The pressure (thermal and magnetic) of the external plasma affects the dynamics [Cui et al. 2010; Cravens et al. 2010] and energetics [Richard et al. 2011; Vigren et al. 2013] of the ionosphere. Magnetic fields are induced in the ionosphere by this interaction, which then acts to help constrain and control the plasma motion. Put simply, plasma flows in response to magnetic forces and thermal pressure forces. INMS data contributed to our understanding of these processes. For example, INMS measurements show that chemically complex species (e.g., $HCNH^+$) flow out the wake (i.e., downstream of the external magnetospheric flow) of Titan eroding Titan's atmosphere [Westlake et al. 2012a, 2012b].

Data from the open source supra thermals mode from Titan showed ions escaping from Titan. In this mode, we tuned the quadrupole switching lens to look for ions with velocities above the spacecraft ram velocity. We fine-tuned these sweeps to look for ions of mass 2, 15, 16, 17, 28, 29, and 30 to characterize Titan's ion outflow and determine the actual velocity of these ions, looking for changes in their apparent temperature, understanding their spatial distribution, looking for acceleration mechanisms, and understanding the instrument response. We have included a Figure INMS-13 that shows these observations for several ions during the T100 flyby.

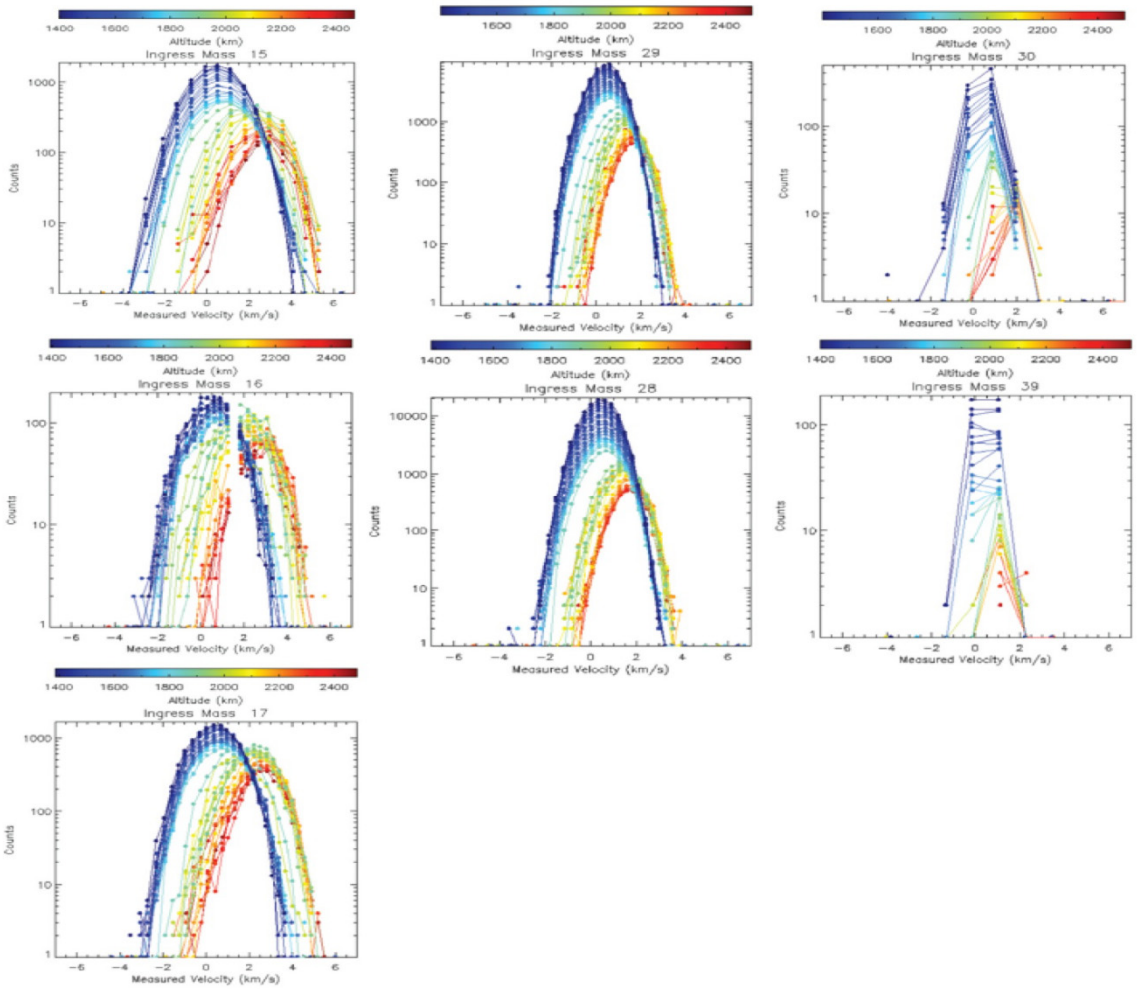

Figure INMS-13. INMS ion measurements from the T100 flyby.

Titan open questions

1. INMS discovered a new regime for organic chemistry in the solar system in Titan's upper atmosphere. Observations indicated the presence of large organic molecules with masses greater than 100 u. This could include biological precursors such as amino acids and nucleotide bases, but the mass range and resolution were insufficient for unique identifications. Thus, detailed knowledge of the organic composition, including the extent of nitrogen incorporation into the large organic molecules, and the associated chemistry remains an open question.

2. INMS found that the thermal structure of Titan's upper atmosphere was highly variable both in space and time. The mean temperature is ~150 K but pass-to-pass variability can be as large as 50 K and there may be long term trends. The variability has been poorly characterized and the cause of the variability has not been

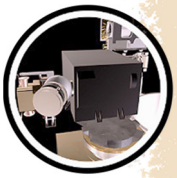

definitively identified. The high level of variability has stymied studies of the dynamics of Titan's upper atmosphere.

3. We have numerous examples of the effect of Titan's interaction with Saturn's magnetosphere on the structure of Titan's upper atmosphere, but insufficient data to thoroughly characterize the interaction.

    a. Why is there no Titan torus about Saturn?

    b. What is the energetic ion environment along Titan's orbit?

    c. How do the upstream plasma conditions affect Titan?

    d. What is the energy and momentum deposited into Titan's atmosphere as a result of the different bulk plasma conditions?

    e. What effect do the deposition of energetic ions have on Titan's atmosphere and its plasma interaction?

    f. How do the different upstream plasma conditions affect ion loss from Titan?

    g. How do the answers to these questions vary along Titan's orbit about Saturn?

    h. How does re-configurations of Saturn's magnetosphere effect Titan's plasma interaction?

    i. How does Titan respond to changes in the upstream conditions and how long does it take those changes to occur?

    j. What role do negative ions play in each of these situations?

4. INMS measured the structure of Titan's ionosphere but a factor of 2–3 disagreement between the observed and modeled electron densities has not yet been fully resolved. What explains the difference between the modeled ionospheric electron densities and the observed ionospheric electron densities? Is there a missing loss process? Are new recombination rates needed? Might ion transport be an answer?

5. There is evidence for both in situ ionization on the nightside of Titan and transport of ions from the dayside, but the relative contributions and characteristics of these two sources remain an open question.

6. How does the coupled neutral and ion dynamics in the ionosphere affect the magnetic structure that is observed? In fact, ionospheric dynamics at Titan was not well-described with Cassini data.

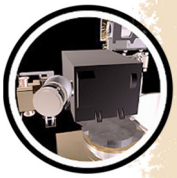

7. The variability of major gasses in the upper atmosphere as a response to solar input? Are there differing variations across species?

8. What are the large volatiles in Titan's upper atmosphere and how are they created?

    a. What is the extent of nitrogen in the larger organic compounds?

    b. What is the relative importance of day/night transport and in situ ion production on the nightside ionosphere?

    c. What is the role of day to night transfer in maintaining the ionosphere.

9. How does the system change with the solar cycle?

10. How does the system change throughout the Saturn year?

11. What are the boundary conditions at Titan? Is there a subsurface ocean and could it be detectable from the Cassini data?

12. What controls the magnetic field signatures below 1200 km? What role does the ionosphere and atmosphere play?

    a. How does the magnetic field topology around Titan and in its ionosphere effect ion and electron transport within Titan's ionosphere and linking them to Saturn's magnetosphere?

    b. What is the role of the Hall and Pederson conductivities in controlling Titan's ionospheric dynamo region? What role do the resulting ion and electron current have in heating Titan's ionosphere/atmosphere?

    c. What are the time constants of the remnant magnetic fields in Titan's ionosphere?

    d. How might atmospheric processes (such as gravity waves) effect Titan's ionosphere and its' resulting plasma interaction?

    e. What is the day to night ion transport rate in the ionosphere?

    f. How do the above processes affect the ion loss rate from Titan?

    g. What happens during morning energetic neutral atom (ENA) storms?

    h. Why is there no Titan torus about Saturn?

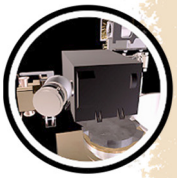

Enceladus Science

The initial INMS planning considered Enceladus as another small icy satellite albeit of some additional interest due to the fact that it was embedded in the E-ring. This perception soon changed. The Cassini MAG measurements on the first flyby of Enceladus redirected flyby E2 close to the satellite and thus began the important compositional exploration of Enceladus by INMS that culminated in a startling assessment that the internal global ocean was habitable; there was food for the microbes.

The first close flyby of Enceladus with a ram pointing orientation for INMS occurred on the July 14, 2005 when Cassini passed within 168.2 km of the flank of Enceladus. The presence of water vapor emanating from the south polar cap was noted over 4000 km before the encounter. Water, carbon dioxide, methane, and a mass 28 compound (carbon dioxide and molecular nitrogen were suggested) were observed during the flyby. Trace detections of ammonia, acetylene, and propane were noted. Figure INMS-14 shows a reproduction of the integrated mass spectra during the E2 flyby (~8 km/s relative velocity) taken from Waite et al. [2006], Figure 2.

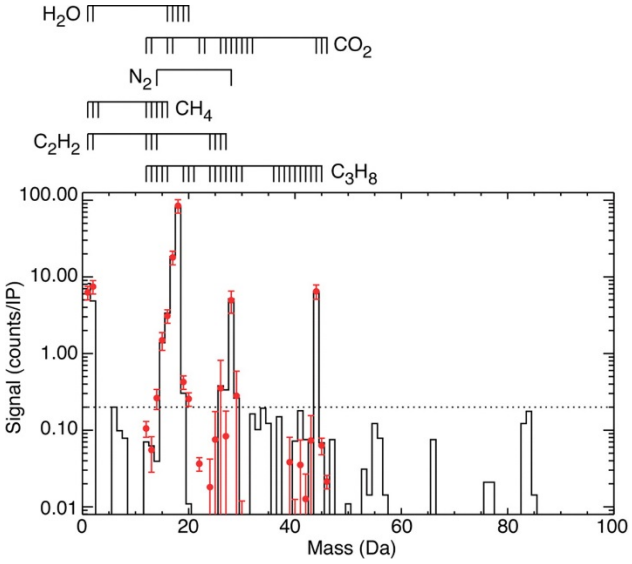

Figure INMS-14. Average mass spectrum for altitudes below 500 km. (Reproduced from Waite et al. [2006], Figure 2). The solid *black line* indicates the measured average spectrum and the *red symbols* represent the reconstructed spectrum. The *error bars* displayed are the larger of the 20% calibration uncertainty or the 1σ statistical uncertainty. The *dotted line* is indicative of the 1σ noise level. The dissociative ionization products produced by the electron ionization source for each constituent are also shown in the figure. Legend: Da = Daltons; IP = integration period.

Enceladus highlights

1. Determination of the major composition of the Enceladus plume gas.

2. Measurement of the deuterium/hydrogen ratio of water in the Enceladus plume.

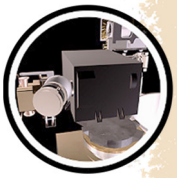

3. Discovery of organic molecules in the Enceladus plume. From fragmentation we know that there are large organic molecules.

4. Discovery of molecular hydrogen in the Enceladus plume.

5. Dynamics of the plume—speed of the gas measured with the open source and more evidence of it with the closed source. Also, angular structure told us about the dynamics. See very narrow jets that suggest that some jets have very high-Mach numbers.

6. Discovery of grains in an intermediate size range between CDA and CAPS.

7. The ion composition measured in Enceladus's plume by INMS confirms the strong interaction between the plume and the external Saturnian magnetosphere and was strongly dominated by H_3O^+.

Velocity-dependent mass spectra and impact fragments

The next major milestone occurred during the E5 flyby that occurred at a much higher relative velocity of ~18 km/s, approached from the Northern hemisphere and flyout along the south polar axis. This produced the highest signal to noise mass spectra of Enceladus of the entire mission due to the long outbound duration in the plume. The integrated mass spectra in Figure INMS-15 (reproduced from Waite et al. [2009], Figure 1) shows a much more complex spectrum extending out to the limits of the INMS mass range (99 u).

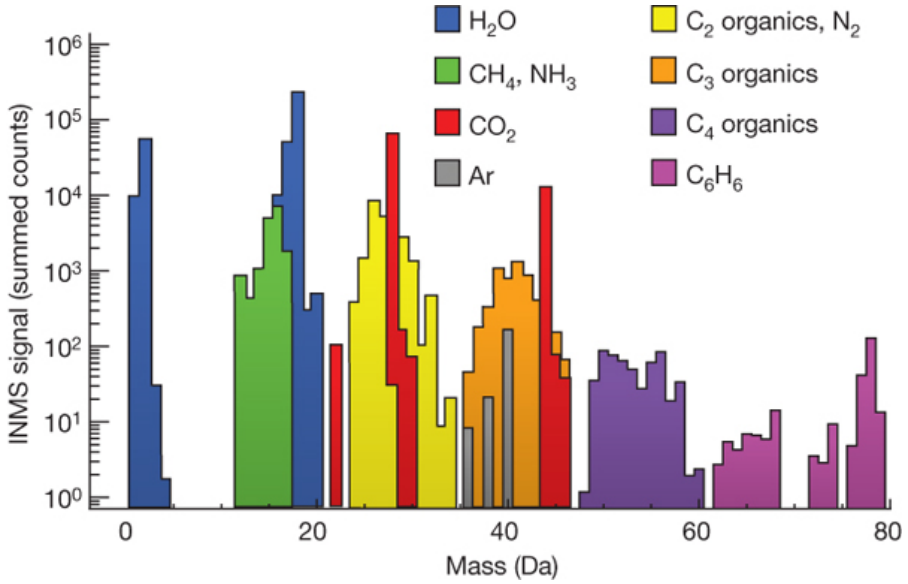

Figure INMS-15. A complex spectrum extending out to the limits of the INMS mass range (99 u). From Waite et al. [2009], Figure 1.

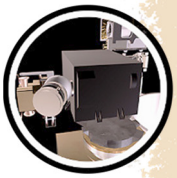

A mass deconvolution of the E5 integrated mass spectra is given in Table INMS-3 indicating a host of complex organic compounds, as well as, the compounds previously cited on flyby E2: water, carbon dioxide, methane, mass 28, ammonia, acetylene, and propane. Of particular note was that water seems to be converted into molecular hydrogen and some other compounds abundance altered due to the high flyby speed. This conversion was interpreted and later verified [Walker et al. 2015] as due to raw titanium vapor from ice grain impacts reacting with water to form TiO and TiO_2 and leaving behind the H_2. The serendipitous side effect of this reaction allowed the INMS team to determine the D/H ratio in water from Enceladus, which was found to be similar to comet Halley ($2.9\ (+1.5/-0.7) \times 10^{-4}$) suggesting that Enceladus had never come into chemical equilibrium with the protoplanetary nebula of Saturn otherwise the ratio would have been much closer to the protoplanetary value of 2×10^{-5}.

The first INMS measurements of the plume's composition were made in the plume's outer edge on July 15, 2005 (E2 encounter), and revealed that the plume consists predominantly of water vapor, with small amounts of carbon dioxide, methane, a species of mass 28, and trace quantities of acetylene and propane. During the October 9, 2008 (E5) encounter, favorable spacecraft pointing and the high spacecraft velocity relative to Enceladus significantly increased the neutral gas density in the closed source antechamber. This density enhancement, together with the proximity of the measurements to the center of the plume, enabled a considerably improved signal-to-noise ratio compared with that obtained during the earlier four encounters. (The y-axis shows counts summed over the period of plume influence.) With their higher signal-to-noise ratio, the E5 measurements provide the first clear evidence of the presence of higher-order (C_4^+) hydrocarbons in the plume, including benzene, and allow the tentative identification of individual species within each hydrocarbon group and of other organics, such as methanol and formaldehyde (Table INMS-3). As described in the Supplementary Information of Waite et al. [2009], interpretation of the INMS spectra requires careful deconvolution of a complex pattern of mass peaks representing both parent species and dissociative ionization products. Fractionation by energetic impact as well as interaction of the gas with the titanium antechamber walls must also be taken into account. Owing to the low mass resolution of INMS, overlapping mass peaks cannot in a number of cases be uniquely separated, resulting in some ambiguity in the interpretation of the data.

The mixing ratios shown for CO and H_2 (values in parenthesis) are included in the mixing ratios for H_2O and CO_2 (first two rows). Analysis of the data from all five encounters shows that the ratios of mass 44 (CO_2) to mass 28, and mass 18 (H_2O) to mass 2 (H_2) decrease with increasing spacecraft velocity, suggesting that H_2 and CO are produced by the dissociation of H_2O and CO_2 through hypervelocity impact on (and reaction with) the walls of the INMS antechamber, see supplementary information of Waite et al. [2009]. We estimate that 40–80% of the signal in mass channel 28 is due to CO produced in this way. A small contribution of CO from Enceladus is also possible, but cannot be distinguished from the dissociation product. The residual mass 28 signal is attributed to N_2, C_2H_4, or a combination of both, with either HCN or the ethene dissociation product C_2H_3 contributing to the signal in mass channel 27. The values given for these species are upper limits based on the two alternative scenarios (N_2 + HCN versus C_2H_4). Neither scenario can be given preference over the other on the basis of the present INMS data set.

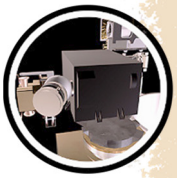

Table INMS-3. With higher signal-to-noise ratio, E5 measurements provide the first clear evidence of the presence of higher-order hydrocarbons in the plume, including benzene, and allow the tentative identification of individual species within each hydrocarbon group and of other organics. From Waite et al. [2009], Table 1.

Species	Volume Mixing Ratio
H_2O	0.90 ±0.01
CO_2	0.053 ±0.001
CO	(0.044)
H_2	(0.39)
H_2CO	$(3.1 \pm 1) \times 10^{-3}$
CH_3OH	$(1.5 \pm 0.6) \times 10^{-4}$
C_2H_4O	$< 7.0 \times 10^{-4}$
C_2H_6O	$< 3.0 \times 10^{-4}$
H_2S	$(2.1 \pm 1) \times 10^{-5}$
^{40}Ar	$(3.1 \pm 0.3) \times 10^{-4}$
NH_3	$(8.2 \pm 0.2) \times 10^{-3}$
N_2	< 0.011
HCN†	$< 7.4 \times 10^{-3}$
CH_4	$(9.1 \pm 0.5) \times 10^{-3}$
C_2H_2	$(3.3 \pm 2) \times 10^{-3}$
C_2H_4	< 0.012
C_2H_6	$< 1.7 \times 10^{-3}$
C_3H_4	$< 1.1 \times 10^{-4}$
C_3H_6	$(1.4 \pm 0.3) \times 10^{-3}$
C_3H_8	$< 1.4 \times 10^{-3}$
C_4H_2	$(3.7 \pm 0.8) \times 10^{-5}$
C_4H_4	$(1.5 \pm 0.6) \times 10^{-5}$
C_4H_6	$(5.7 \pm 3) \times 10^{-5}$
C_4H_8	$(2.3 \pm 0.3) \times 10^{-4}$
C_4H_{10}	$< 7.2 \times 10^{-4}$
C_5H_6	$< 2.7 \times 10^{-6}$
C_5H_{12}	$< 6.2 \times 10^{-5}$
C_6H_6	$(8.1 \pm 1) \times 10^{-5}$

Later, subsequent orbits at relative flyby velocities of < 8 km/s E14, E17, and E18 also helped establish that much of the organic content beyond the C_3 (> mass 40 u) were likely fragments of a heavier organic compound CDA identified in E-ring ice grains. This is the subject of a paper in Science [Postberg et al. 2018]. Figure INMS-16 shows the differences of the combined E14, E17, and E18 relative to the E5 spectra.

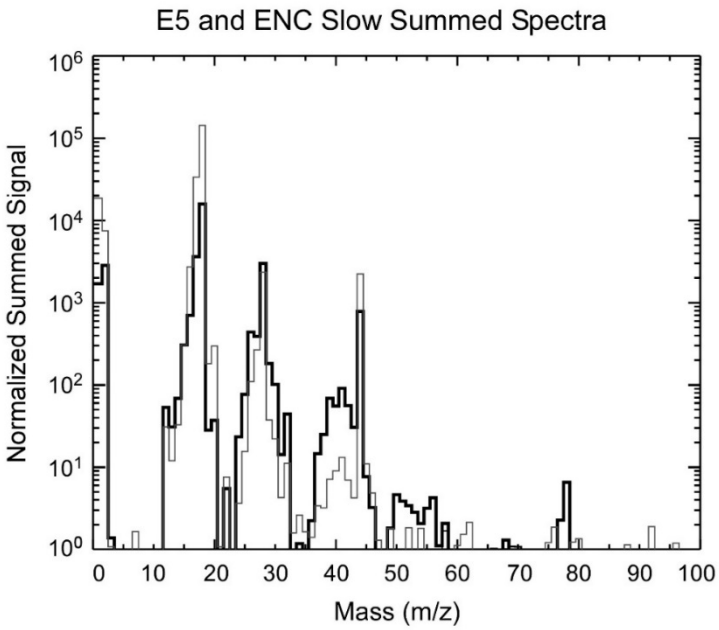

Figure INMS-16. The effects of impact fragmentation of organics within the ice grains and the effect of Titanium vapor on the water signal can be seen in this comparison mass spectra. The E5 spectra are the bold lines, and the summed E14, E17, and E18 spectra are the light lines. The normalization is performed by setting the spectra equal at mass 15 u.

The composition of plume vapor

The data obtained during the E14, E17, and E18 flybys all at relative flyby speeds of 7–8 km/s and all along or in parallel tracks near the Baghdad tiger stripe provide a consistent and repeatable depiction of the mass spectra at relative speeds low enough that fragmentation effects are minimized. These spectra are shown in Figure INMS-17. The spectra above 50 u (not shown) were near the noise level and further reinforce the point that the relative speeds above 8 km/s can lead to significant fragmentation of heavy organics buried in ice grains that complicate the interpretation of the mass spectra from E3 (~14 km/s) and E5 (~18 km/s). One can mass deconvolve the combined spectra from the slower flybys (E14, E17, and E18). The detailed analysis of this data set is the subject of Magee and Waite [2017]. A preliminary deconvolution is shown in Table INMS-4 taken from Magee and Waite [2017].

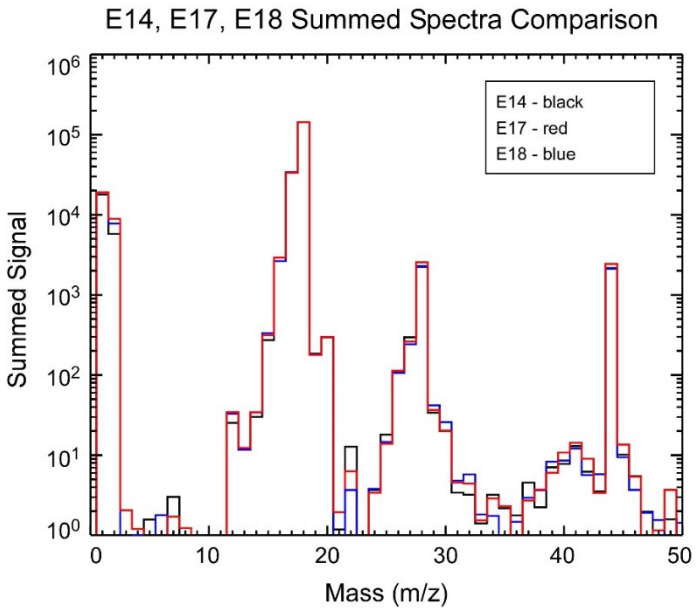

Figure INMS-17. Overlaid mass spectra for flybys E14, E17, and E18. Note the consistency of the spectra.

Table INMS-4. Preliminary mass deconvolution of mass spectra from E14, E17, and E18.

Minor Species I	Minor Species II				
Moderate Ambiguity	High Ambiguity				
< 0.2% and > 100 ppm	< 100 ppm				
	Hydrocarbons	**N-bearing**	**O-bearing**	**NO-bearing**	**Others**
C_2H_2 (26)	C_3H_4 (40)	CH_5N (31)	O_2 (32)	C_2H_7NO (61)	H_2S (34)
HCN (27)	C_3H_6 (42)	C_2H_3N (41)	CH_3OH (32)	$C_2H_5NO_2$ (75)	PH_3 (34)
C_2H_4 (28)	C_3H_8 (44)	C_2H_7N (45)	C_2H_2O (42)	$C_3H_7NO_2$ (89)	Ar (36, 38, 40)
CO (28)	C_4H_8 (56)	$C_2H_6N_2$ (58)	C_2H_4O (44)		C_3H_5Cl (76)
N_2 (28)	C_4H_{10} (58)	C_4H_9N (71)	C_2H_6O (46)		
C_2H_6 (30)	C_5H_{10} (70)	$C_4H_8N_2$ (84)	C_3H_6O (58)		
CH_2O (30)	C_5H_{12} (72)	$C_6H_{12}N_4$ (140)	C_3H_8O (60)		
NO (30)	C_8H_{18} (114)		$C_2H_4O_2$ (60)		
			$C_2H_6O_2$ (62)		
			$C_4H_{10}O$ (74)		
			$C_4H_6O_2$ (86)		

INMS measurement of ice-grain composition

Another serendipitous data product that INMS obtained from the Enceladus plume was a record of the ice grain composition. When an ice grain impacted the antechamber, a burst of material passed through the instrument creating a spike in the data [Perry et al. 2015; Teolis et al. 2010b]. Since

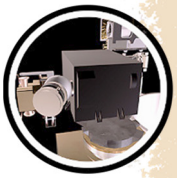

material flowed through the instrument in 2–3 milliseconds, these bursts occurred within one sampling period (i.e., one mass step), which had a dwell time of 31 milliseconds. Compiling the spikes from the E14, E17, and E18 data sets produces a mass spectrum of the portion of the ice grain material that does not chemically interact with the walls of the antechamber. This spectrum is shown in Figure INMS-18 (reproduced from Postberg et al. [2018], Figure 10).

The ice grain spectrum is related but distinct from the spectrum of the plume vapor. If present, C_2H_4 is limited to less than approximately 6% of the 28-u signal, and N_2 has an upper limit of approximately 10% due to the low signal at 14 u. This leaves a requirement for CO as the dominant species at 28 u, which matches well the signal at 12 u and 14 u (C^+ and CO^{++} dissociative peaks). Acetonitrile (C_2H_3N) also appears to be present. The signal pattern of 39–42 u suggests a species with its highest signal peak at 41 u and lower signal in the surrounding masses. C_2H_3N is the best candidate as it matches this stairstep pattern.

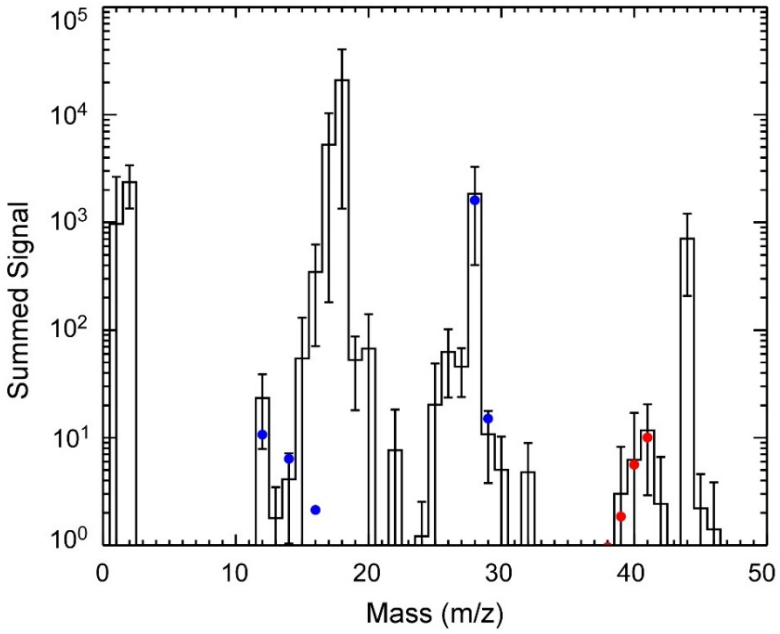

Figure INMS-18. Co-added INMS ice grain spike spectrum from three plume encounters. *Error bars* are derived from the dispersion of the count rate from the three encounters. The spectrum proves the presence of CO fragments (*blue circles*) as an oxygen bearing species: N_2 has very low abundance and contributes < ~10% of the 28 u signal. CO_2 and C_2H_4 collectively contribute < ~10% of the 28 u signal. CO (*blue circles*) is required to fit the rest of the 28 u signal and matches its other dissociative peaks well. The spectrum also indicates the presence of nitrogen bearing species: the stairstep pattern around 41 u matches best to the C_2H_3N spectrum (*red circles*). From Postberg et al. [2018], Figure 10.

Velocity of plume vapor

During four Enceladus encounters between November 2009 and October 2015, INMS operated in its seldom-used OSNB mode. In the OSNB mode, INMS makes direct measurement of the

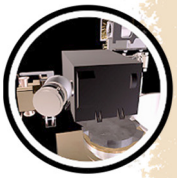

velocities of the neutrals. Although the velocity data from OSNB measurements are coarse, they provide strong constraints on the speed distribution of H_2O molecules within and surrounding the plumes.

In the OSNB mode, the velocity of the neutrals measured by INMS are determined by the angle of the INMS boresight, which sets the direction of the molecules, and the INMS compensation velocity parameter (V_{COMP}), which sets the speed of the molecules. The vector addition of this velocity with Cassini's velocity provides the neutrals' velocity relative to Enceladus. During E8, E11, and E16, V_{COMP} was fixed, but Cassini rotated so that INMS scanned the velocity of neutrals. (E21 operations were different: Cassini's attitude was fixed and V_{COMP} was scanned throughout the encounter to purposely sample the velocity distribution of the plume multiple times.) For each encounter, Cassini's rotation produced a single velocity scan, where the measured molecules had velocities that were radial from Enceladus with speeds increasing from 0 to 2 km/s. Figure INMS-19 shows the results of the velocity scan for E8. The fitted shape peaks at 1.25 km/s, but reduces to 1.1 ±0.2 after correction for INMS pointing calibration. The width of 300 m/s corresponds to a temperature of 65 K, which is similar to the low temperatures predicted by the models of Yeoh et al. [2015].

The ultimate velocity of adiabatic expansion for water at its triple point reflects the energy available per molecule of H_2O and is equivalent to 1.0 km/s, which is within the uncertainty of the measurement for the bulk velocity of E8. These results are reconciled with a previous higher-velocity estimate due to the modeling that shows the observed high-Mach jets have lower temperatures than previously assumed. INMS measured molecules leaving Enceladus at both high and low velocities.

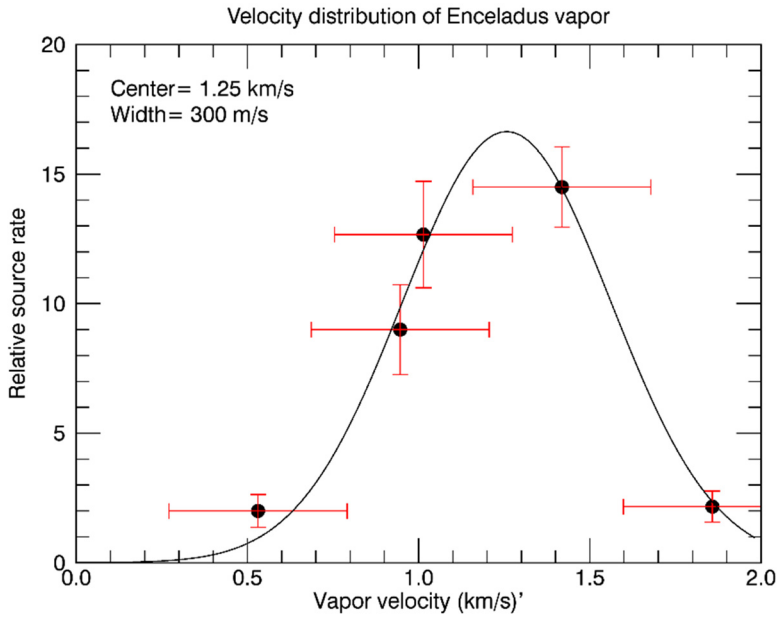

Figure INMS-19. Results of the E8 OSNB velocity scan. After adjustment for pointing calibration, the distribution peaks at ±0.2 km/s.

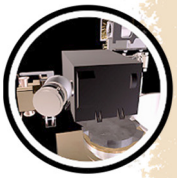

The measurements from the other OSNB encounters show a range of speeds that reflect the different environments surrounding Enceladus (Figure INMS-20).

- E8 had the highest velocities, and was sampling the strong jets.
- E11 velocities are slower and may represent the broader plume, outside of the dense, fast jets. E11 velocities are also consistent with early modeling of data from the higher-altitude encounters where the jets had merged with lower-velocity sources such as the tiger stripes, and the broad distribution of E11 may indicate a combination of multiple sources.
- E16 measured the neutral cloud that surrounds Enceladus and is fed by the plumes.

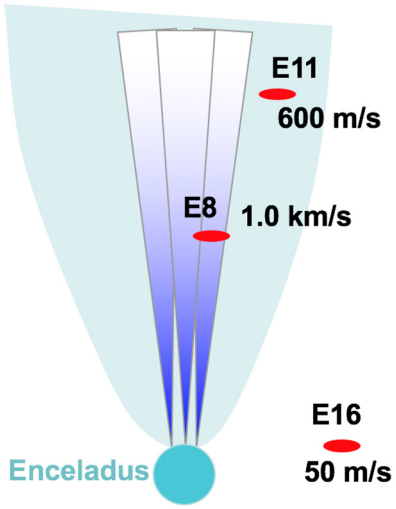

Figure INMS-20. The vertical speed of H_2O molecules measured during the E8, E11, and E16 encounters, showing several different velocity regimes.

The vapor-density structure of the Enceladus plumes

During six encounters between 2008 and 2013, the Cassini INMS made in situ measurements deep within the Enceladus plumes (Table INMS-5). Throughout each encounter, those measurements showed density variations that reflected the nature of the source, particularly of the high-velocity jets. Since the dominant constituent of the vapor, H_2O, interacted with the walls of the INMS inlet, changes in the external vapor density are tracked by using more-volatile species that responded promptly to those changes. To understand the plumes requires examination of each of the three components of Enceladus ejecta, fast and dense jets, slower diffuse gas, and ice grains.

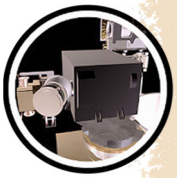

Table INMS-5. Information on the Enceladus encounters with the best INMS data. Perry et al. [2015] contains plume-structure data for the six un-shaded encounters. The last three encounters follow nearly identical trajectories but are offset several kilometers from each other.

Encounter	Features
E2	Relatively far from ejected vapor; minimal data useful for plume structure; first INMS identification of H_2O.
E3, E5	Steeply inclined, fast (14, 17 km/s) north-south trajectories, following the plume.
E7	Horizontal, slow pass (7 km/s) at 100 km min altitude, perpendicular to stripes, outbound from Saturn.
E8	Horizontal, slow pass south of Enceladus 1,200 km below the equatorial plane. Includes vapor velocity measurements from OSNB data. Minimal closed source neutral (CSN) data.
E14	Horizontal, slow pass at 100 km, high res, parallel to stripes, inbound to Saturn.
E17	Horizontal, slow pass at 75 km, high res, parallel to stripes, inbound to Saturn.
E18	Horizontal, slow pass at 75 km, high res, parallel to stripes, inbound to Saturn.

When INMS operated in the Closed Source Neutral (CSN) mode, Teolis et al. [2010b] described H_2O adsorption onto the walls of the INMS inlet system and the consequential delayed passage of H_2O through INMS. The delays can be tens of seconds to hours, depending on the amount of water already adsorbed onto the walls, and measurements of H_2O do not represent the conditions at the time and location of the measurement. Molecules with higher volatility respond to external flux in a tenth of an IP, 34 milliseconds, the temporal resolution of INMS [Waite et al. 2004], and these volatile gases (referred to as volatiles) are used to track changes in density.

The ice grains entering the INMS aperture add complexity and uncertainty to the physical interpretation of the data because the grains modified the INMS measurements. On entering the CSN aperture, an ice grain causes a high count or spike for a single measurement. The larger grains cause spikes that mask the gas density, confuse interpretation of INMS measurements, and add uncertainty. Since the resident time for volatiles in the INMS CSN inlet system is 2−3 milliseconds, the grain usually affects the measurement of only one IP.

The size of ice grains spans a range from molecular clusters to several microns in radius [Spahn et al. 2006; Jones et al. 2009; Coates et al. 2010]. Only grains that cause count rates much larger than the neighboring measurements can be clearly identified, and these were removed from the vapor-density data. Slightly smaller grains can cause two types of ambiguity in the INMS measurement: small spikes may be misinterpreted as local increases in vapor density, and rapid density variations may be misinterpreted as grain spikes. Grains that are still smaller cannot individually cause a noticeable change in count rate, but nanometer-scale grains are so plentiful that many enter the INMS aperture during a single IP, and these combine to create a background. Figure INMS-21 shows an example of INMS data with ice-grains spikes removed.

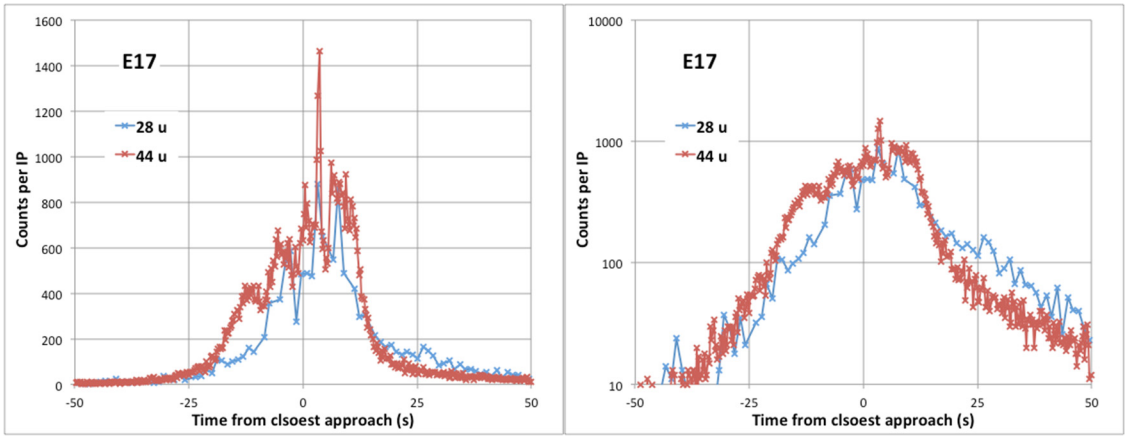

Figure INMS-21. Linear and log-plot profiles for the E17 Enceladus encounters. (Perry et al. [2015] has the profiles for all Enceladus encounters before 2016 with structure data.) The plots contain count rates for species with masses of 28 u and 44 u. Measurements that were clearly affected by ice grains have been removed.

For molecules emitted at the same supersonic velocity and in thermal equilibrium with each other at the time they are emitted, the cone angle or spreading of the molecules depends on mass (Figure INMS-22). This behavior causes differences in spatial composition that are measured by INMS and are independent of variations in source composition. Depending on the temperature, bulk velocity and mass, spreading angles vary from 10 to 45 degrees for Mach numbers from 1 to higher than 5, see Teolis et al. [2017].

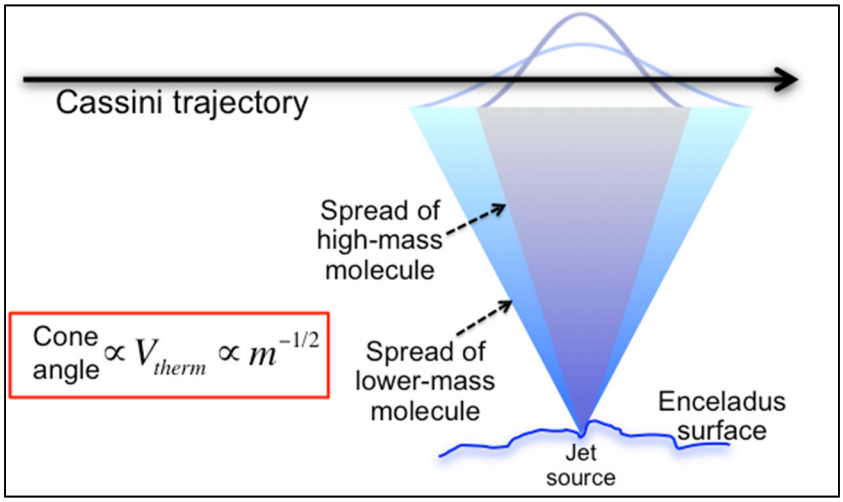

Figure INMS-22. Illustration of the mass-dependent behavior of high-velocity molecules emitted by the jets.

Based on ground [Waite et al. 2004] and flight calibration at Titan [Teolis et al. 2015], each INMS count during E7, E14, E17, and E18, corresponds to 2,100 molecules/cm^3 for the 28 u mass channel and 1,500 molecules/cm^3 for the 44 u channel (25% uncertainty). For E3 and E5, which had higher velocities, the calibration factors are 890 and 660 molecules/cm^3 for 28 u and 44 u

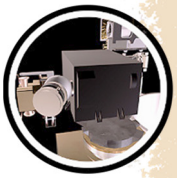

channels, respectively. Since high-velocity fragmentation products of molecules with masses greater than 100 u increase the counts of lower masses, E3 and E5 counts are higher than they would be without the added molecular fragments. Consequently, the actual 28 u and 44 u densities for E3 and E5 are a factor of two-to-five lower than the values based on the calibration factor provided for E7, E14, E17, and E18 [Teolis et al. 2015].

In lieu of modeling each individual molecule separately to account for mass-dependent behavior, the total-count ratios between the 18 u mass channel and the volatile masses provide an approximate density for H_2O. For the later, lower-velocity encounters, the total counts summed over the flyby for the 28 u and 44 u channels were each 0.5 % to 1% of the total 18 u counts after adjusting for the higher measurement frequency of the 44 u channel. At the high velocity of E3 and E5, larger molecules dissociate on impact with the INMS inlet, modifying the measurements for lower masses. This increased the counts for the measured volatiles and the ratio to water counts increased to 2–5% for each species [Teolis et al. 2015].

The vapor plumes show variability that was first reported by Hedman et al. [2013]. A comparison of data from the last three encounters, E14, E17, and E18, are consistent with the Visual and Infrared Imaging Spectrometer (VIMS) observation of variability in jet production and a slower, more diffuse gas flux from the four sulci or tiger stripes. Teolis et al. [2017] used data from all INMS and Ultraviolet Imaging Spectrograph (UVIS) encounters to constrain a time-dependent and high-resolution model of the plumes.

Two-component and multi-component models of INMS plumes

During the final low-altitude flybys of Enceladus, the most abundant, non-sticky species in the plume, CO_2 at 44 u, was sampled at a higher rate, to enable higher-resolution measurements of local density variations along Cassini's trajectory, achieving resolution of 0.25 s temporal and 1.9 km spatial. As shown in Figure INMS-24, CO_2 data from E17 clearly resolved density variations, indicative of gas jets, along Cassini's trajectory. Hurley et al. [2015] suggested on the basis of Monte Carlo models (Figure INMS-23) that the plume source may be continuously distributed, albeit variable, along the tiger stripes. These models included one lower-velocity component for the tiger stripes and a second, higher-velocity component for the jets. The complete plume three-dimensional structure is difficult to uniquely constrain solely on the basis of the few INMS flybys as multiple combinations of jet pointing directions and intensities can fit the data, and temporal variability further increases the potential solutions.

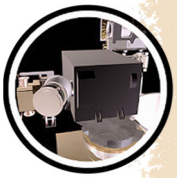

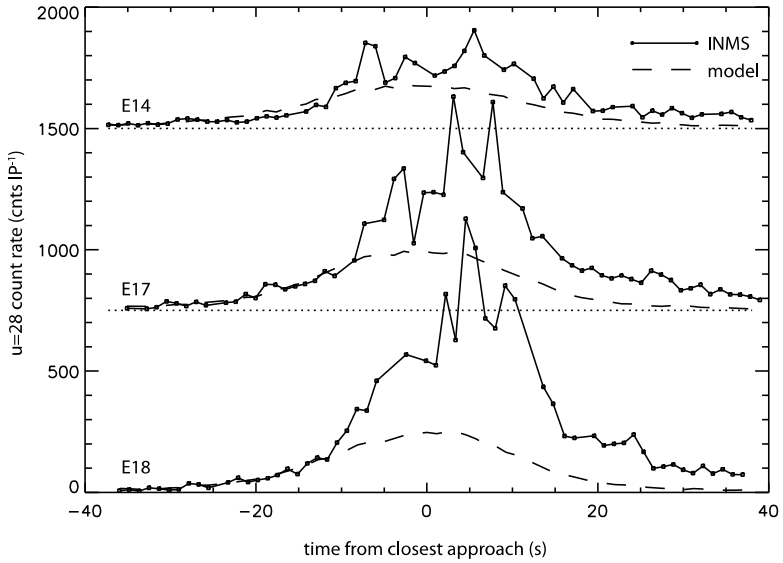

Figure INMS-23. Using the model described in Hurley et al. [2015], the *dashed lines* are simulated count rates with a continuous source along the tiger stripes as the only source of vapor. The temperature (270 K) and velocity (500 m/s) of the emitted tiger-stripe vapor were chosen to fit the rise and fall of the INMS data for mass 28 u. The best fit to the data is for E14, which occurred during a phase that corresponds to lower activity in the jets according to Hedman et al. [2013]. E17 and E18 occurred near Enceladus' apoapsis, when VIMS observed higher ice-grain emissions, and the higher, variable measurements in E17 and E18 may be due to more-active jets.

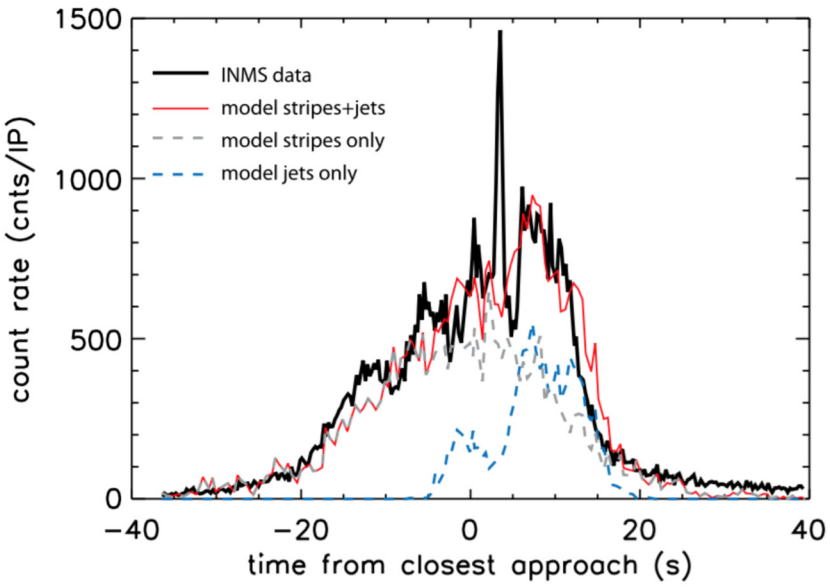

Figure INMS-24. INMS measurements of mass 44 u species during the E17 flyby are shown in *black*. Model [Hurley et al. 2015] predictions using constant emission along the tiger stripes at 500 m/s and 270 K (*gray dashed line*) are selected to match the rise and fall on the outskirts of the plume. The jet model using Mach 4 (1500 m/s and 270 K) are included (*blue dashed line*) to reproduce the overall enhancement near closest approach. The sum of the two models (*red line*) reproduces the overall structure of the plume, but misses some of the fine structure.

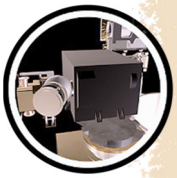

Alternate Enceladus plume structure

During Cassini's close (99, 74, 74 km) E14, E17 and E18 flybys through the Enceladus gas/dust plume on October 1, 2011, March 27, 2012, and April 14, 2012, the INMS measured in situ the detailed spatial structure of the neutral gas along the trajectories. These encounters were the first to fly close enough to the plume sources with the required pointing and sufficient data acquisition rate, to enable resolution of individual gas jets within the broad plume by INMS. During these flybys two INMS objectives were to: 1) constrain the locations, magnitudes and gas velocity from the plume surface sources, and 2) extrapolate the three-dimensional structure of the plume, including the diffuse plume and individual major jets. Since these flybys, the INMS team have carried out detailed plume modeling, combining the along-track densities measured at different times/dates by INMS, with and occultation, surface temperature, and imaging data from UVIS, Composite Infrared Spectrometer (CIRS) and ISS. The goals were to constrain the physics of the jet sources, i.e., the nozzle dimension and gas thermodynamic properties including temperature, density, flow and expansion rate, and provide necessary inputs for future modeling of the plume interaction with the Saturn system, i.e., the E-ring and magnetospheric sources and mass loading.

The results of our studies are now published in the papers by Perry et al. [2015] and Teolis et al. [2017]. Teolis et al. [2017] describes a detailed comparison of several plume source scenarios. The findings indicate that a time variable source, consisting of a source continuously (but non-uniformly) distributed along the tiger stripes, and sharp gas jets as inferred from ISS data [Porco et al. 2014], provide the best fit to the INMS and UVIS data. Figures INMS-26–INMS-30 compare the results of plume modeling for several different plume source models, considering both a curtain source with upward (normally) directed emission continuously distributed along the tiger stripes, and a source consisting of discrete gas jets with locations and pointing direction matching the grain jets identified by Porco et al. [2014] in ISS data.

In both the curtain and jet cases, the model suggests that a gas source with a Mach number distribution, containing a slow (with thermal velocity, Mach 0) isotropic emission, and a super-sonic (high velocity) component, was required to fit the broad distribution, and the fine structure, respectively, observed in the UVIS/INMS data. The fits use a 4-point Mach number distribution ranging from zero (gas at rest) to 16 (the fast component), as necessary to best fit the shapes of the features in the INMS and UVIS data. The curtain model considered three cases: 1) a uniform emission along the tiger stripes; 2) emission correlated to the tiger stripe temperature from CIRS data (Figure INMS-25); and 3) emission optimized to fit the INMS and UVIS data. For jets, the model considered two cases: 1) jets with equal intensities; and 2) jet intensity optimized to fit the data. The optimized models typically give multiple solutions, corresponding to reductions/enhancements in different combinations of jets, or different vapor source distributions along the tiger stripes. Figures INMS-26–INMS-30 show the averages over these solution families to compare and contrast the quality of the fits in the cases of continuous distributed emission and of discrete gas jets. It is clear on the basis of the plots, that neither the thermal plume cases, nor the cases of uniform curtains or jets, provide very good fits to the data. Both optimized curtains and jets yield rough agreement with the data but, as shown in the plots, some features of the data are better matched by the jets. The models could not fit all of the INMS and UVIS data simultaneously

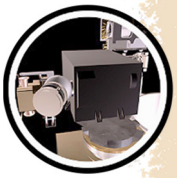

with a unique model solution. Therefore, given the curtain and [Porco et al. 2014], jets as a modeling constraint, an assumption of time variability of plume source distribution and/or individual jets between the Cassini flybys, is required to fit the data. The changes over time of the individual jets appears to be chaotic, exhibiting no obvious correlation to the Enceladus mean anomaly, as seen (for the plume as a whole) in VIMS data [Hedman et al. 2013].

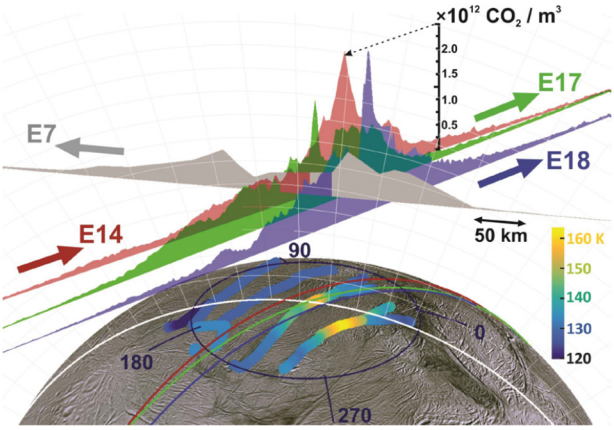

Figure INMS-25. Emission correlated to the tiger stripe temperature from CIRS data. To scale 3-D representation of the E14, E17, E18, and also (lower resolution) E7 INMS data with vertical areas representing (in linear scale) the density, and the flat base of the areas corresponding to the Cassini trajectories. Lines across the surface are the ground tracks. The Tiger stripes are colored according to the temperature estimated by CIRS. Figure from Teolis et al. [2017].

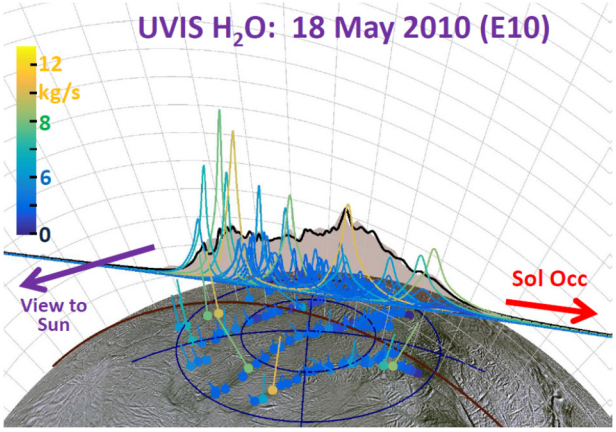

Figure INMS-26. Results of plume modeling. To scale 3-D representation of the 2010 Enceladus plume UVIS Solar Occultation with vertical areas representing (in linear scale) the occulted intensity fraction (corresponding to the water vapor column density), and the flat base of the area corresponding to the line of minimum ray height (*brown line* on surface is the ground track of this ray). For example, Cassini's viewpoint onto the plume is from the upper right of the figure, and UVIS is scanned from left to right as shown by the *arrow*. *Dots on surface:* [Porco et al. 2014] jet source locations, with *straight lines* showing jet directions. The colors and jet line lengths are given by the optimized jet strength; i.e., *orange* (*blue*), long (short) jets represent high (low) intensity jets. Colored curves: line height from min ray height line gives the estimated column density profile of each jet along the UVIS line of sight. *Black curve:* the best fit total column density of all jets across the UVIS line of sight: the colored curves sum to yield the *black curve*. Figure from Teolis et al. [2017].

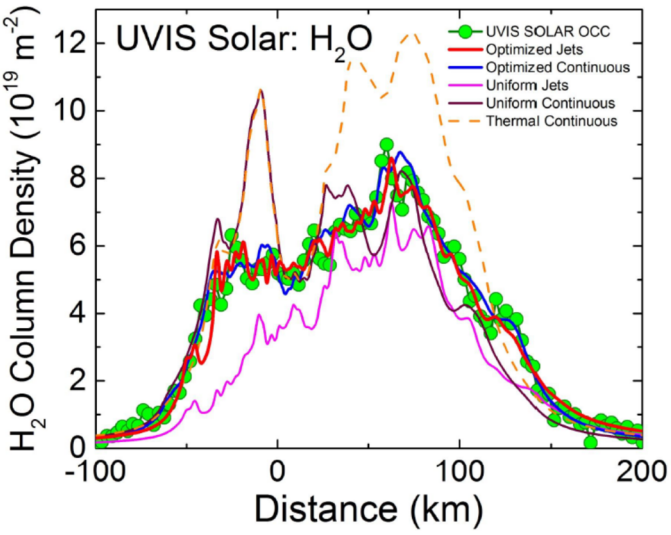

Figure INMS-27. Results of plume modeling. Enceladus plume water vapor column density measurement from the UVIS 2010 solar occultation (*Green circles*), plotted versus distance across the plume along the occultation line of sight minimum ray height. *Red line:* Average model solution for the optimized [Porco et al. 2014] jets. *Blue line:* Average solution for continuous emission along the tiger stripes. *Magenta line:* Jets with equal intensity. *Brown line:* Uniformly distributed continuous emission along the tiger stripes. *Orange dashed line:* Continuous emission with emission strength dependent on tiger stripe temperature (proportional in this example to Tn, with n = 7). Figure from Teolis et al. [2017].

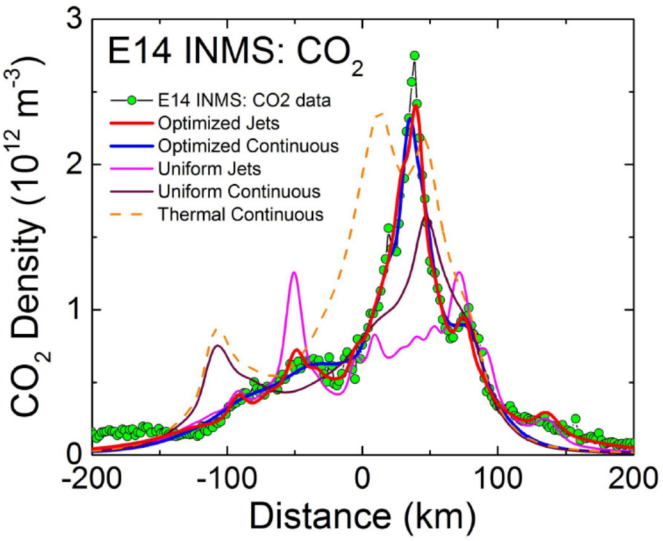

Figure INMS-28. Results of plume modeling. INMS CO_2 density measurement (*Green circles*) along the E14 flyby trajectory showing structure in the plume density along trajectory. *Red line:* Average model solution for the optimized (Porco et al., 2014) jets. *Blue line:* Average solution for continuous emission along the tiger stripes. *Magenta line:* Jets with equal intensity. *Brown line:* Uniformly distributed continuous emission along the tiger stripes. *Orange dashed ine:* Continuous emission with emission strength dependent on tiger stripe temperature. Figure from Teolis et al. (2017).

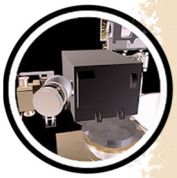

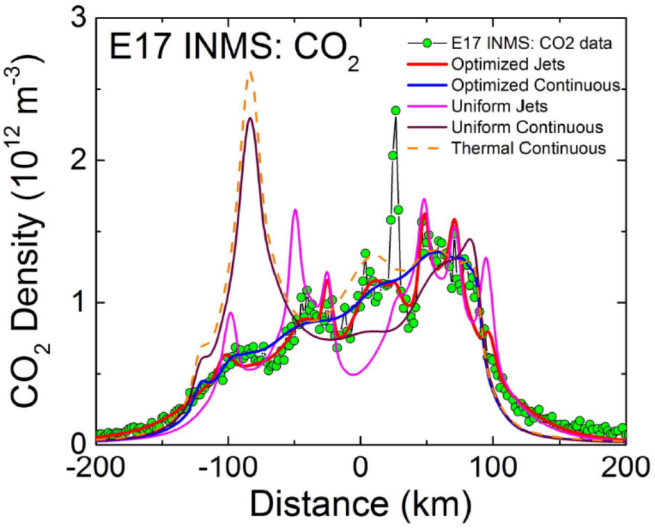

Figure INMS-29. Results of plume modeling. Same as Figure INMS-28 for the E17 flyby. Figure from Teolis et al. [2017].

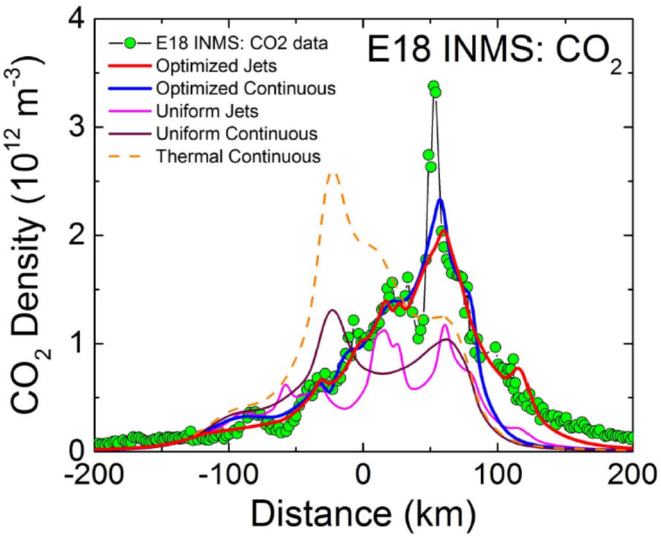

Figure INMS-30. Results of plume modeling. Same as Figures INMS-28 and INMS-29 for the E18 flyby. Figure from Teolis et al. [2017].

Confirmation of H_2 in the plume vapor and hydrothermal activity

Finally, one of the most important findings of the Cassini mission by INMS was the open source detection of molecular hydrogen within the plume. Previous observations by the closed source had indicated the presence of molecular hydrogen, but were fraught with ambiguity due to the unearthing of fresh titanium from the walls of the antechamber from ice grain impacts as noted in the E5 discussion in the section entitled Velocity-Dependent Mass Spectra and Impact Fragments. E21 used the open source to measure molecular hydrogen and then after a lengthy and careful

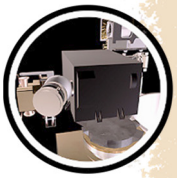

study of the instrumental background this result was verified and published in Science [Waite et al. 2017]. Figure INMS-31 data (reproduced from Waite et al. [2017], Figure 2) indicates a two sigma detection of molecular hydrogen in the plume and an indication of the other important minor constituents, see Table INMS-6 (reproduced from Waite et al. [2017] Table1). The important implications of this measurement are shown in Figure INMS-32 (reproduced from Waite et al. [2017], Figure 4), which illustrates that a positive chemical affinity for the reaction that represents methanogenesis in Earth's ocean can be shown to be present on Enceladus. This constitutes evidence that food for microbes is present Enceladus' ocean, the crowning achievement for demonstrating habitability at Enceladus.

Comparison of OSNB measurements of mass 2 (H_2) with the estimated total mass 2 instrumental background

The detected count rates and estimated background rates are plotted (Figure INMS-31) as a function of time from closest approach to Enceladus. The bottom panel of the plot is on a linear scale showing all the data points at or below ten counts. The top panel, plotted on the common log scale, shows the remaining data points that are above ten counts. Data points are color-coded according to the statistical uncertainties and background estimation: **open black circles** - no distinguishable separation from the background signal; **light blue circles** - at least one sigma separation; **dark blue diamonds** - at least two sigma separation; **purple triangles** - at least three sigma separation.

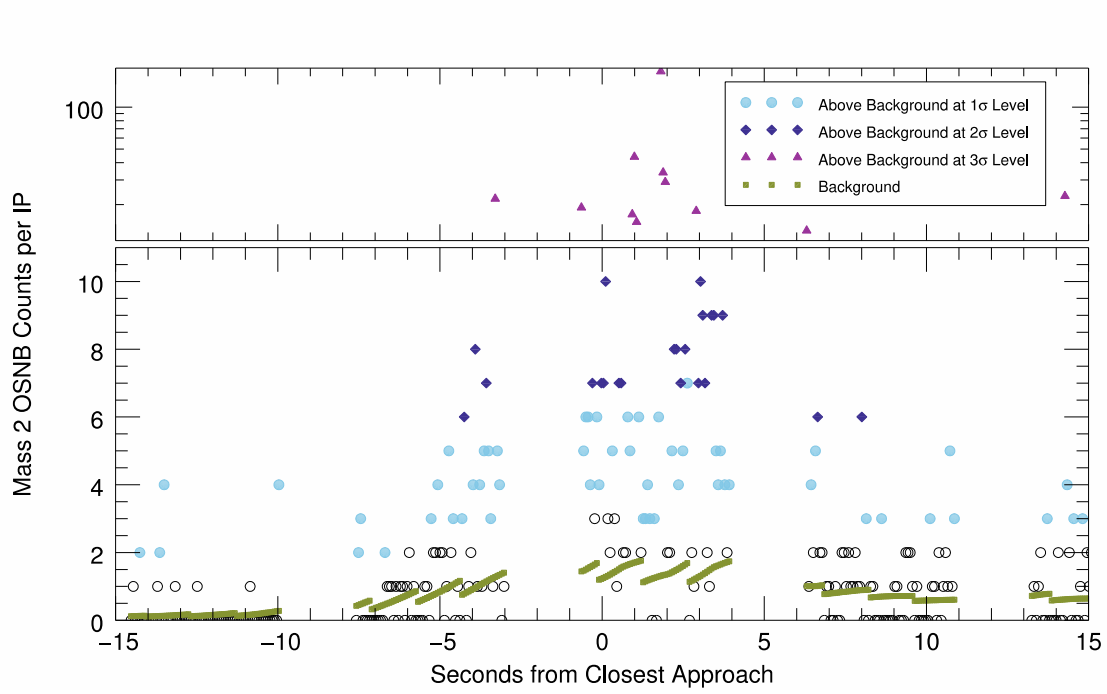

Figure INMS-31. Detection of molecular hydrogen in the plume. Figure from Waite et al. [2017].

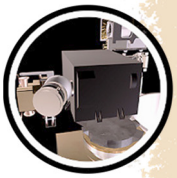

Table INMS-6. Other important minor constituents. Table from Waite et al. [2017]*.

Constituent	Mixing Ratio (%)
H_2O	96 to 99
CO_2	0.3 to 0.8
CH_4	0.1 to 0.3
NH_3	0.4 to 1.3
H_2	0.4 to 1.4

* Waite et al. [2017], Table 1. The major species composition of Enceladus' plume gas. Volume mixing ratios are derived from Cassini INMS measurements—supplementary materials [20], sections 2.4 and 3.2.

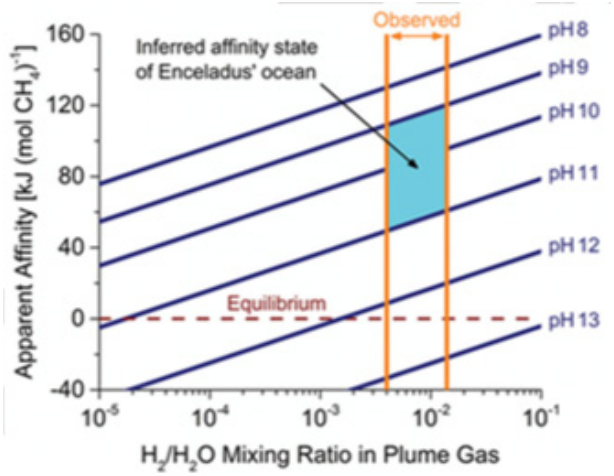

Figure INMS-32. A positive chemical affinity for the reaction that represents methanogenesis in Earth's ocean can be shown to be present on Enceladus. (Reproduced from Waite et al. [2017] Figure 4.) Apparent chemical affinity for hydrogenotrophic methanogenesis in Enceladus' ocean (273 K, 1 bar). The *orange lines* bracket the observed range in the mixing ratio of H_2 in the plume gas (Waite et al. [2017], Table 1). The *blue lines* are contours of constant ocean pH, a key model parameter. The *cyan region* indicates affinities for a pH range that may provide the greatest consistency between the results of (13, 15, 25). The *dashed red line* designates chemical equilibrium, where no energy would be available from methanogenesis. These nominal model results are based on CH_4/CO_2 = 0.4 (Waite et al. [2017], Table 1), a chlorinity of 0.1 molal, and 0.03 molal total dissolved carbonate (*25*). Reported ranges in these parameters propagate to give an uncertainty in the computed affinities of ~10 kJ (mol CH_4)$^{-1}$.

Detection of a plume ionosphere by INMS

As will be discussed later, the INMS (and CAPS) measured plasma in the Enceladus torus that mainly consisted of H_2O^+, OH^+, and O^+. In addition to closed source measurements of neutrals, INMS during the E3 flyby of Enceladus also made measurements in its open source ion mode [Cravens et al. 2009c]. The mass spectrum primarily showed a species with a mass of 19 u, and localized to the region of the neutral plume. Almost no signal at mass 18 was detected. Mass 19 corresponds to H_3O^+. We interpret the INMS measurements of cold H_3O^+ ions and the almost complete absence of cold H_2O^+ ions as being a consequence of ion-neutral chemistry taking place

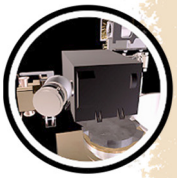

in a plume "ionosphere" where the H_3O^+ is produced by reaction of H_2O^+ ions (incident from outside or locally from phototionization of water) with H_2O [Sakai et al. 2016].

Enceladus Open Questions

1. Extremely narrow vapor jets with Mach numbers as high as ten were sampled by INMS along Cassini's E14, E17 and E18 trajectories. What is the temperature and speed of the gas in the jets?

2. Drastic stochastic time variability in the vapor jets detected by INMS between Cassini's plume traversals. How does the time variability relate to subsurface tidal stresses and fluid flow in the tiger stripes?

3. What chemistry produces a mass 28 species in the closed source of INMS?

4. What is the isotopic composition of non-water plume gases?

5. Are there noble gases in the plume?

6. Is the methane detected by INMS abiotic or biotic in origin?

7. What is the relationship between plume gas abundances and the concentrations of dissolved species in Enceladus's ocean?

8. What is the composition of those large organics that are outside the mass range of the instrument?

Icy Satellite Science

INMS results provide essential clues regarding the origin of O_2 and CO_2 at Dione and Rhea, and invaluable insight into the physics of icy satellite exospheres generally.

A major original objective of the Cassini mission, and of the INMS in particular, was to measure the abundance and composition of atmospheric gases around Saturn's large icy moons. Unlike Enceladus, which has insufficient gravity to retain an appreciable bound exosphere, sputtered and/or cryovolcanic emissions from Saturn's other large airless moons may fall back to their surfaces, and more volatile molecules can accumulate in the exosphere, adsorbing and desorbing to and from the surface many times before escaping to space. The ability of INMS to capture and analyze exospheric ions (with the OS) and/or neutrals (with the CS) is a strong function of Cassini's distance from these moons, with close flybys most likely to encounter detectable exospheric densities. Of Saturn's five large airless moons Mimas, Tethys, Dione, Rhea, and Iapetus, Cassini only flew close enough to

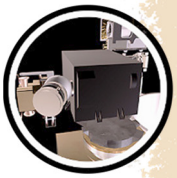

two, Dione and Rhea, to enable the detection of neutral O_2 and CO_2 exospheres by INMS at both moons (Figure INMS-33 and Figure INMS-34). INMS found evidence that the exospheres of Dione and Rhea exhibit complex structure, and observed drastic changes in the exosphere over time during the mission, as the Saturn system transitioned between equinox and solstice.

Owing to the diversity of multiple flyby dates and geometries (altitude, latitude, local time) the INMS was able to carry out exospheric density measurements over different geographic regions of Dione and Rhea, and at different flyby dates throughout the Saturnian year. The constraints provided by these INMS data, provide critical context and interpretation for the exospheric pickup ions detected by Cassini CAPS, and paint a highly detailed picture of the exospheric structure and time evolution. These data, together with high fidelity exospheric modeling, reveal highly seasonal exospheres at both Dione and Rhea, and inform interpretation of the exospheric measurements reported by Cassini's other instruments at these two moons [Simon et al. 2011; Tokar et al. 2012]. INMS results provide essential clues regarding the origin of O_2 and CO_2 at Dione and Rhea, and invaluable insight into the physics of icy satellite exospheres generally. For these reasons, INMS exploration of Saturn's large icy moons must be judged a spectacular success, meeting and in fact exceeding the original science objectives.

Icy satellites highlights

1. Discovery of oxygen and carbon dioxide exospheres at Dione and Rhea.
2. The exospheres change with time seasonally.
3. The exospheres have complex structure.
4. The measurements of the INMS place limits on the exospheric density that allowed aspects of the magnetometer data to be interpreted such that new types of current systems were discovered.

The Rhea and Dione flybys

Table INMS-7 summarizes Cassini's close flybys of Dione and Rhea, and the flybys for which INMS (and CAPS) had priority. At Rhea, Cassini carried out five major flybys ranging in speed from 6.8 to 9.3 km/s: the high altitude R1 and R1.5 flybys through the plasma wake, the low altitude R2 and R3 flybys approximately over the north and south poles, and the high altitude R4 flyby over the northern hemisphere. At Dione, five 6.5–9.0 km/s flybys were performed: the high altitude D1 flyby over the south, the high-altitude D2 flyby through the plasma wake, the low altitude D3 flyby near the dusk terminator, and the high altitude D4 and D5 flybys over the north. Cassini's traversal across the solar terminator, from night to day on all of the low altitude flybys (R2, R3, D3, see Figure INMS-33, Figure INMS-35, Figure INMS-36), was fortunate and essential, enabling INMS to detect the drastic differences of exospheric density between the night and day hemispheres. This constraint is key to the interpretation and understanding of the INMS data as discussed in the rest of this section.

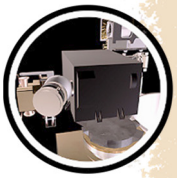

Table INMS-7. Dione and Rhea flyby observations.

Flyby	Body	Date	UTC	Speed	Alt	Detection	Species	References	Description
D1	Dione	11-Oct-05	17:52:00	9.12 km/s	500 km	MAG	-	Simon et al. 2011	Upstream southern flux tube, Saturn inbound.
R1	Rhea	26-Nov-05	22:37:38	7.28	500	CAPS	CO_2^+, O^-	Teolis et al. [2010a]; Teolis and Waite [2016]	Equatorial Wake, toward night side, Saturn inbound.
R1.5	Rhea	30-Aug-07	01:18:55	6.76	5725	CAPS	CO_2^+	Teolis and Waite [2016]	Northern Wake, toward night side, Saturn outbound.
R2	Rhea	2-Mar-10	17:40:36	8.58	100	INMS	O_2, CO_2	Teolis et al. [2010a]; Teolis and Waite [2016]	Low altitude, north polar, toward day side, Saturn inbound.
D2	Dione	7-Apr-10	05:16:11	8.34	500	CAPS	O_2^+	Tokar et al. [2012]	Equatorial Wake, toward day side, Saturn inbound.
R3	Rhea	11-Jan-11	04:53:25	8.05	72	INMS	O_2	Teolis and Waite [2016]	Low altitude, south polar, toward day side, Saturn outbound.
D3	Dione	12-Dec-11	09:39:23	8.73	99	INMS	O_2, CO_2	Teolis and Waite [2016]	Low altitude, equatorial wake, toward day side, Saturn outbound. CAPS offline.
R4	Rhea	9-Mar-13	18:17:26	9.29	996	-	None	Teolis and Waite [2016]	South-to-north, over anti-Saturn night side. CAPS offline. Altitude too high, and pointing poor, for INMS: Non-detection.
D4	Dione	16-Jun-15	20:11:52	7.32	516	INMS	O_2	Teolis and Waite [2016]	North polar, toward night side, Saturn outbound. CAPS offline.
D5	Dione	17-Aug-15	18:33:25	6.45	476	-	None	Teolis and Waite [2016]	North polar, toward night side, Saturn inbound. CAPS offline.

Detection of exospheric oxygen and carbon dioxide

Figure INMS-33 and Figure INMS-34 show the densities of exospheric O_2 and CO_2 at Rhea and Dione as they were measured by the INMS closed source along Cassini's flyby trajectories [Teolis et al. 2010a; Teolis and Waite 2016]. While O_2 is an expected product of sputtering, produced by radiolysis of highly abundant water ice on the surfaces of many icy satellites, the detection of exospheric CO_2 at a high relative abundance compared to O_2 was not expected.

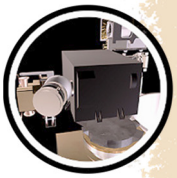

Before addressing the origin of CO_2, we first point to several other extraordinary aspects of these INMS data sets that are key to their interpretation:

- Exospheric densities, as measured during the R2, R3 and D3 flybys, were higher over the dayside than the night side (Figure INMS-33).
- The day-night asymmetry is in all cases far more pronounced for CO_2 than for O_2 (Figure INMS-33).
- Despite the lower altitude of the R3 flyby (minimum 72 km) relative to R2 (minimum 100 km), ten times less O_2, and no CO_2 was detected on R3 (Figure INMS-33).

The observation of higher exospheric densities over the daysides of Dione and Rhea is consistent with higher exospheric scale heights over that hemisphere, as exospheric gas interacts and thermally accommodates to the warmer dayside surface temperatures. However, the day-night exospheric asymmetry is far more pronounced for CO_2 than for O_2 at both Dione and Rhea (Figure INMS-33, Figure INMS-35, Figure INMS-36), suggesting that the less volatile CO_2 molecules may, unlike O_2, actually freeze out onto the night sides of both moons.

However, the detection of far less O_2, and non-detection of CO_2 at R3 was entirely unexpected at the time of the flyby, since the R3 trajectory was at a lower altitude than the previous R2 flyby. This raised the question of whether the drastically different O_2 and CO_2 densities between R2 and R3 were the result of exospheric spatial structure (a gas source in the north), or changes in the exospheric structure with time?

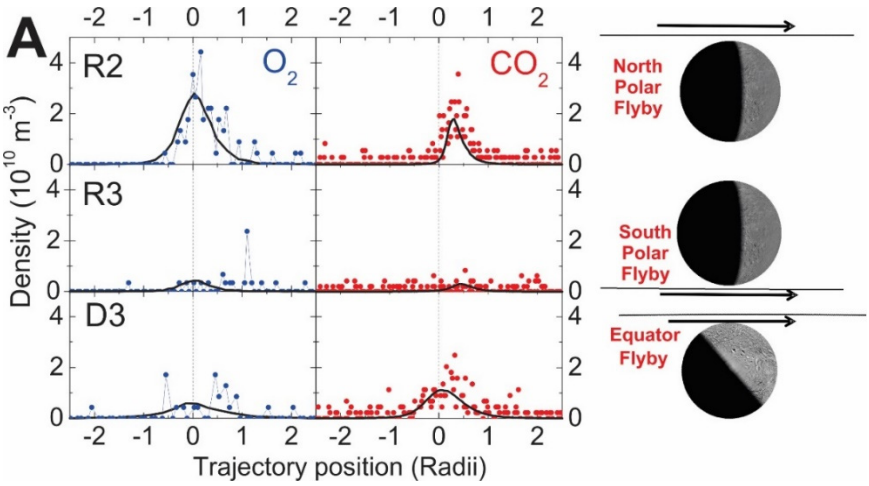

Figure INMS-33. Densities of exospheric O_2 and CO_2 at Rhea and Dione as they were measured by the INMS closed source along Cassini's flyby trajectories. The Dione and Rhea O_2 and CO_2 exospheric densities measured by Cassini INMS versus distance (in planetary radii) from closest approach (*dashed line*) along the night-to-day R2, R3 and D3 trajectories (*shown on right*). The data are un-binned, such that single counts are visible. Time increases left to right in the plots, with Cassini moving from the night to the dayside hemisphere on all flybys. As shown, the exospheric profiles are concentrated (especially for CO_2) over the dayside when equivalent inbound-outbound altitudes are compared. Lines: exosphere model results, see Figure INMS-35 and Figure INMS-36. Figure from Teolis and Waite [2016].

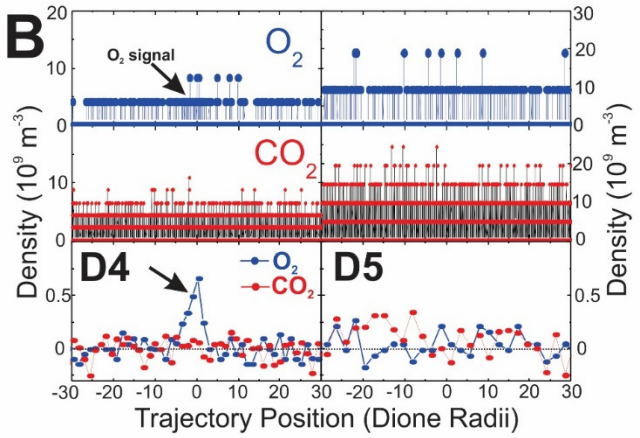

Figure INMS-34. Densities of exospheric O_2 and CO_2 at Rhea and Dione as they were measured by the INMS closed source along Cassini's flyby trajectories. Exospheric data (*top-center:* raw counts converted to density; *bottom:* binned/background subtracted) from the recent Dione northern high (516 km) altitude (day-to-night) D4 and D5 flybys, showing the detection of O_2 but not CO_2 at D4 and the non-detection of either species at D5. Time increases left to right with Cassini moving from the day to the night side hemisphere on both flybys. Figure from Teolis and Waite [2016].

Exospheric structure and seasons at Dione and Rhea

To address this puzzle Teolis et al. [2010a] and Teolis and Waite [2016] created a state-of-the-art icy satellite exospheric model code that specifically takes into account the effects of surface thermal accommodation and sticking observed by INMS. The model considers the rotation of Dione and Rhea, the variability of surface temperature between day and night, and the change in the solar declination with Saturn's seasons, which varies from between ±26.7 degrees over the 29.5 (Earth) year Saturn orbit. Molecules of O_2 and CO_2 are ejected into the simulated exosphere uniformly from all points on the surface to approximate a surface sputtered source, but can stick (transiently) to the night side and (for much longer periods) at the winter latitudes.

The exospheres of Dione and Rhea are, according to the models, highly seasonal with exospheric O_2 and CO_2 freezing onto the cold terrain in the winter latitudes, which remain in shadow drop as low as 20 Kelvin over the 14 year Saturn system winter [Howett et al. 2016]. However, with the approach of spring equinox the solar terminator advances across the polar terrain resulting in the rapid desorption of condensed gasses and a drastic ramp up of the exospheric gas density. In fact, the Rhea R2 flyby over the north occurred shortly after northern equinox and thus the exospheric O_2 and CO_2 were still desorbing from the northern terrain as previously shadowed areas were coming into sunlight. The main exospheric gas source was in the north at the time of the R2 and R3 flybys, due to desorption of condensed O_2 and CO_2 (built up over the prior winter) from that region. This can be seen in Figure INMS-35 and Figure INMS-36 where we plot the modeled exospheric CO_2 and O_2 densities at Rhea and compare predicted with measured densities along the R2 and R3 flyby trajectories. For CO_2 it can be seen (Figure INMS-35) that Rhea's exospheric gas density was higher over the north than the south according to the model, since CO_2 was

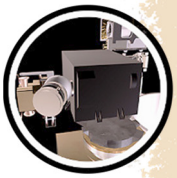

desorbing from the north at that time. This interpretation, shown in Figure INMS-35, successfully accounts for INMS non-detection of CO_2 on R3 in the south.

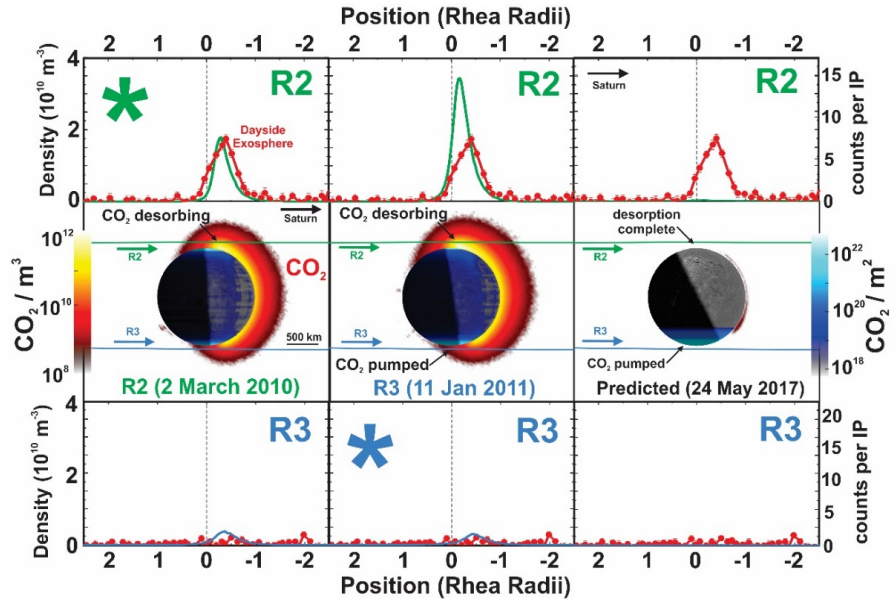

Figure INMS-35. Plot of the modeled exospheric CO_2 and O_2 densities at Rhea, and the comparison of predicted with measured densities along the R2 and R3 flyby trajectories. Rhea CO_2 exospheric model results, showing (*center row*) the surface solar illumination (dawn terminator as viewed over the equator), and predicted gas density cross-sections and surface frost column density at the R2 (*left*) and R3 (*center column*) flyby dates and times, and prediction (*right*) for the 2017 Saturn solstice. *Top*: comparison of the observed (*red points*, data binned) and predicted (*green line*) CO_2 densities versus position from closest approach along the R2 trajectory (x-axis, in Rhea radii, *dashed line:* closest approach). *Bottom*: same for the R3 flyby trajectory. *Asterisks* denote model-data comparisons with the same flyby date; all other plots show model projections to different dates. The model assumed a 3.7 × 10^{21} CO_2/s source rate as required to match the observed peak density on both flybys. The observation of CO_2 concentrated on the dayside is consistent with the modeled exospheric structure due to night side and polar cryopumping. CO_2 was desorbing from the north, and cryopumping onto the southern polar surface during the flybys. Accordingly, as anticipated by the model (*bottom center*), CO_2 was undetectable in the south on R3. As shown (*right*) exhaustion of the northern frost cap should result in the collapse of the CO_2 exosphere by the time of the 2017 solstice. Figure from Teolis and Waite [2016].

Surprisingly the O_2 data has a somewhat different interpretation than CO_2 according to the model, owing to the greater volatility of O_2 as compared to CO_2. The less volatile CO_2 (unlike O_2) is was beginning to freeze out onto the south polar terrain at the time of the R2 flyby according to the model, even before its desorption from the north had completed. For CO_2 (unlike O_2) the adsorption of exospheric gas onto one pole overlaps in time with its desorption from the opposite pole, meaning that CO_2 exhibited a more drastic difference of density between north and south at the time of the R2 and R3 flybys than O_2. Therefore, as can be seen in Figure INMS-36, the drop in O_2 between R2 and R3 is indicative of a rapid collapse of the entire exosphere in the ten months between R2 and R3. The exosphere's collapse occurs as all of the O_2 frozen onto the northern terrain is depleted, having fully desorbed off of the northern surface. The CO_2, being less volatile, takes longer to desorb from the north, and therefore CO_2 exosphere is predicted to have collapsed

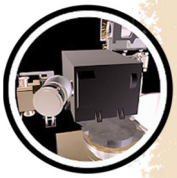

only after the R3 flyby took place. In this way exospheric O_2 and CO_2 desorb and re-freezing, moving from pole to pole every equinox, in a repeating seasonal cycle, leading to changing exospheric densities at Dione and Rhea that are minimal near Saturn's solstices and maximal near the its equinox's. The model of a seasonal exosphere not only accounts for the INMS data, but also the spatial distribution, composition, flux of pickup ions observed by CAPS discussed by Teolis and

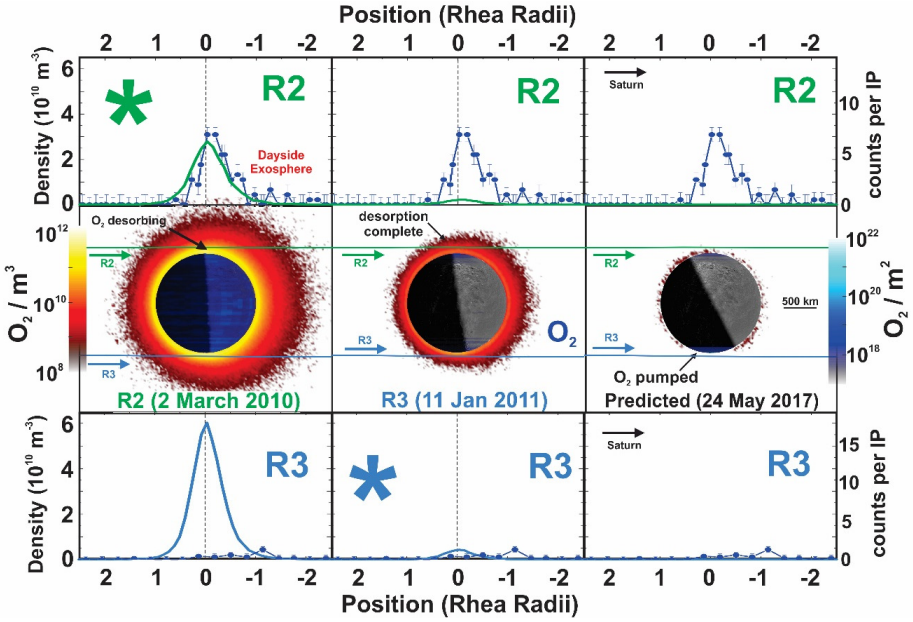

Figure INMS-36. Plot of the modeled exospheric CO_2 and O_2 densities at Rhea, and the comparison of predicted with measured densities along the R2 and R3 flyby trajectories. Rhea O_2 exospheric model results, showing (center row) the surface solar illumination (dawn terminator as viewed over the equator), and predicted gas density cross-sections and surface frost column density at the R2 (left) and R3 (center) flyby dates and times, and prediction (right) for the 2017 Saturn solstice. (Top) comparison of the observed (data binned) and predicted O_2 densities versus position from closest approach along the R2 trajectory (x-axis, in Rhea radii, dashed line: closest approach). (Bottom) same for the R3 flyby trajectory. Asterisks denote model-data comparisons with the same flyby date; all other plots show model projections to different dates. The model assumed a 7.2 × 10^{21} O_2/s source rate as required to match the observed peak density on both flybys. An O_2 tail is detected on the dayside, consistent with the anticipated greater dayside scale height. Unlike CO_2, the southern latitudes are not yet cold enough to cryopump O_2 from the southern exosphere on the R2 and R3 flybys dates. However, the modeled O_2 frost cap is exhausted between the R2 and R3 flybys, resulting in an anticipated collapse of the global exosphere, consistent with the reduced O_2 detection on R3. Figure from Teolis and Waite [2016].

Waite [2016]. CAPS observed 50% more CO_2^+ pickup ions during the distant 2007 R1.5 flyby than the 2005 R1 flyby, consistent with the expected ramp up of Rhea's exospheric CO_2 densities as the 2009 Saturn system equinox was approaching. See the publication by Teolis and Waite [2016] for a much more detailed description of these (and other) aspects of the analysis.

The source of O_2 and CO_2 at icy satellites

Another spectacular facet of these INMS data and models is that, together, they fully constrain the source rates O_2 and CO_2 to the exospheres of Dione and Rhea. Since both the exospheric density

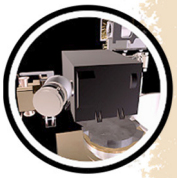

and ionization/escape rates are constrained by INMS and CAPS, the O_2 and CO_2 source rates can be directly estimated by fitting the exospheric model to obtain agreement with the INMS and CAPS data—as Teolis and Waite [2016] have done. These source rates can, in the case of O_2, be compared to known yields of sputtered radiolytic O_2 from water ice measured in the laboratory [Teolis et al. 2017a] to infer the composition and radiation chemistry of the surface material on Rhea and Dione subject to magnetospheric sputtering.

The results of this analysis are remarkable—the O_2 source rates at Dione and Rhea are lower, by approximately two orders of magnitude, than that expected from water ice subject to sputtering by Saturn's magnetospheric plasma [Thomsen et al. 2010]. Teolis and Waite [2016] concluded that, if pure water ice were present on their surfaces, Dione and Rhea ought to have two orders of magnitude more O_2 in their exospheres than observed.

A clue to this puzzle may be the high CO_2 abundance CO_2 (relative to O_2) in the exospheres of Dione and Rhea. Teolis and Waite [2016] proposed that preferential sputtering and removal of radiolytic volatile water products such as O_2 and H_2, and of H_2O itself, may enrich the topmost nanometers of surface material of these moons in carbonaceous sputter-resistant refractory material. As a result, the surfaces of surface regolith grains, composed in bulk of water ice and (likely) small amounts of carbon-bearing organic species, may be coated with a nanometer thick rind of radiolytically processed refractory material, for example, graphitic oxide, which is carbon-rich and yields small amounts of O_2 and CO_2 when sputtered. Recent composition analysis [Desai et al. 2018] of negative pickup ions detected by Cassini CAPS during the Rhea R1 flyby [Teolis et al. 2010] also supports the interpretation of a carbonaceous material on Rhea's surface ice. Thus, by constraining the source rates of O_2 and CO_2 to the exospheres of Dione and Rhea, the findings of Cassini INMS at these two Saturnian icy satellites have provided fundamental clues about the physics of surface sputtering and radiolysis, and of exospheric gas production, at icy bodies generally.

… the findings of Cassini INMS at these two Saturnian icy satellites have provided fundamental clues about the physics of surface sputtering and radiolysis, and of exospheric gas production, at icy bodies generally.

ICY SATELLITES OPEN QUESTIONS

1. O_2 and CO_2 exospheres at Rhea and Dione confirmed by INMS. Is CO_2, like O_2, a sputtered surface radiolysis product?

2. Exospheric seasonal variability, and complex spatial structure, in the exospheres of Dione and Rhea, suggests that diurnal and seasonal adsorption and desorption play a major role in exospheric structure and dynamics. What is the effect of regolith porosity on the exospheric gas adsorption, desorption and diffusion rates on the surfaces of Dione, Rhea, and other solar system icy satellites?

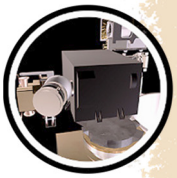

3. Lower than expected O_2 exospheric densities at Dione and Rhea O_2 suggest surface sputtering rates two orders of magnitude less than those measured from water ice in the laboratory. Do surface refractory impurities suppress sputtering from ice satellites, and do carbonaceous refractories contribute radiolytic CO_2 to their atmospheres?

4. Rhea's INMS-measured exospheric densities are insufficient to account for strong magnetic perturbations in Rhea's vicinity, leading to the conclusion that Cassini's Magnetometer measured two new electric current systems never before observed at a plasma absorbing planetary body. These are an Alfvenic current system generated by Rhea's plasma wake, and a thermo-electric flux-tube current system which maintains electric charge balance on Rhea's surface. How widespread are these newly discovered current systems at other plasma absorbing planetary bodies in the solar system?

Magnetosphere–icy satellite Interactions science

Saturn inner magnetosphere highlights

1. INMS measured the individual ions and determined the fractional abundance within the water group (O^+, H_2O^+, OH^+, H_3O^+) and derived those fractions relative to the various parameters (velocity phase space and distance from Saturn).

2. INMS measured neutral water and was able to derive an azimuthal distribution with respect to Enceladus via in situ measurements.

Current systems at Rhea

The constraints provided by INMS on the exospheric gas abundances at Dione and Rhea have been essential to the interpretation of the Magnetometer (MAG) readings from these two moons, resulting in the discovery of two previously unknown current systems at inert plasma absorbing planetary bodies. These discoveries a fantastic demonstration of the power of a diverse instrument payload; in this case Cassini’s INMS, CAPS and MAG; to reveal new and previously unknown fundamental physics operating in planetary systems.

MAG has been a powerful tool for the detection of exospheres in the Saturn system, having been in part responsible for the initial discovery of the Enceladus plume. Exospheric neutral gas disrupts the flow of Saturn’s co-rotating magnetosphere plasma by contributing new pickup ions to magnetosphere, generating electric currents and draped magnetic field perturbations, which can be measured by MAG to infer the presence of an exosphere. In addition to Enceladus, a major effort was made to detect the exospheres of Saturn’s other large icy satellites with the magnetometer, and to compare these data with the in situ measurements from CAPS and INMS. In fact, MAG did detect field-aligned currents at both Dione [Simon et al. 2011] and Rhea [Khurana

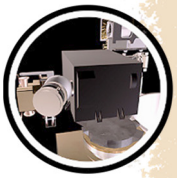

et al. 2017; Santolik et al. 2011; Simon et al. 2012] which appeared, initially, to be consistent with exospheres at these moons as found by INMS. Remarkably, after taking into consideration the rates of pickup ion generation and the electrical conductivity, it became clear that the exospheres measured by CAPS [Tokar et al. 2012] and INMS [Teolis et al. 2010] at Dione at Rhea (Chapter 1.4) were two orders of magnitude too tenuous to account for the Magnetometer data. At Rhea these limits on the exospheric abundances from INMS spurred a fundamental new re-interpretation of the MAG data which, together with new modeling approaches, resulted in the discovery of two new current systems. In the next few paragraphs we briefly summarize these current systems at Rhea, but we refer the reader to papers by [Khurana et al. 2017; Simon et al. 2012; Teolis et al. 2014] for a much more detailed analysis.

The first current system, detected by MAG in Rhea's plasma wake, results from the combination of ion kinetic effects in a hot plasma, and relative motion between the plasma and an inert plasma absorbing body like Rhea. As the wake is refilled with plasma in the downstream co-rotation flow [Roussos et al. 2008], the plasma pressure gradient directed back toward Rhea results in diamagnetic current closure across the wake and perpendicular to the co-rotation flow. The pressure gradient exerts a force directed towards Rhea and mimics a real exosphere by generating a field-aligned Alfvénic current system, which extracts momentum from the co-rotating plasma outside the wake and transfers it to the wake. The Alfvén wings from the wake [Khurana et al. 2017] produce flow-directed magnetic field perturbations north and south of Rhea's equatorial plane, detected by MAG at the locations of R2 and R3 and also during two distant (102 R_H and 54 R_H away from Rhea on June 3 and October 17, 2010 [Khurana et al. 2012] downstream flybys. However, MAG also found indications of a second field aligned current system in Rhea's flux tube which, remarkably, is not generated by Rhea's motion relative to the plasma. Evidence for this current system comes from sharp magnetic field perturbations detected during Cassini's R2 and R3 flybys through Rhea's northern and southern flux tubes [Teolis et al. 2014]. The perturbations point in opposite directions on opposite sides of the flux tube, indicating a field twisting about the flux tube, consistent with a wire of flux tube current flowing away, north and south, from Rhea [Santolik et al. 2011; Simon et al. 2012]. The small ~100 km thickness of these field perturbations, much less than the ~500 km ion inertial length, makes them too small to be Alfvénic.

This current system, investigated by [Teolis et al. 2014], results from the requirement to balance ion and electron currents at Rhea's non-conductive surface, and the difference of gyroradius between the positive (ion) and negative (electron) charge carriers. The ions which (owing to their larger gyroradius) discharge into the plasma absorber's surface from all directions are balanced by the electrons, which are constrained to flow along the magnetic field lines. More magnetic field lines connect to the planetary equator due to the oblique angle and, therefore, the electron current is most intense at the edge of the flux tube. The resulting magnetic field perturbation circles about the flux tube and is maximal at the edges, as observed by the Cassini spacecraft. A fundamental property of this flux tube current system is its proportionality only to the ion flux into Rhea, i.e., the plasma density times the ion thermal speed, and its independence of the motion of the moon's conductive atmosphere through the magnetosphere. This spectacular, albeit unexpected outcome of Cassini's magnetic field data at Rhea, would not have been possible

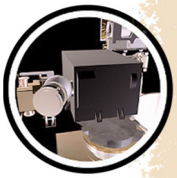

without the exospheric abundance limits provided by Cassini CAPS [Tokar et al. 2012] and INMS [Teolis and Waite 2016].

Inner magnetosphere science

INMS has extracted the water-group ion fractions from OSI measurements in Saturn's inner magnetosphere. These fractions are sensitive probes of the source, transport, and loss mechanisms that govern Saturn's magnetosphere. INMS samples only a small portion of velocity space at a time (Figure INMS-37), which enables investigation of the distributions within velocity space but also limits sensitivity and complicates the separation of various factors that affect the relative ion fractions. Densities and count rates can be low, sometimes requiring the sum of 10,000 IPs for a two-sigma result. Figure INMS-38 shows that ion fractions depend on distance from the orbit of Enceladus. Models show that the water-group fractions depend most strongly on the local fraction of neutrals. In contrast to CAPS results, INMS data show H_3O^+ fractions less than 0.1 except for measurements taken directly in the plumes. These fractions are now being used to calibration ion and neutral models of Saturn's magnetosphere.

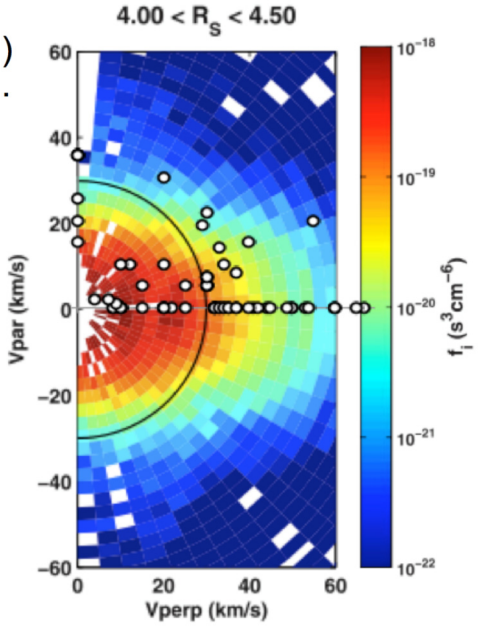

Figure INMS-37. INMS samples only a small portion of velocity space at a time. The *small white circles*, displayed on the CAPS distribution of ion density in velocity space [Tokar et al. 2008], show the location of the INMS measurements of water-group fractions. Although coverage is sparse, the INMS measurements take spot samples of a wide region of velocity space.

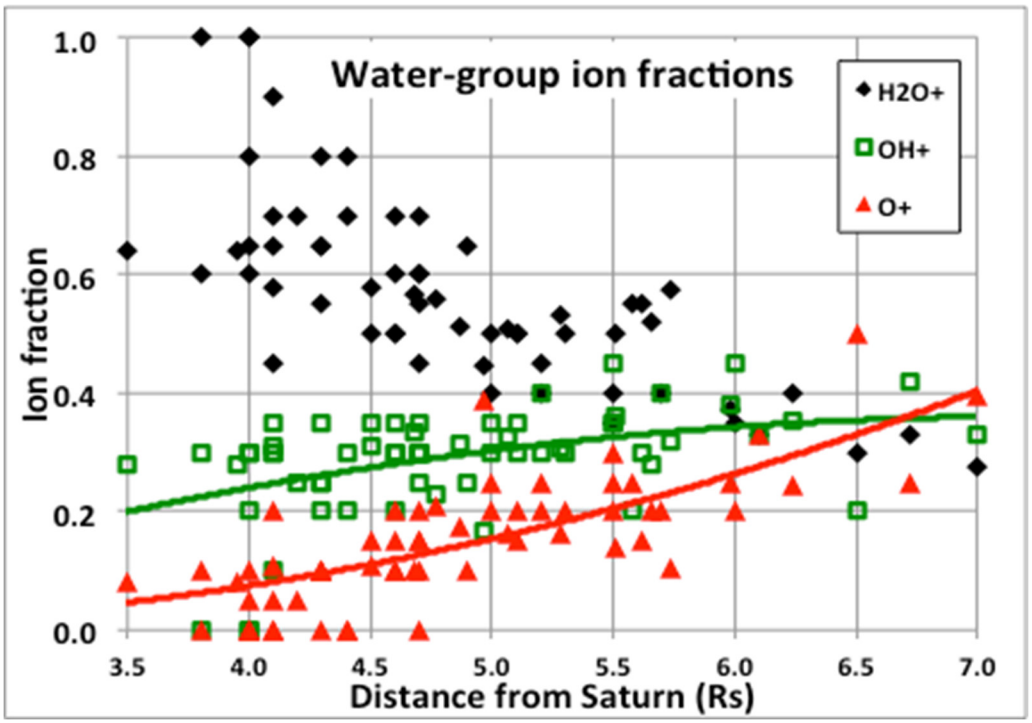

Figure INMS-38. The fraction of water-group ions plotted as a function of distance from Saturn. INMS finds that the highest fraction of H_3O^+ is near 4 R_S, as expected, as that is the orbit of Enceladus, the source of the neutral water that becomes the plasma.

Neutrals in Saturn's inner magnetosphere

In 2008, the Cassini INMS investigation made in situ measurements of neutral species near Saturn's equatorial plane within 0.5 Saturn radii (R_S) of the orbit of Enceladus. After removing the large background and modeling to interpret instrumental effects, the data provide constraints on the neutral distribution and composition. These data show an azimuthal asymmetry in the neutral densities (Figure INMS-39) and provide measurements used to compare simulations of neutral H_2O emitted from Enceladus (Figure INMS-40). Far from Enceladus, the neutral water densities, at a few times 10^3 molecules/cm^3, are near the detection limit of INMS. Near Enceladus, but outside of the plumes and north of the equatorial plane, the INMS detects particles within 5,000 km of Enceladus, with the density increasing to approximately 10^5 molecules/cm^3 at the equatorial plane.

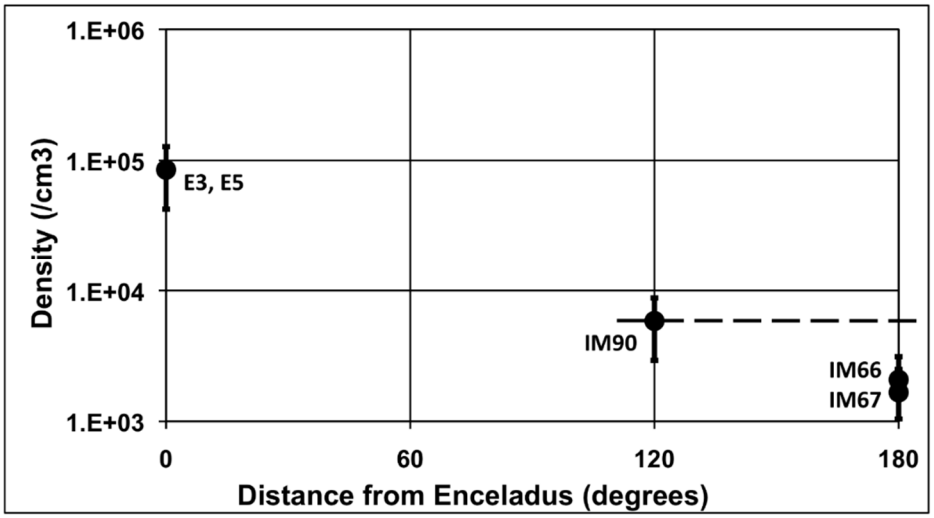

Figure INMS-39. Average densities near 4 R_S show the dependence on azimuth. The densities at 0 (near Enceladus) are north of Enceladus, outside the plumes. The difference between the measurements at 0° and 120° are much larger than the uncertainties. The measurements at 180° are at 4.5 R_S. The data at 180° are a factor of three below the data at 120°. The displayed *error bars* are ±50%.

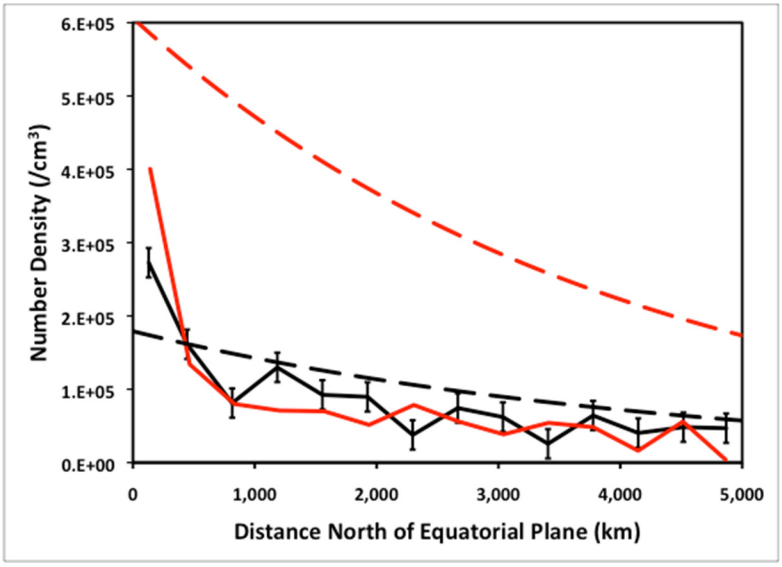

Figure INMS-40. Neutral cloud density north of Enceladus, before close approach and outside of proximal influence of the south-pole plumes. The solid lines are the INMS data. The *dashed lines* are simulations using the charge-exchange model of the neutral cloud [Smith et al. 2010]. The E5 simulation is based on the source rate derived from modeling the E5 plumes, and the E3 simulation is based on the source rate derived from modeling the E3 plumes. The E3 and E5 INMS densities are similar to each other and to the E3 simulation. E5 error bars (not shown to reduce clutter) are the same size as E3 error bars.

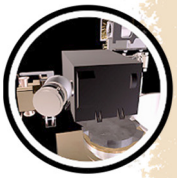

28 u neutrals in Saturn's inner magnetosphere

INMS observes inner-magnetosphere neutrals with a mass of 28 u that have unexpectedly high densities, no apparent source, and no clear molecular identification. With densities as high as 30% of the neutral-water density, the candidate molecules, N_2 and CO, should be abundant in the Enceladus emissions, but multiple observational approaches show that neither molecule comprises more than 3% of the H_2O density (Figure INMS-41).

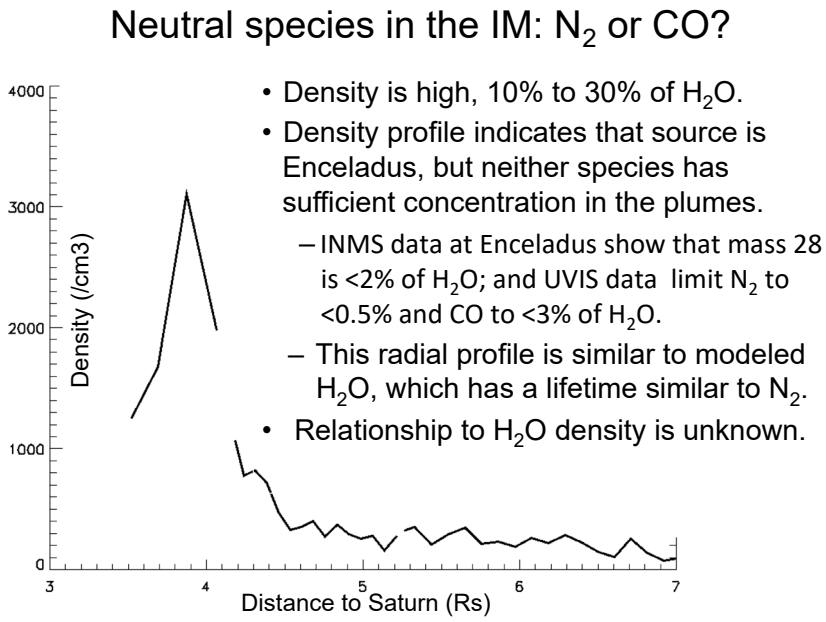

Figure INMS-41. Mass 28 u mystery compound in the inner magnetosphere.

SATURN INNER MAGNETOSPHERE OPEN QUESTIONS

1. What explains the mass 28 signal?

F-ring Science

F-ring observations: primary neutrals

INMS found two neutral species with remarkable consistency during the F-ring passes: H_2 and a species at 28 u (Figure INMS-42). The scale height, or the half-width-half-max of the INMS counts, for both of these species was approximately 3,000 km, or 0.05 Saturn radii (R_S). This parameter and the total counts were nearly identical in each pass.

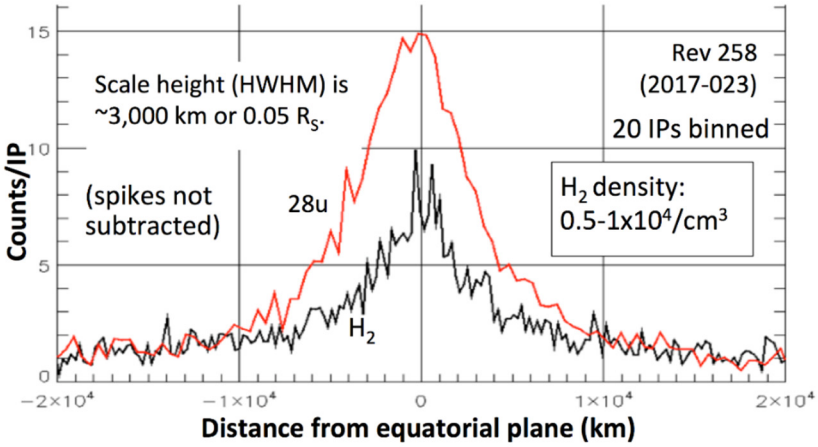

Figure INMS-42. The major neutrals measured by INMS in the F-ring. Twenty measurements (integration periods or IPs) were binned for this plot.

Although H_2 was expected in this area of the rings, models and Earth-based observations predicted a larger scale height for H_2 from Saturn's atmosphere, and the narrow distribution of the observed H_2 suggests that it is more liked to originate in the rings. The lack of variability indicates a stable ring atmosphere. Atomic hydrogen is not measured by INMS due to instrumental noise at 1 u.

A complication for INMS neutral observations is the high speed of Cassini relative to the ring particles. At 20 km/s, the molecules carry 2.1 eV per nucleon, which is sufficient energy to cause some dissociation in the INMS antechamber, particularly for larger molecules. If a molecule dissociates, only volatile products are measured. Without considering dissociation, the density of the H_2 is 0.5-1 × 10^4 cm^{-3}.

F-ring observations: other neutrals and 28 u

CH_4 (16 u) and CO_2 (44 u) are the only other measured species. They both have a count rate that is approximately 20% of the H_2 rate. CH_4 is confirmed by the presence of 15 u counts at the correct electron impact dissociative ionization ratio, the amount produced from CH_4 in the INMS ionization chamber. CO_2 is not a common dissociation product and may be a native species, it exists on the surface of several icy moons. Count rates for both CH_4 and CO_2 are depressed due to dissociation and they may be more abundant than indicated by the measurements. There are small amounts of 26 u and 27 u, which are expected products from ionization of C_2H_4, one possibility for the 28 u measurements. However, the count rates for these two cracking products are lower than expected if the entire 28 u signal was produced by C_2H_4. This deficiency implies that another species such as CO may contribute to the 28 u signal.

Several expected neutral species are missing, most notably H_2O and O_2. Since water is temporarily adsorbed onto the walls of the INMS inlet, H_2O counts are suppressed and delayed. Combined with the radiation background, which increases after passing through the equatorial plane, INMS would not detect low densities of H_2O particularly after some loss due to high-velocity

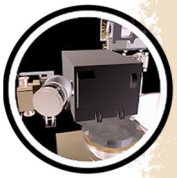

dissociation. Models show that O_2 could be abundant, but that densities decrease a factor of 1,000 approaching the location of Cassini's trajectory, moreover, much of the O_2 would be lost due to dissociation.

F-ring observations: ions

INMS observed only water-group ions in the F-ring. Unlike the neutrals, the ion densities were not symmetrical with respect to the equatorial plane, varying in both total density and the relative fractions within the water group (Figure INMS-43). The predominance of O^+ versus the other water-group ions indicates that there may be a source of O^+ other than as a byproduct of water. One possibility is that CH_4^+ contributes a fraction of the 16 u ions.

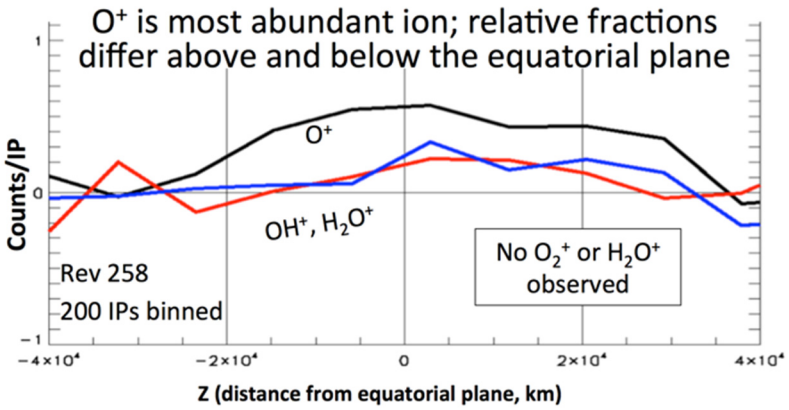

Figure INMS-43. Distribution of water-group ions south and north of the equatorial plane. O+ comprises a higher fraction of the ions in the south.

The velocity distribution of the ions (Figure INMS-44) shows that the ions are cold, with a mean velocity below the pickup velocity of 8 km/s, corresponding to a temperature of approximately 3 eV. These results are consistent with analyses and modeling of data from the CAPS.

The lack of O_2^+ in the F-ring, which INMS previously observed during Cassini's insertion into orbit about Saturn, is likely due to the INMS energy limit at the F-ring speeds—O_2^+ exceeds the INMS energy limit for ions. The lack of H_2^+ is surprising and not yet explained. As with neutrals, noise prevents INMS measurement of H^+ at 1 u.

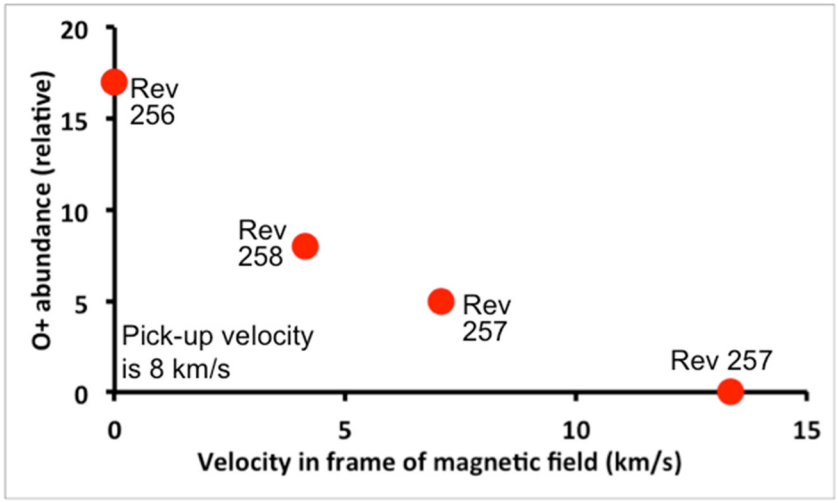

Figure INMS-44. The distribution of ions in the rest frame of the magnetic field. Ions are concentrated near the core, as expected for cold ions.

Saturn Ionosphere, Atmosphere, and Atmosphere-Ring Interaction Science

Saturn Upper Atmosphere Major Findings (Neutral Thermosphere):

- INMS made the first in situ measurements of Saturn's atmosphere, and made surprising discoveries of several species of high mass neutrals, e.g., CH_4, CO, CO_2.
- The INMS made the first in situ characterization of the thermal structure in the upper atmosphere of Saturn, indirectly through its measurements of the H_2 densities.
- Helium has been measured for the first time in Saturn's upper atmosphere, providing constraints on possible deep-atmosphere mixing ratios of Helium and whether or not Saturn has a solar-like composition or something else.

During the Cassini Grand Finale, the INMS made an unprecedented series of measurements of Saturn's upper atmosphere during the Proximal Orbit Phase, sampling from ~3500–1370 km altitude above the one bar pressure level. Prior to these orbits, it was anticipated that Saturn's upper atmosphere consisted primarily of H, H_2, with trace amounts of H_2O and He. However, the INMS measurements revealed an atmosphere with an unexpectedly rich composition, containing significant amounts of organics spanning the entire mass range sampled by INMS, shown in Figure INMS-45. These results were completely unanticipated and they have effectively turned our understanding of the high altitude thermosphere-ionosphere chemistry on its head [Waite et al. 2018; Perry et al. 2018; Yelle et al. 2018].

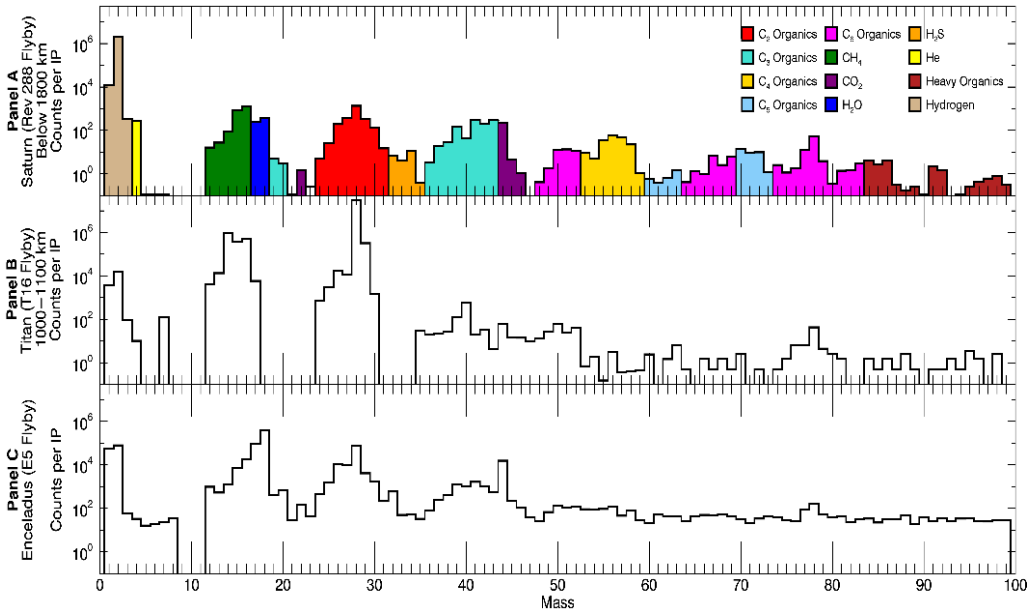

Figure INMS-45. INMS mass spectra from the Grand Finale orbits at Saturn (*Panel A*), compared with those of Titan (*Panel B*), and Enceladus (*Panel C*). Horizontal axis is in units of mass per charge. See Waite et al. [2018] for details.

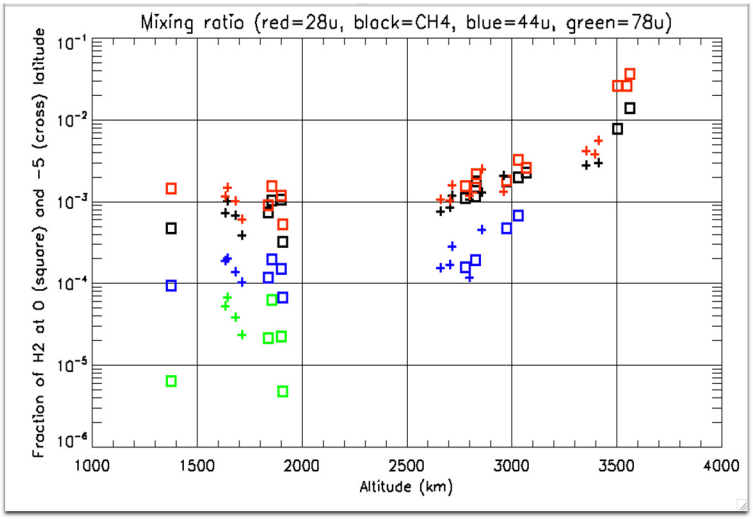

Figure INMS-46. Volume mixing ratios (*vertical axis*) of the heavy species identified by INMS in the Saturnian upper atmosphere as a function of altitude above the 1-bar pressure level (*horizontal axis*).

In particular, INMS has identified methane (CH_4) as a significant component of the upper atmosphere of Saturn above 1370 km. As shown in Figure INMS-46, INMS has found significant amounts of methane that reach up to ~10% of the composition near 3500 km altitude above the 1-bar pressure level. Additional heavy species (masses 28 u, 44 u, and 78 u) have also been

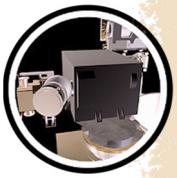

identified. All of these species can potentially play major photochemical roles in the atmosphere of Saturn [cf. Moses and Bass 2000; Kim et al. 2014].

Using a combination of National Institute of Standards and Technology (NIST) data and calibration data collected using the refurbished engineering unit, preliminary fits to spectra at altitudes between 1700 and 1800 km for three representative orbits were made to identify contributing species in the measured mass spectra (for example, Figure INMS-45). In general, the spectrum below ~70 u can be fit by a combination of species that is dominated by hydrocarbons. Ammonia (NH_3) is detected at 17 u. Other N-bearing species are neither excluded nor required by the spectra. The same is true for O-bearing organics. Inclusion of S species, especially H_2S, improves the fit of the spectrum. However, of the non-H_2, non-He material, less than 1 mol percent is contributed by S-bearing species. We estimate that between 30 and 50 mol percent of the non-H_2, non-He material measured by INMS is comprised of organics other than methane, which may constitute an additional 20 to 35 mol percent. C_4 species, including butane (C_4H_{10}) at 58 u, are particularly abundant compared to other hydrocarbons. Above 70 u, the spectra are consistent with contributions from heavier aromatic species, including species such as naphthalene ($C_{10}H_8$, 128 amu) with primary peaks that are beyond the range of INMS.

Other Cassini instruments, including the Charge-Energy-Mass Spectrometer (CHEMS) from the MIMI, reported detections of heavy (8,000 to 40,000 amu) particles during the Grand Finale orbits [Mitchell et al. 2018]. To understand the relationship of these particles to INMS data, we compared the total amount of material detected by INMS to the particle sizes observed by MIMI [Perry et al. 2018]. The results suggest that INMS may have mainly sampled smaller particles that were dominated by volatile and organic material with very little contribution from refractory mineral phases. The altitude-density profiles of these particles indicate very low densities, likely on the order of 0.1 g/cm^3 or less. These densities may be consistent with the densities of interplanetary dust particles from small bodies [Rietmeijer 1993]. Some masses, including 15 u (mainly from CH_4), 28 u (possibly N_2 or CO) and 17 u (mainly NH_3), have altitude-density profiles that are consistent with molecular radii. Other masses, including 58 u (possibly butane, C_4H_{10}) and 78 u (possibly benzene, C_6H_6), have profiles that suggest larger radii, on the order of nanometers or tens of nanometers.

In addition to the heavy species in the upper atmosphere of Saturn, INMS has also made the first in situ measurements of H_2, He, and H-D in the atmosphere of Saturn (shown in Figure INMS-47). Molecular hydrogen (H_2) is the dominant species in the thermosphere, and its density scale height reveals the expected background temperature of Saturn's upper atmosphere. Thus, measurements of H_2 reveal information about the thermal state of Saturn's upper atmosphere. Prior to the INMS measurements, only remote sensing observations were possible [cf. Koskinen et al. 2015; Vervack and Moses 2015], which provide temperatures through inversion techniques. The measurements in **SIA3**, however, provide the first-ever direct sampling of the Saturn atmosphere [Waite et al., 2018; Yelle et al. 2018], allowing us to infer thermal structure from these measurements using models of the atmosphere, such as Müller-Wodarg et al. [2006b, 2012].

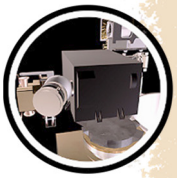

Finally, there has been considerable uncertainty about the amount of Helium in the Saturnian atmosphere [Ben-Jaffel and Abbes 2015]. He abundances are key to determining the most likely formation scenarios for Saturn's atmosphere. Currently, it has been suggested that Saturn would be depleted in Helium relative to Jupiter (~13.5% volume mixing ratio) or the protosolar value (~15.6%) due to Helium raining out in the lower atmosphere. The measurements provided by INMS, combined with diffusive modeling, can lead to constraints on the Helium content in the lower atmosphere providing a missing component in our understanding of planetary evolution.

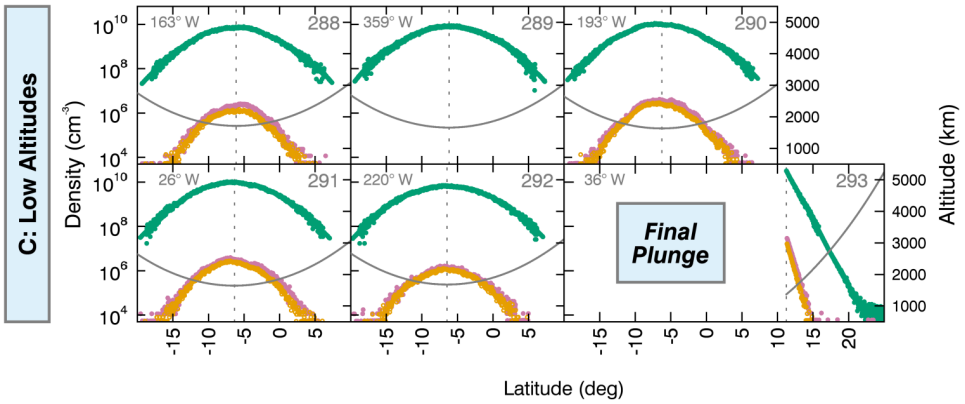

Figure INMS-47. INMS measurements of H_2 (green), He (red), and Mass 3 u (orange) as a function of altitude (*right-hand axis*) and latitude (*horizontal axis*).

Saturn Upper Atmosphere Major Findings (Charged Gases, i.e, the Ionosphere):

- The INMS made the first in situ measurements of the ion composition of the ionosphere of a gas giant planet (i.e., Saturn), allowing the first determination of ion mixing ratios and number densities as well as their temporal variabilities.
- INMS measurements of the minor ion (H_2^+) represent a strong constraint on local ion production rates providing a check on outer planet projections of solar irradiances, including evidence for ring shadowing of the ionosphere.
- Combined with RPWS and MIMI measurements, INMS in situ data paint a clear picture of Saturn's equatorial ionosphere being dominated by heavy molecular ions that result from ring-derived material.

Prior to the Cassini Grand Finale, observations of Saturn's ionosphere were limited to altitude profiles of electron density (the presumed sum of the ion densities) at dawn or dusk, periods of rapid change in an ionosphere. Trace emissions from an expected major ion (H_3^+) were also detected, but column-integrated densities could only be derived at auroral latitudes. Therefore, ion densities throughout the majority of Saturn's ionosphere were based solely on model comparisons with radio occultation measurements, for example, Moses and Bass [2000]; Moore et al. [2006, 2010]. In situ measurements by INMS provided key constraints on the expected major ion species, H^+ and H_3^+ [Waite et al. 2018; Cravens et al. 2018; Moore et al. 2018], finally providing closure on a decades-long debate regarding the dominant chemical losses of H^+, for example, Connerney and Waite [1984].

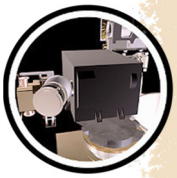

In addition, INMS was able to measure the expected minor ion species H_2^+ and He^+. The chemistry of these ions is relatively straightforward, and the extremely short chemical lifetime of H_2^+ makes it an ideal tracer of the in situ ion production rate. Therefore, H_2^+ densities from INMS measurements can be used to gauge the accuracy of commonly used projections of solar irradiances at Saturn. These projections rely on Earth-based data, and the assumption of a relatively stable solar irradiance over a period of days. Comparisons between measured H_2^+ with modeled H_2^+ based on projected solar irradiances find a ~50% discrepancy, implying that future outer planet modeling will require better estimates of the solar irradiance. A drop-off in the H_2^+ density (i.e., ionization rate) observed by INMS near 15° S latitude is consistent with shadowing by the B-ring [Waite et al. 2018; Cravens et al. 2018].

Finally, Cassini's high speed near periapsis during the Grand Finale (~32 km s^{-1}), meant that INMS could only sample ions with masses up to 7 u. The sums of the light ion densities measured by INMS were found to be an excellent match with the electron densities from RPWS, for example, Persoon et al. [2019], at high altitudes (> ~2200 km), implying that Saturn's high-altitude ionosphere was charge-neutral and dominated by H^+ with minor contributions from H_3^+, as expected (Figure INMS-48). However, at low altitudes the total ion densities from INMS differed significantly from the electron densities. This massive discrepancy was interpreted as a signature of an ionosphere dominated by heavy (> 7 u) ions, which would be entirely consistent with the expected ion chemistry to follow from the ring-derived influx of complex neutrals measured by INMS (Figure INMS-46). Detailed model-data comparisons indicated that in the main ionosphere, a complex, and heavy, neutral species was needed to react with H^+ and H_3^+, and thus reduce the model densities of these light species to measured values [Cravens et al. 2018; Moore et al. 2018]. The neutral mixing ratios required were consistent with the values measured by the closed source and described earlier. The ion species produced by these reactions were suggested to be those needed to fill the ion-electron density gap evident in Figure INMS-48.

The ionosphere was demonstrated to be chemically controlled at lower altitudes where the heavy ions are dominant [Cravens et al. 2018; Moore et al. 2018], but at higher altitudes, where H^+ dominates the measured ion composition, transport processes should become important. During the relatively high altitude proximal orbit 287, the INMS open source was operated in a special energy scan mode and some limited information on proton flow speeds was obtained [Cravens et al. 2018]. Proton speeds of a couple km/s were detected in the Northern Hemisphere at latitudes connecting to the B-ring shadow in the Southern Hemisphere.

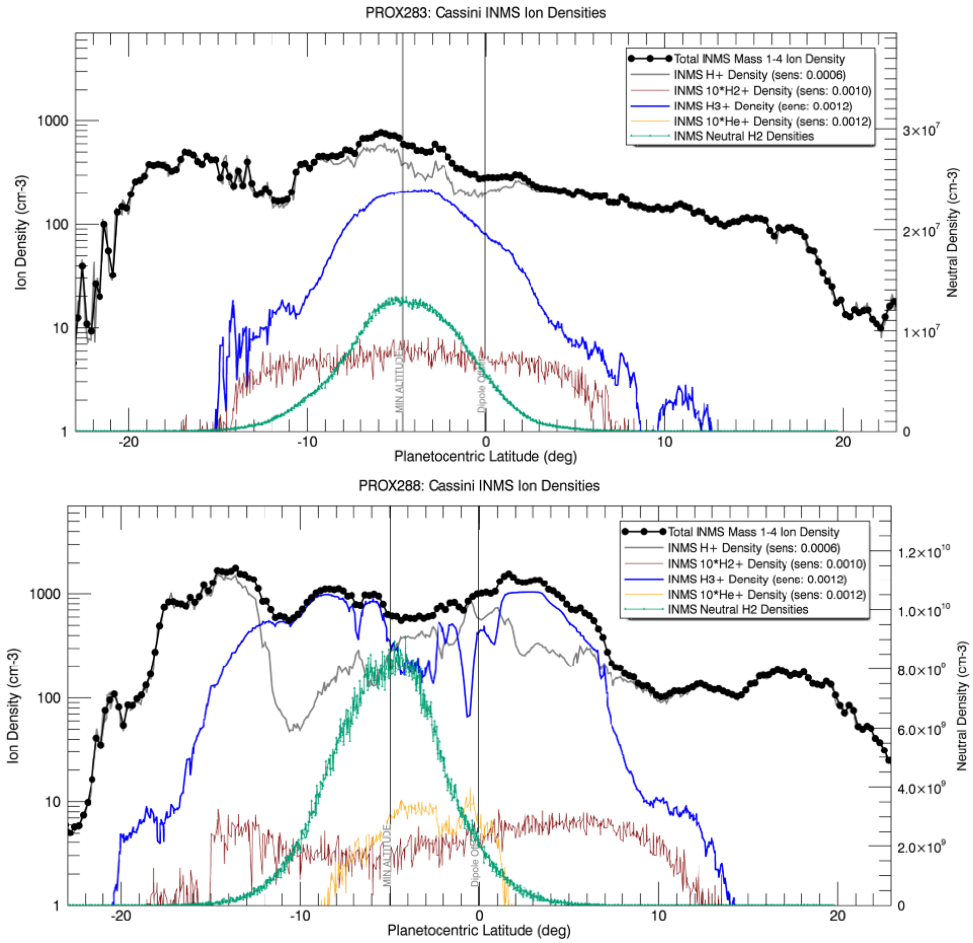

Figure INMS-48. INMS measurements of H_2 (*green*), H^+ (*gray*), H_2^+ (*red*, multiplied by 10), H_3^+ (*blue*), He^+ (*gold*, multiplied by 10), and total light ion density (1–4 u, *black*) as a function of planetocentric latitude (*horizontal axis*). Ion measurements were taken for four proximal orbits, 283, 287, 288, and 292, though only one representative high altitude (283, top) and low altitude (288, bottom) orbit is presented here.

Saturn proximals open questions

1. INMS made the first in situ measurements of He and HD in Saturn's atmosphere. What are the implications of the upper atmosphere He measurements for the abundance of He in the bulk atmosphere? How is the measured HD affected by ring inflow?

2. INMS measured the temperature structure of Saturn's upper atmosphere with significantly higher precision and altitude resolution than is possible with remote sensing techniques. The energy balance in Saturn's upper atmosphere remains an open question.

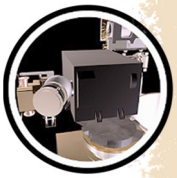

3. INMS measurements revealed significant influx of material from the rings to the atmosphere.

    a. What causes this inflow, how it relates to ring erosion processes and magnetospheric processes, as well as the implications for atmospheric chemistry remain open questions.

    b. Is the ring influx uniformly distributed about Saturn?

    c. Is the ring influx constant or is there a time dependence?

    d. Does the ring influx respond to magnetospheric processes or solar wind drivers?

    e. How long has the ring influx been taking place? Is the time the same for all species (methane, nanograins, etc.)?

    f. What are the dynamics in equatorial region and how are they affected by the Joule heating measured by MAG??

    g. Presence of negative ions in the equatorial region (and auroral regions too)?

    h. What is the balance between chemistry and transport operating in the low-latitude Saturnian ionosphere?

Open Questions for Saturn System Science

The open questions are found under each subtopic. The big open question for the Saturn system—Is there life in the ocean of Enceladus?

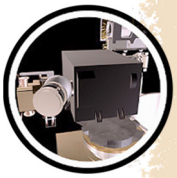

ACRONYMS

Note: For a complete list of Acronyms, refer to Cassini Acronyms – Attachment A.

AACS	Attitude and Articulation Control System
AO	Announcement of Opportunity
CAPS	Cassini Plasma Spectrometer
CDA	cosmic dust analyzer
CHEMS	Charge-Energy-Mass Spectrometer
CIRS	Composite Infrared Spectrometer
CS	closed source
CSM	Cassini Solstice Mission
CSN	Closed Source Neutral
Da	Daltons
ELS	Electron Spectrometer
ENA	energetic neutral atom
EUV	extreme ultraviolet
GCM	General Circulation Model
IBS	Ion Beam Spectrometer
IP	integration period
ISE	Ion Source Enclosure
ISS	Imaging Science Subsystem
LP	Langmuir probe
MAG	Magnetometer
MAPS	Magnetospheres and Plasma Science
MHD	magneto-hydrodynamic
MIMI	Magnetospheric Imaging Instrument
NAV	Navigation
NIST	National Institute of Standards and Technology
OS	open source
OSI	open source ion
OSNB	open source neutral beam
OSNT	open source neutral thermal
PA	proton affinities
PAH	polycyclic aromatic hydrocarbon
QMA	quadrupole mass analyzer
RPWS	Radio and Plasma Wave Science
TAMWG	Titan Atmospheric Working Group
UVIS	Ultraviolet Imaging Spectrograph
UVS	Ultraviolet Spectrometer
VIMS	Visual and Infrared Imaging Spectrometer

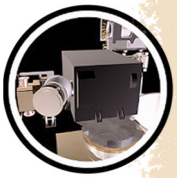

REFERENCES

Disclaimer: The partial list of references below correspond with in-text references indicated in this report. For all other Cassini references, refer to Attachment B – References & Bibliographies; Attachment C – Cassini Science Bibliographies; the sections entitled References contributed by individual Cassini instrument and discipline teams located in Volume 1 Sections 3.1 and 3.2 Science Results; and other resources outside of the Cassini Final Mission Report.

Ågren, K., J. E. Wahlund. R. Modolo, D. Lummerzheim, M. Galand, I. Müller-Wodarg, P. Canu, W. S. Kurth, T. E. Cravens, R. V. Yelle, J. H. Waite Jr., A. J. Coates, G. R. Lewis, D. T. Young, C. Bertucci, M. K. Dougherty, (2007), On magnetospheric electron impact ionisation and dynamics in Titan's ram-side & polar ionosphere-a Cassini case study, Annales Geophysicae, 25.

Anicich, V. G. and M. J. McEwan, (1997), Ion-molecular chemistry in Titan's ionosphere, Planetary Space Science, 45, 897–921, doi: 10.1016/S0032-00633(97)00053-6.

Bauschlicher, C. W., A. Ricca, M. Rosi, (2002), Mechanisms for the growth of polycyclic aromatic hydrocarbon (PAH) cations, Chemical Physics Letters, vol. 355, issues 1–2, pp. 159–163.

Bauschlicher Jr., C. and A. Ricca, (2000), Mechanisms for polycyclic aromatic hydrocarbon (PAH) growth, Chemical Physics Letters, vol. 326, Issues 3–4, 283–287.

Bell, J. M., J. H. Waite, J. H. Westlake, S. W. Bougher, A. J. Ridley, R. Perryman, K. Mandt, (2014), Developing a self-consistent description of Titan's upper atmosphere without hydrodynamic escape, Journal of Geophysical Research, 119, 4957–4972.

Bell, J. M., J. Westlake, J. H. Waite Jr., (2011a), Simulating the time-dependent response of Titan's upper atmosphere to periods of magnetospheric forcing, Geophysical Research Letters, 38, L06202.

Bell, J., S. W. Bougher, J. H. Waite Jr., A. J. Ridley, B. Magee, K. Mandt, J. Westlake, A. D. DeJong, A. Bar-Nun, R. Jacovi, G. Toth, V. de la Haye, (2011b), Simulating the one-dimensional structure of Titan's upper atmosphere, Part III: Mechanisms determining methane escape, Journal of Geophysical Research, 116, E11002.

Bell, J., S. W. Bougher, J. H. Waite Jr., A .J. Ridley, B. Magee, K. Mandt, J. Westlake, A. D. DeJong, A. Bar-Nun, R. Jacovi, G. Toth, V. de la Haye, (2010a), Simulating the one-dimensional structure of Titan's upper atmosphere, Part I: Formulation of the Titan global ionosphere-thermosphere model and benchmark simulations, Journal of Geophysical Research, 115, E12002.

Bell, J., S. W. Bougher, J. H. Waite Jr., A.J. Ridley, B. Magee, K. Mandt, J. Westlake, A. D. DeJong, V. de la Haye, D. Gell, G. Fletcher, A. Bar-Nun, R. Jacovi, G. Toth, (2010b), Simulating the one-dimensional structure of Titan's upper atmosphere, Part II: Alternative scenarios for methane escape, Journal of Geophysical Research, 115, E12018.

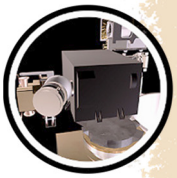

Ben-Jaffel, L. and I. Abbes, (2015), Helium abundance in giant planets and the local interstellar medium, Journal of Physics: Conference Series, 577, doi: 10.1088/1742-6596/577/1/012003.

Bird, M. K., R. Dutta-Roy, S. W. Asmar, T.A. Rebold, (1997), Detection of Titan's ionosphere from Voyager 1 radio occultation observations, Icarus, vol. 130, issue 2, pp. 426—436, doi: 10.1006/icar.1997.5831.

Blanc, M., S. Bolton, J. Bradley, M. Burton, T. E. Cravens, I. Dandouras, M. K. Dougherty, M. C. Festou, J. Feynman, R. E. Johnson, T. G. Gombosi, W. S. Kurth, P. C. Liewer, B. H. Mauk, S. Maurice, D. Mitchell, F. M. Neubauer, J. D. Richardson, D. E. Shemansky, E. C. Sittler, B. T. Tsurutani, P. Zarka, L. W. Esposito, E. Grün, D. A. Gurnett, A. J. Kliore, S. M. Krimigis, D. Southwood, J. H. Waite Jr., D. T. Young, (2002), Magnetospheric and plasma science with Cassini-Huygens, Space Science Reviews, 104, 1, 253–346.

Bohme, D. K., (1992), PAH [polycyclic aromatic hydrocarbons] and fullerene ions and ion/molecule reactions in interstellar and circumstellar chemistry, Chemical Reviews, 92 (7), 1487.

Bouquet, A., C. R. Glein, D. Wyrick, J. H. Waite Jr., (2017), Alternative energy: Production of H2 by radiolysis of water in the rocky cores of icy bodies, The Astrophysical Journal Letters, 840, L8, doi:10.3847/2041-8213/aa6d56.

Brecht, S. H., J. G. Luhmann, D. J. Larson, (2000), Simulation of the Saturnian magnetospheric interaction with Titan, Journal of Geophysical Research, vol. 105, issue A6, 13119–13130, doi: 10.1029/1999JA900490.

Carrasco, N., J. Westlake, P. Pernot, J. H. Waite Jr., (2013), Nitrogen in Titan's Atmospheric Aerosol Factory, The Early Evolution of the Atmospheres of Terrestrial Planets, 35, doi: 10.1007/978-1-4614-5191-4_11.

Coates, A. J., A. Wellbrock, G. R. Lewis, G. H. Jones, D. T. Young, F. J. Crary, J. H. Waite, R. E. Johnson, T. W. Hill, E. C. Sittler Jr., (2010), Negative ions at Titan and Enceladus: recent results, Faraday Discussions, 147(1), 293-305, doi: 10.1039/C004700G2010.

Coates, A. J., A. Wellbrock, G. R. Lewis, G. H. Jones, D. T. Young, F. J. Crary, J. H. Waite Jr., (2009), Heavy negative ions in Titan's ionosphere: Altitude and latitude dependence, Planetary and Space Science, 57, 1866–1871.

Coates, A. J., F. J. Crary, G. R. Lewis, D. T. Young, J. H. Waite, Jr., E. C. Sittler Jr., (2007), Discovery of heavy negative ions in Titan's ionosphere, Geophysical Research Letters, 34, L22103, doi: 10.1029/2007GL030978.

Connerney, J. and J. Waite, (1984), New model of Saturn's ionosphere with an influx of water from the rings, Nature, 312, 136–138.

Coustenis, A., J. I. Lunine, J.-P. Lebreton, D. Matson, C. Erd, K. Reh, P. Beauchamp, R. Lorenz, J. H. Waite Jr., C. Sotin, L. Gurvits, M. Hirtzig, (2009), Earth-based support for the Titan Saturn System Mission, Earth, Moon and Planets, 105, 135–142.

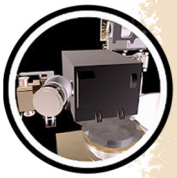

Coustenis, A., S. K. Atreya, T. Balint, R. H. Brown., et al., (2008), TandEM: Titan and Enceladus mission, Experimental Astronomy, 23, issue 3, pp. 893–946, doi: 10.1007/s10686-008-9103-z.

Crary, F. J., B. A. Magee, K. E. Mandt, J. H. Waite, J. Westlake, D. T. Young, (2009), Heavy ions, temperatures and winds in Titan's ionosphere: Combined Cassini CAPS and INMS observations, Planetary and Space Science, 57, 1847–1856.

Cravens, T. E., M. Morooka, A. Renzaglia, L. Moore, J. H. Waite Jr., R. Perryman, et al., (2019). Plasma transport in Saturn's low-latitude ionosphere: Cassini data, Journal of Geophysical Research: Space Physics, 124, 4881–4888, doi: 10.1029/2018JA026344.

Cravens, T. E., L. Moore, J. H. Waite Jr., R. Perryman, M. Perry, J.-E. Wahlund, A. Persoon, W. Kurth, (2018), The ion composition of Saturn's equatorial ionosphere as observed by Cassini. Geophysical Research Letters, doi: 10.1029/2018GL077868.

Cravens, T. E., M. Richard, Y.-J. Ma, C. Bertucci, J. G. Luhmann, S. Ledvina, I. P. Robertson, J.-E. Wahlund, K. Ågren, J. Cui, I. Müller-Wodarg, J. H. Waite, M. Dougherty, J. Bell, D. Ulusen, (2010), Dynamical and Magnetic Field Time Constants for Titan's Ionosphere - Empirical Estimates, Journal of Geophysical Research, 115, A08319.

Cravens, T. E., R. V. Yelle, J.-E. Wahlund, D. E. Shemansky, A. F. Nagy, (2009a), Composition and structure of the ionosphere and thermosphere, In Titan from Cassini-Huygens, Chapter 11, (eds.) R. H. Brown, J. P. Lebreton, J. H. Waite, Springer, Dordrecht, pp. 259–295, doi: 10.1007/978-1-4020-9215-2_11.

Cravens, T. E., I. P. Robertson, J. H. Waite Jr., R. V. Yelle, V. Vuitton, A. J. Coates, J.-E. Wahlund, K. Ågren, M. S. Richard, V. De La Haye, A. Wellbrock, F. N. Neubauer, (2009b), Model-data comparisons for Titan's nightside ionosphere, Icarus, 199, 174–188, doi: 10.1016/j.icarus.2008.09.005.

Cravens, T. E., R. L. McNutt Jr., J. H. Waite Jr., I. P. Robertson, J. G. Luhmann, R. V. Yelle, W. Kasprzak, W.-H. Ip, (2009c), Plume ionosphere of Enceladus as seen by the Cassini Ion and Neutral Mass Spectrometer, Geophysical Research Letters, 36, L08106, doi: 10.1029/2009GL037811.

Cravens, T. E., I. P. Robertson, S. A. Ledvina, D. Mitchell, S. M. Krimigis, J. H. Waite Jr., (2008a), Energetic ion precipitation at Titan, Geophys. Res. Lett., 35, L03103, doi: 10.1029/2007GL032451.

Cravens, T. E., I. P. Robertson, J. H. Waite Jr., R. V. Yelle, V. Vuitton, A. J. Coates, J.-E. Wahlund, K. Ågren, M. S. Richard, V. De La Haye, A. Wellbrock, F. N. Neubauer, (2008b), Model-data comparisons for Titan’s nightside ionosphere, Icarus, doi: 10.1016/j.icarus.2008.09.005.

Cravens, T. E., I. P. Robertson, J. H. Waite Jr., R. V. Yelle, W. T. Kasprzak, C. N. Keller, S. A. Ledvina, H. B. Niemann, J. G. Luhmann, R. L. McNutt, W.-H. Ip, V. De La Haye, I. Müller-Wodarg, J.-E. Wahlund, V. G. Anicich, V. Vuitton, (2006), The composition of Titan's ionosphere, Geophysical Research Letters, 33, L07105.

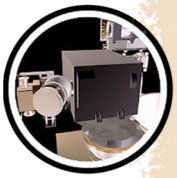

Cravens, T. E., I. P. Robertson, J. Clark, J.-E. Wahlund, J. H. Waite Jr., S. A. Ledvina, H. B. Niemann, R. V. Yelle, W. T. Kasprzak, J. G. Luhmann, R. L. McNutt, W.-H. Ip, V. De La Haye, I. Müller-Wodarg, D. T. Young, A. J. Coates, (2005), Titan's ionosphere: Model comparisons with Cassini Ta data, Geophysical Research Letters, vol. 32, issue 12, doi: 10.1029/2005GL023249.

Cravens, T. E., J. Vann, J. Clark, J. Wu, C. N. Keller, C. Brull, (2004), The ionosphere of Titan: An updated theoretical model, Advances in Space Research, 33, 212.

Cravens, T. E., C. N. Keller, B. Ray, (1997), Photochemical sources of non-thermal neutrals for the exosphere of Titan, Planetary and Space Science, 45, 889.

Cui, J., R. V. Yelle, T. Li, D. S. Snowden, I. C. F. Müller-Wodarg, (2014), Density waves in Titan's upper atmosphere, Journal of Geophysical Research, 119, 490–518, doi: 10.1001/2013JA019113.

Cui, J., Y. Lian, I. C. F. Müller-Wodarg, (2013), Compositional effects in Titan's thermospheric gravity waves, Geophysical Research Letters, 40, 43–47, doi: 10.1029/2012GL054621.

Cui, J., R. V. Yelle, D. F. Strobel, I. C. F. Müller-Wodarg, D. S. Snowden, T. T. Koskinen, M. Galand, (2012), The CH4 structure in Titan's upper atmosphere revisited, Journal of Geophysical Research, 117, E11006, doi: 10.1029/2012JE004222.

Cui, J., R. V. Yelle, I. C. F. Müller-Wodarg, P. P. Lavvas, M. Galand, (2011), The implications of the H2 variability in Titan's exosphere, Journal of Geophysical Research, 116, A11324.

Cui, J., M. Galand, R. V. Yelle, J.-E. Wahlund, K. Ågren, J. H. Waite Jr., M. K. Dougherty, (2010), Ion transport in Titan's upper atmosphere, Journal of Geophysical Research, 115, A06314.

Cui, J., R. V. Yelle, V. Vuitton, J. H. Waite, W. T. Kasprzak, D. A. Gell, H. B. Niemann, I. C. F. Müller-Wodarg, N. Borggren, G. G. Fletcher, E. L. Patrick, E. Raaen, B. A. Magee, (2009a), Analysis of Titan's neutral upper atmosphere from Cassini ion neutral mass spectrometer measurements, Icarus, 200, 581–615, doi: 10.1016/j.icarus.2008.12.005.

Cui, J., M. Galand, R. V. Yelle, V. Vuitton, I. C. F. Müller-Wodarg, J. -E. Wahlund, P. P. Lavvas, T. E. Cravens, W. T. Kasprzak, J. H. Waite Jr., (2009b), Diurnal variations of Titan's ionosphere, Journal of Geophysical Research, 114, A06310.

Cui, J., R. V. Yelle, K. Volk, (2008), Distribution and escape of molecular hydrogen in Titan's thermosphere and exosphere, Journal of Geophysical Research, 113, E10004, doi: 10.1029/2007JE003032.

De La Haye, V., J. H. Waite Jr., T. E. Cravens, I. P. Robertson, S. Lebonnois, (2008a), Coupled ion and neutral rotating model of Titan's upper atmosphere, Icarus, 197, 110–136, doi: 10.1016/j.icarus.2008.03.022.

De La Haye, V., J. H. Waite Jr., T. E. Cravens, S. W. Bougher, I. P. Robertson, J. M. Bell, (2008b), Heating Titan's upper atmosphere, Journal of Geophysical Research, 113, A11314.

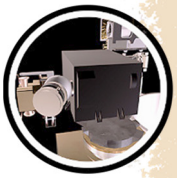

De La Haye, V., J. H. Waite, R. E. Johnson, R. V. Yelle, et al., (2007a), Cassini Ion and Neutral Mass Spectometer data in Titan's upper atmosphere and exosphere: Observation of a suprathermal corona, Journal of Geophysical Research, 12, A07309.

De La Haye, V., J. H. Waite Jr., T. E. Cravens, A. F. Nagy, R. E. Johnson, S. Lebonnois, I. P. Robertson, (2007b), Titan's Corona: The contribution of exothermic chemistry, Icarus, 191, 236–250.

Desai, R. T., S. A. Taylor, L. H. Regoli, A. J. Coates, et al. (2018), Cassini CAPS identification of pickup ion compositions at Rhea, Geophysical Research Letters, vol. 45, Issue 4, pp. 1704–1712, doi: 10.1002/2017GL076588.

Dong, Y., T. W. Hill, B. D. Teolis, B. A. Magee, J. H. Waite Jr., (2011), The water vapor plumes of Enceladus, Journal of Geophysical Research, 116, A10204.

Edberg, N. J. T., D. J. Andrews, O. Shebanits, K. Ågren, J.-E. Wahlund, H. J. Opgenoorth, T. E. Cravens, Z. Girazian, (2013a), Solar cycle modulation of Titan's ionosphere, Journal of Geophysical Research, 118, 5255–5264, doi: 10.1002/jgra.50463.

Edberg, N. J. T., D. J. Andrews, O. Shebanits, K. Ögren, J.-E. Wahlund, H. J. Opgenoorth, E. Roussos, P. Garnier, T. E. Cravens, S. V. Badman, R. Modolo, C. Bertucci, M. K. Dougherty, (2013b), Extreme densities in Titan's ionosphere during the T85 magnetosheath encounter, Geophysical Research Letters, 40, 2879–2883, doi: 10.1002/grl.50579.

Farrell, W. M., W. S. Kurth, D. A. Gurnett, R. E. Johnson, M. L. Kaiser, J.-E. Wahlund, J. H. Waite Jr., (2009), Electron density dropout near Enceladus in the context of water-vapor and water-ice, Geophysical Research Letters, 36, L10203.

Fox, J. L. and R. V. Yelle, (1997), Hydrocarbon ions in the ionosphere of Titan, Geophysical Research Letters, 24, Issue 17, pp. 2179–2182.

Galand, M., A. J. Coates, T. E. Cravens, J.-E. Wahlund, (2014), Titan's ionosphere, In Titan: Interior, Surface, Atmosphere, and Space Environment, Chapter 11, (eds.) I. Müller-Wodarg, C. A. Griffith, E. Lellouch, T. E. Cravens, Cambridge University Press, pp. 376–419.

Garnier, P., J.-E. Wahlund, L. Resnqvist, R. Modolo, K. Ågren, N. Sergis, P. Canu, M. Andre, D. A. Gurnett, W. S. Kurth, S. M. Krimgis, A. Coates, M. Dougherty, J. H. Waite Jr., (2009), Titan's ionosphere in the magnetosheath: Cassini RPWS results during the T32 flyby, Annales Geophysicae, 27, 4257–4272.

Glein, C. R., (2017), A whiff of nebular gas in Titan's atmosphere – Potential implications for the conditions and timing of Titan's formation, Icarus, 293, 231–242.

Glein, C. R., J. A. Baross, J. H. Waite Jr., (2015), The pH of Enceladus' ocean, Geochimica et Cosmochimica Acta, 162, 202–219, doi: 10.1016/j.gca.2015.04.017.

Hansen, C. J., D. E. Shemansky, L. W. Esposito, A. I. F. Stewart, B. R. Lewis, J. E. Colwell, A. R. Hendrix, R. A. West, J. H. Waite Jr., B. Teolis, B. A. Magee, (2011), The composition and structure of the Enceladus plume, Geophysical Research Letters, 38, L11202.

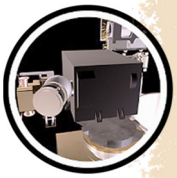

Hedman, M. M., C. M. Gosmeyer, P. D. Nicholson, C. Sotin, R. H. Brown, R. N. Clark, K. H. Baines, B. J. Buratti, M. R. Showalter, (2013), An observed correlation between plume activity and tidal stresses on Enceladus, Nature, 500, 182–184.

Howett, C. J. A., J. R. Spencer, T. Hurford, A. Verbiscer, M. Segura, (2016), Thermal properties of Rhea's poles: Evidence for a meter-deep unconsolidated subsurface layer, Icarus, 272, 140, doi: 10.1016/j.icarus.2016.02.033.

Hurley, D. M., M. E. Perry, H. J. Waite Jr., (2015), Modeling insights into the locations of density enhancements from the Enceladus water vapor jets, Journal of Geophysical Research, 120, 1763–1773, doi: 10.1002/21015JE004872.

Ip W.-H., (2006), On a ring origin of the equatorial ridge of Iapetus, Geophysical Research Letters, 33, L16203.

Ip, W.-H., (2005), An update on the ring exosphere and plasma disc of Saturn, Geophysical Research Letters, doi: 10.1029/2004GL022217.

Johnson, R. E., J. G. Luhmann, R. L. Tokar, M. Bouhram, J. J. Berthelier, E. C. Sittler, J. F. Cooper, T. W. Hill, H. T. Smith, M. Michael, M. Liu, F. J. Crary, D. T. Young, (2006), Production, ionization and redistribution of O2 in Saturn's ring atmosphere, Icarus, 180, 393.

Jones, G. H., C. S. Arridge, A. J. Coates, G. R. Lewis, S. Kanani, A. Wellbrock, D. T. Young, F. J. Crary, R. L. Tokar, R. J. Wilson, R. E. Johnson, D. G. Mitchell, J. Schmidt, S. Kempf, U. Beckmann, C. T. Russell, Y. D. Jia, M. K. Dougherty, J. H. Waite Jr., B. A. Magee, (2009), Fine jet structure of electrically charged grains in Enceladus' plume, Geophysical Research Letters, 36, L16204.

Kasprzak, W. T., H. Niemann, D. Harpold, J. Richards, H. Manning, E. Patrick, P. Mahaffy, (1996), Cassini orbiter ion neutral mass spectrometer instrument, Proceedings SPIE, vol. 2803, Cassini-Huygens: A Mission to the Saturnian Systems, International Symposium on Optical Science, Engineering, and Instrumentation, Denver, CO, doi: 10.1117/12.253413.

Keller, C. N., V. G. Anicich, T. E. Cravens, (1998), Model of Titan's ionosphere with detailed hydrocarbon ion chemistry, Planetary and Space Science, 46, 1157.

Keller, C. N., T. E. Cravens, L. Gan, (1992), A model of the ionosphere of Titan, Journal of Geophysical Research: Space Physics, vol. 97, Issue A8, pp. 12117–12135, doi: 10.1029/92JA00231.

Khurana, K. K., S. Fatemi, J. Kindkvist, E. Roussos, N. Krupp, M. Holmstrom, C. T. Russell, M. K. Dougherty, (2017), The role of plasma slowdown in the generation of Rhea’s Alfvén wings, Journal of Geophysical Research: Space Physics, 122, doi: 10.1002/2016JA023595.

Khurana, K. K., N. Krupp, M. G. Kivelson, E. Roussos, M. K. Dougherty, (2012), Cassini’s flyby through Rhea’s distant Alfven wing, in European Planetary Science Congress 2012, pp. EPSC2012-2309, Europlanet RI, Madrid.

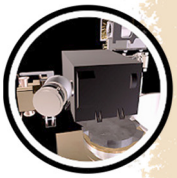

Kim, Y. H., J. L. Fox, J. H. Black, J. I. Moses, (2014), Hydrocarbon ions in the lower ionosphere of Saturn, Journal of Geophysical Research: Space Physics, 119, 1–12, doi: 10.1002/2013JA019022.

Koskinen, T. T., B. R. Sandel, R. V. Yelle, D. F. Strobel, I. C. F. Müller-Wodarg, J. T. Erwin, (2015), Saturn's variable thermosphere from Cassini/UVIS occultations, Icarus, 260, 174–189, doi: 10.1016/j.icarus.2015.07.008.

Lavvas, P., A. Coustenis, I. Vardavas, (2008a), Coupling photochemistry with haze formation in Titan's atmosphere, part I: Model description, Planetary and Space Science, 56(1), 27–66.

Lavvas, P., A. Coustenis, I. Vardavas, (2008b), Coupling photochemistry with haze formation in Titan's atmosphere, Part II: Results and validation with Cassini/Huygens data, Planetary and Space Science, 56(1), 67–99.

Lebonnois, S., (2005), Benzene and aerosol production in Titan and Jupiter's atmospheres: a sensitivity study, Planetary and Space Science, 53(5), 486–497.

Ledvina, S. A. and S. H. Brecht, (2012a), Consequences of negative ions for Titan's plasma interaction, Geophysical Research Letters, 39, L20103, doi: 10.1029/2012GL053835.

Ledvina, S. A., S. H. Brecht, T. E. Cravens, (2012b), The orientation of Titan's dayside ionosphere and its effects on Titan's plasma interaction, Earth Planets Space, 64, 207–230.

Ledvina, S. A., Y. Ma, E. Kallio, (2008), Modeling and simulating flowing plasmas and related phenomena, Space Science Reviews, doi: 10.1007/s11214-008-9384-6.

Ledvina, S. A., T. E. Cravens, K. Kecskemety, (2005), Ion distributions in Saturn's magnetosphere near Titan, Journal of Geophysical Research, 110, A06211, doi: 10.1029/2004JA010771.

Ledvina, S. A., J. G. Luhmann, S. H. Brecht, T. E. Cravens, (2004a), Titan's induced magnetosphere, Advances in Space Research, 33, 2092.

Ledvina, S. A., J. G. Luhmann, T. E. Cravens, (2004b), Ambient ion distributions in Saturn's magnetosphere near Titan during a non-Voyager type interaction, Advances in Space Research, 33, 221.

Ledvina, S. A., S. H. Brecht, J. G. Luhmann, (2004c), Ion distributions of 14 amu pickup ions associated with Titan's plasma interaction, Geophysical Research Letters, 31, L17S10, doi: 10.1029/2004GL019861.

Lee, A. Y. and G. Hanover, (2005), Cassini spacecraft attitude control system flight performance, in AIAA Guidance, Navigation, and Control Conference, American Institute of Aeronautics and Astronautics, San Francisco, CA, AIAA-2005-6269.

Luhmann, J. G., D. Ulusen, S. A. Ledvina, K. Mandt, B. Magee, J. H. Waite, J. Westlake, T. E. Cravens, I. Robertson, N. Edberg, K. Ågren, J.-E. Wahlund, Y.-J. Ma, H. Wei, C. T. Russell, M. K. Dougherty, (2012), Investigating magnetospheric interaction effects of Titan's ionosphere with the Cassini orbiter ion neutral mass spectrometer, Langmuir Probe and magnetometer observations during targeted flybys, Icarus, 219, 534–555, doi: 10.1016/j.icarus.2012.03.015.

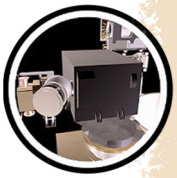

Luhmann, J. G., R. E. Johnson, R. L. Tokar, S. A. Ledvina, T. E. Cravens, (2006), A model of the ionosphere of Saturn's rings and its implications, Icarus, 181 (2), 465–474.

Luhmann, J. G., S. A. Ledvina, C. T. Russell, (2004), Induced magnetospheres, Advances in Space Research, 33, 1905.

Luhmann, J. G., (1996), Titan's ion exosphere wake: A natural ion mass spectrometer? Journal of Geophysical Research, 101, E12, pp. 29387–29393, doi: 10.1029/96JE03307.

Ma, Y., K. Altwegg, T. Breus, M. R. Combi, et al., (2008), Plasma flow and related phenomena in planetary aeronomy, Space Science Reviews, 139, no. 1–4, 311–353, doi: 10.1007/s11214-008-9389-1.

Ma, Y., A. F. Nagy, T. E. Cravens, I. V. Sokolov, K. C. Hansen, J.-E. Wahlund, F. J. Crary, A. J. Coates, M. K. Dougherty, (2006), Comparisons Between MHD Model Calculations and Observations of Cassini Flybys of Titan, Journal of Geophysical Research, 111, A05207, doi: 10.1029/2005JA011481.

Ma, Y.-J., A. F. Nagy, T. E. Cravens, I. G. Sokolov, J. Clark, K. C. Hansen, (2004), 3-D global MHD model prediction of the first close flyby of Titan by Cassini, Geophysical Research Letters, 31, doi: 10.1029/2004GL021215.

Madanian, H., T. E. Cravens, M. S. Richard, J. H. Waite, N. J. T. Edberg, J. H. Westlake, J.-E. Wahlund, (2016), Solar cycle variations in ion composition in the dayside ionosphere of Titan, Journal of Geophysical Research, 121, 8013–8037, doi: 10.1002/2015JA022274.

Magee, B. A. and J. H. Waite, (2017), Neutral gas composition of Enceladus' plume - Model parameter insights from Cassini-INMS, 48th Lunar and Planetary Science Conference, 20–24 March 2017, The Woodlands, TX, LPI Contribution No. 1964, id. 2974.

Magee, B. A., J. H. Waite, K. E. Mandt, J. Bell, J. Westlake, D. A. Gell, V. De la Haye, (2009), INMS derived composition of Titan's upper atmosphere: Analysis methods and model comparison, Planetary and Space Science, 57, 1895–1916.

Mahhafy, P. M. and K. Lai, (1990), An electrostatic quadrupole deflector for mass spectrometer applications, Journal of Vacuum Science A8, 3244.

Mandt, K. E., J. H. Waite Jr., B. Teolis, B. A. Magee, J. Bell, J. Westlake, C. Nixon, O. Mousis, J. Lunine, (2012a), The 12C/13C ratio on Titan from Cassini INMS measurements and implications for the evolution of methane, Astrophysical Journal, 749, 160, doi: 10.1088/0004-637X/749/2/160.

Mandt, K. E. , D. A. Gell, M. Perry, J. H. Waite Jr., F. A. Crary, D. Young, B. A. Magee, J. H. Westlake, T. Cravens, W. Kasprzak, G. Miller, J.-E. Wahlund, K. Ågren, N. J. T. Edberg, A. N. Heays, B. R. Lewis, S. T. Gibson, V. de la Haye, M.-C. Liang, (2012b), Ion densities and composition of Titan's upper atmosphere derived from the Cassini ion neutral mass spectrometer: Analysis methods and comparison of measured ion densities to photochemical model simulations, Journal of Geophysical Research, 117, E10006, doi: 10.1029/2012JE004139.

- - - - - - - - - - - - - -

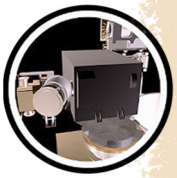

Mandt, K. E., J. H. Waite Jr., W. Lewis, J. I. Lunine, O. Mousis, J. Bell, B. A. Magee, D. Cordier, (2009), Isotopic evolution of the major constituents of Titan's atmosphere based on Cassini data, Planetary and Space Science, 57, 1917–1930.

Michael, M., R. E. Johnson, F. Leblanc, M. Liu, J. G. Luhmann, V. I. Shematovich, (2005), Ejection of nitrogen from Titan's atmosphere by magnetospheric ions and pick-up ions, Icarus, vol. 175, Issue 1, pp. 263–267, doi: 10.1016/j.icarus.2004.11.004.

Mitchell, D. G., M. E. Perry, D. C. Hamilton, J. H. Westlake, P. Kollmann, H. T. Smith, J. F. Carbary, J. H. Waite Jr., R. Perryman, H.-W. Hsu5, J.-E. Wahlund, M. W. Morooka, L. Z. Hadid, A. M. Persoon, W. S. Kurth, (2018), Dust grains fall from Saturn’s D-ring into its equatorial upper atmosphere, Science, 362, no. 6410, p. eaat2236.

Moore, L., T. E. Cravens, I. Müller-Wodarg, M. E. Perry, J. H. Waite Jr., R. Perryman, et al., (2018), Models of Saturn’s equatorial ionosphere based on in situ data from Cassini’s Grand Finale, Geophysical Research Letters, 45, 9398–9407, doi: 10.1029/2018GL078162.

Moore, L., I. Müller-Wodarg, M. Galand, A. Kliore, M. Mendillo, (2010), Latitudinal variations in Saturn’s ionosphere: Cassini measurements and model comparisons, Journal of Geophysical Research, 115(A11), A11317, doi: 10.1029/2010JA015692.

Moore, L., A. F. Nagy, A. J. Kliore, I. Müller-Wodarg, J. D. Richardson, M. Mendillo, (2006), Cassini radio occultations of Saturn’s ionosphere: Model comparisons using a constant water flux, Geophysical Research Letters, 33(22), L22202, doi: 10.1029/2006GL027375.

Moses, J. and S. Bass, (2000), The effects of external material on the chemistry and structure of Saturn’s ionosphere, Journal of Geophysical Research, 105(1999), 7013–7052.

Mousis, O., J. I. Lunine, S. Picaud, D. Cordier, J. H. Waite Jr., K. E. Mandt, (2011), Removal of Titan's atmospheric noble gases by their sequestration in surface clathrates, The Astrophysical Journal, 740, L9.

Mousis, O., J. I. Lunine, J. H. Waite Jr., B. Magee, W. S. Lewis, K. E. Mandt, D. Marquer, D. Cordier, (2009a), Formation conditions of Enceladus and origin of its methane reservoir, The Astrophysical Journal Letters, 701, L39-L42.

Mousis, O., J. I. Lunine, M. Pasek, D. Cordier, J. H. Waite Jr., K. E. Mandt, W. S. Lewis, M.-J. Nguyen, (2009b), A primordial origin for the atmospheric methane of Saturn's moon Titan, Icarus, 204, 749–751.

Müller-Wodarg, I. C. F., L. Moore, M. Galand, S. Miller, M. Mendillo, (2012), Magnetosphere–atmosphere coupling at Saturn: 1 – Response of thermosphere and ionosphere to steady state polar forcing, Icarus, 221(2), 481–494, doi: 10.1016/j.icarus.2012.08.034.

Müller-Wodarg, I. C. F., R. V. Yelle, J. Cui, J. H. Waite, (2008), Horizontal structures and dynamics of Titan’s thermosphere, Journal of Geophysical Research, 113, E10003, doi: 10.1029/2007JE003031.

Müller-Wodarg, I. C. F., R. V. Yelle, N. Borggren, J. H. Waite, (2006a), Waves and horizontal structures in Titan’s thermosphere, Journal of Geophysical Research, 111, A12315.

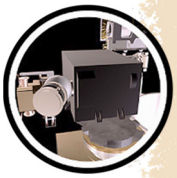

Müller-Wodarg, I. C. F., M. Mendillo, R. Yelle, A. Aylward, (2006b), A global circulation model of Saturn's thermosphere, Icarus, 180(1), 147–160, doi: 10.1016/j.icarus.2005.09.002.

Müller-Wodarg, I. C. F., R. V. Yelle, M. J. Mendillo, A. D. Aylward, (2003), On the global distribution of neutral gases in Titan's upper atmosphere and its effect on the thermal structure, Journal of Geophysical Research: Space Physics, vol. 108, issue A12, doi: 10.1029/2003JA010054.

Müller-Wodarg, I. C. F. and R. V. Yelle, (2002a), The effect of dynamics on the composition of Titan's upper atmosphere, Geophysical Research Letters, vol. 29, issue 23, 54-1–54-4, doi: 10.1029/2002GL016100.

Müller-Wodarg, I. C. F., (2002b), The application of general circulation models to the atmospheres of terrestrial-type moons of the giant planets, In Atmoshperes in the Solar System: Comparative Aeronomy, Volume 120, Part IV: Models of Aeronomic Systems, (eds.) M. Mendillo, A. Nagy, J. H. Waite, American Geophysical Union, Geophysical Monograph Series, pp. 307–318, doi: 10.1029/GM130.

Müller-Wodarg, I. C. F., R. V. Yelle, M. Mendillo, L. A. Young, A. D. Aylward, (2000), The thermosphere of Titan simulated by a global three-dimensional time-dependent model, Journal of Geophysical Research, 105, pp. 20833–20856, doi: 10.1029/2000JA000053.

Nagy, A. F. and T. E. Cravens, (1998), Titan's ionosphere: A review, Planetary and Space Science, 46, 1149, doi: 10.1016/S0032-0633(98)00049-X.

Neubauer, F. M., et al., (2006). Titan's near magnetotail from magnetic field and electron plasma observations and modeling: Cassini flybys, TA, TB and T3, Journal of Geophysical Research, 111, doi: 10.1029/2006011676.

Neubauer, F. M., D. A. Gurnett, J. D. Scudder, R. E. Hartle, (1984), Titan's magnetospheric interaction, Saturn, 1, 760–787.

Ozak, N., T. E. Cravens, G. H. Jones, A. J. Coates, I. P. Robertson, (2012), Modeling of electron fluxes in the Enceladus plume, Journal of Geophysical Research, 117, A06220, doi: 10.1029/2011JA017497.

Patrick, E. L., (2006), Silicon carbide nozzle for producing molecular beams, Review of Scientific Instruments, 77, 043301, doi:10.1063/1.2188907.

Perry, M. E., J. H. Waite Jr., D. G. Mitchell, K. E. Miller, T. E. Cravens, R. S. Perryman, et al., (2018), Material flux from the rings of Saturn into its atmosphere, Geophysical Research Letters, 45, 10,093–10,100, doi: 10.1029/2018GL078575.

Perry, M. E., B. D. Teolis, D. M. Hurley, B. A. Magee, J. H. Waite, T. G. Brockwell, R. S. Perryman, R. L. McNutt, (2015), Cassini INMS measurements of Enceladus plume density, Icarus, 257, 139–162, doi: 10.1016/j.icarus.2015.04.037.

Perry, M. E., B. Teolis, H. T. Smith, R. L. McNutt, G. Fletcher, W. Kasprzak, B. Magee, D. G. Mitchell, J. H. Waite Jr., (2010), Cassini INMS observations of neutral molecules in Saturn's E ring. Journal of Geophysical Research, 115, A10206.

- - - - - - - - - - - - - -

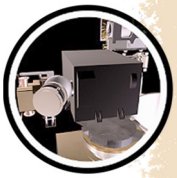

Persoon, A. M., W. S. Kurth, D. A. Gurnett, J. B. Groene, A. H. Sulaiman, J.-E. Wahlund, et al., (2019), Electron density distributions in Saturn's ionosphere, Geophysical Research Letters, 46, 3061–3068, doi: 10.1029/2018GL078020.

Porco, C., D. DiNino, F. Nimmo, (2014), How the geysers, tidal stresses, and thermal emission across the south polar terrain of Enceladus are related, The Astronomical Journal, 148, 45.

Postberg, F., N. Khawaja, B. Abel, G. Choblet, C. R. Glein, M. S. Gudipati, B. L. Henderson, H.-W. Hsu, S. Kempf, F. Klenner, G. Moragas-Klostermeyer, B. Magee, L. Nölle, M. Perry, R. Reviol, J. Schmidt, R. Srama, F. Stolz, G. Tobie, M. Trieloff, J. H. Waite, (2018), Macromolecular organic compounds from the depths of Enceladus, Nature, 558, 564–568, doi: 10.1038/s41586-018-0246-4.

Ricca, A., C. Bauschlicher Jr., E. L. O. Bakes, (2001a), A computational study of the mechanisms for the in- corporation of a nitrogen atom into polycyclic aromatic hydrocarbons in the Titan haze, Icarus, 154(2), 516–521.

Ricca, A., C. Bauschlicher Jr., M. Rosi. (2001b), Mechanisms for the incorporation of a nitrogen atom into polycyclic aromatic hydrocarbon cations, Chemical Physics Letters, 347(4-6), 473–480.

Richard, M. S., T. E. Cravens, C. Wylie, D. Webb, Q. Chediak, R. Perryman, K. Mandt, J. Westlake, J. H. Waite, I. Robertson, B. A. Magee, N. J. T. Edberg, (2015a), An empirical approach to modeling ion production rates in Titan's ionosphere I: Ion production rates on the dayside and globally, Journal of Geophysical Research, 120, 1264–1280, doi: 10.1002/2013JA019706.

Richard, M. S., T. E. Cravens, C. Wylie, D. Webb, Q. Chediak, K. Mandt, J. H. Waite, A. Rymer, C. Bertucci, A. Wellbrock, A. Windsor, A. J. Coates, (2015b), An empirical approach to modeling ion production rates in Titan's ionosphere II: Ion production rates on the nightside, Journal of Geophysical Research, 120, 1281–1298, doi: 10.1002/2014JA020343.

Richard, M. S., T. E. Cravens, I. P. Robertson, J. H. Waite, J.-E. Wahlund, F. J. Crary, A. J. Coates, (2011), Energetics of Titan's ionosphere: model comparisons with Cassini data, Journal of Geophysical Research, 116, A09310.

Richter, H. and J. B. Howard, (2000), Formation of polycyclic aromatic hydrocarbons and their growth to soot—a review of chemical reaction pathways, Progress in Energy and Combustion Science, 26, 565.

Rietmeijer, F. J., (1993) Size distributions in two porous chondritic micrometeorites, Earth and Planetary Science Letters, 117, 609–617.

Robertson, I. P., T. E. Cravens, J. H. Waite Jr., R. V. Yelle, V. Vuitton, A. J. Coates, J. E. Wahlund, K. Ågren, B. Magee, K. Mandt, M. S. Richard, (2009), Structure of Titan's ionosphere: model comparisons with Cassini data, Planetary and Space Science, 57, 1834–1846.

Rosenqvist, L., J.-E. Wahlund, K. Ågren, R. Modolo, H. J. Opgenoorth, D. Strobel, I. Müller-Wodarg, P. Garnier, C. Bertucci, (2009), Titan ionospheric conductivities from Cassini

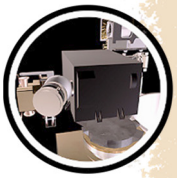

measurements, Planetary and Space Science, 57, 1828–1833, doi: 10.1016/j.pss.2009.01.007.

Roussos, E., J. Wuller, S. Simon, A. Boswetter, U. Motschmann, N. Krupp, M. Franz, J. Woch, K. K. Khurana, M. K. Dougherty, (2008), Plasma and fields in the wake of Rhea: 3-D hybrid simulation and comparison with Cassini data, Annales Geophysicae, 26, 619.

Rymer, A. M., H. T. Smith, A. Wellbrock, A. J. Coates, D. T. Young, (2009), Discrete classification and electron energy spectra of Titan's varied magnetospheric environment, Geophysical Research Letters, 36, L15109, doi: 10.1029/2009GL039427

Sagnières, L. B. M., M. Galand, J. Cui, P. P. Lavvas, E. Vigren, V. Vuitton, R. V. Yelle, A. Wellbrock, A. J. Coates, (2015), Influence of local ionization on ionospheric densities in Titan's upper atmosphere, Journal of Geophysical Research, 120, 5899–5921, doi: 10.1002/2014JA020890.

Sakai, S., T. E. Cravens, N. Omidi, M. E. Perry, J. H. Waite Jr.,(2016) Ion energy distributions and densities in the plume of Enceladus, Planetary and Space Science, 130, 60–79, doi: 10.1016/j.oss.2016.05.007.

Santolik, O., D. A. Gurnett, G. H. Jones, P. Schippers, F. J. Crary, J. S. Leisner, G. B. Hospodarsky, W. S. Kurth, C. T. Russell, M. K. Dougherty, (2011), Intense plasma wave emissions associated with Saturn's moon Rhea, Geophysical Research Letters, 38, L19204.

Shebanits, O., J.-E. Wahlund, N. J. T. Edberg, F. J. Crary, A. Wellbrock, D. J. Andrews, E. Vigren, R. T. Desai, A. J. Coates, K. E. Mandt, J. H. Waite, (2016), Ion and aerosol precursor densities in Titan's ionosphere: A multi-instrument case study, Journal of Geophysical Research, 121, 10075–10090, doi: 10.1002/2016JA022980.

Shematovich, V. I., R. E. Johnson, M. Michael, J. G. Luhmann, (2003), Nitrogen loss from Titan, Journal of Geophysical Research, 108, E8, id. 5087, doi: 10.1029/2003JE002094.

Simon, S., H. Kriegel, J. Saur, A. Wennmacher, F. M. Neubauer, E. Roussos, U. Motschmann, M. K. Dougherty, (2012), Analysis of Cassini magnetic field observations over the poles of Rhea, Journal of Geophysical Research, 117, A07211.

Simon, S., J. Saur, F. M. Neubauer, A. Wennmacher, M. K. Dougherty, (2011), Magnetic signatures of a tenuous atmosphere at Dione, Journal of Geophysical Research, 38, L15102.

Smith, H. T., R. E. Johnson, M. E. Perry, D. G. Mitchell, R. L. McNutt, D. T. Young, (2010), Enceladus plume variability and the neutral gas densities in Saturn's magnetosphere, Journal of Geophysical Research, 115, A10252, doi: 10.1029/2009JA015184.

Snow, T., V. Le Page, Y. Keheyan, V. Bierbaum, (1998), The interstellar chemistry of PAH cations, Nature, 391(6664), 259–260

Snowden, D. and R. V. Yelle, (2014a), The global precipitation of magnetospheric electrons into Titan's upper atmosphere, Icarus, 243, 1–15, doi: 10.1016/j.icarus.2014.08.027.

Snowden, D. and R. V. Yelle, (2014b), The thermal structure of Titan's upper atmosphere, II: Energetics, Icarus, vol. 228, pp. 64–77, doi: 10.1016/j.icarus.2013.08.027.

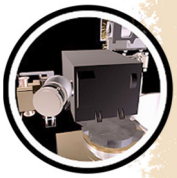

Snowden, D., R. Yelle, J. Cui, J.-E. Wahlund, N. J. T. Edberg, K. Ågren, (2013a), The thermal structure of Titan's upper atmosphere, I: Temperature profiles from Cassini INMS observations, Icarus, vol. 226, pp. 552–582, doi: 10.1016/j.icarus.2013.06.006.

Snowden, D., R. V. Yelle, M. Galand, A. J. Coates, A. Wellbrock, G. H. Jones, and P. Lavvas, (2013b), Auroral electron precipitation and flux tube erosion in Titan's upper atmosphere, Icarus, 226, 186-204, doi: 10.1016/j.icarus.2013.05.021.

Spahn, F., N. Albers, M. Hörning, S. Kempf, A. V. Krivov, M. Makuch, J. Schmidt, M. Seiß, M. Sremčević, (2006), E-ring dust sources: Implications from Cassini's dust measurements, Planetary and Space Science, vol. 54, Issues 9–10, pp. 1024–1032, doi: 10.1016/j.pss.2006.05.022.

Strobel, D. F., (2010), Molecular hydrogen in Titan's atmosphere: Implications of the measured tropospheric and thermospheric mole fractions, Icarus, vol. 208, no. 2, pp. 878–886.

Strobel, D. F., S. K. Atreya, B. Bézard, F. Ferri, F. M. Flasar, M. Fulchignoni, E. Lellouch, I. C. F. Müller-Wodarg, (2009), Atmospheric structure and composition, In Titan from Cassini-Huygens, (eds.) R. Brown, J.-P. Lebreton, J. H. Waite, Springer Dordrecht, pp. 235–257, doi: 10.1007/978-1-4020-9215-2_10.

Strobel, D. F., (2008), Titan's hydrodynamically escaping atmosphere, Icarus, vol. 193, no. 2, pp. 588–594.

Strobel, D. F., (2006), Gravitational tidal waves in Titan's upper atmosphere, Icarus, vol. 182, no. 1, pp. 251–258.

Tenishev, V., D. C. S. Öztürk, M. R. Combi, M. Rubin, J. H. Waite Jr., M. Perry, (2014), Effect of the Tiger Stripes on the water vapor distribution in Enceladus' exosphere, Journal of Geophysical Research, 119, 2658–2667, doi: 10.1002/2014JE004700.

Tenishev, V., M. R. Combi, B. D. Teolis, J. H. Waite Jr., (2010). An approach to numerical simulation of the gas distribution in the atmosphere of Enceladus, Journal of Geophysical Research, 115, A09302.

Teolis, B. D., C. Plainaki, T. A. Cassidy, U. Raut, (2017a), Water Ice Radiolytic O2, H2, and H2O2 Yields for Any Projectile Species, Energy, or Temperature: A Model for Icy Astrophysical Bodies, Journal of Geophysical Research: Planets, 122, doi: 10.1002/2017JE005285.

Teolis, B. D., M. E. Perry, C. J. Hansen, J. H. Waite, C. C. Porco, J. R. Spencer, C. J. A. Howett, (2017b), Enceladus Plume Structure and Temporal Variability: Comparison of Cassini Observations, Astrobiology (special issue), 17, no. 9, 926–940.

Teolis, B. D. and J. H. Waite, (2016), Dione and Rhea seasonal exospheres, revealed by Cassini CAPS and INMS, Icarus, 272, 277–289, doi: 10.1016/j.icarus.2016.02.031.

Teolis, B. D., H. B. Niemann, J. H. Waite, D. A. Gell, R. S. Perryman, W. T. Kasprzak, K. E. Mandt, R. V. Yelle, A. Y. Lee, F. J. Pelletier, G. P. Miller, D. T. Young, J. M. Bell, B. A. Magee, E. L. Patrick, J. Grimes, G. G. Fletcher, and V. Vuitton, (2015), A revised sensitivity model for Cassini INMS: Results at Titan, Space Science Reviews, doi: 10.1007/s11214-014-0133-8.

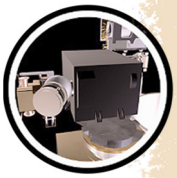

Teolis, B. D., I. Sillanpää, J. H. Waite, K. K. Khurana, (2014), Surface current balance and thermoelectric whistler wings at airless astrophysical bodies: Cassini at Rhea, Journal of Geophysical Research, 119, 8881–8901, doi: 10.1002/2014JA020094.

Teolis, B., G. H. Jones, P. F. Miles, R. L. Takar, B. A. Magee, J. H. Waite, E. Roussos, D. T. Young, F. J. Crary, A. J. Coates, R. E. Johnson, W.-L. Tseng, R. A. Baragiola, (2010a), Cassini Finds an Oxygen-Carbon Dioxide Atmosphere at Saturn's Icy Moon Rhea, Science, 330, 24.

Teolis, B., M. E. Perry, B. A. Magee, J. Westlake, J. H. Waite Jr., (2010b), Detection and measurements of ice grains and gas distribution in the Enceladus plume by Cassini's ion neutral mass spectrometer, Journal of Geophysical Research, 115, A09222.

Thomsen, M. F., D. B. Reisenfeld, D. Delapp, R. L. Tokar, D. T. Young, F. J. Crary, E. C. Sittler, M. A. McGraw, J. D. Williams, (2010), Survey of Ion Plasma Parameters in Saturn’s Magnetosphere, Journal of Geophysical Research, 115, A10220.

Tokar, R. L., R. E. Johnson, M. F. Thomsen, E. C. Sittler, A. J. Coates, R. J. Wilson, F. J. Crary, D. T. Young, G. H. Jones, (2012), Detection of Exospheric O2+ at Saturn’s Moon Dione, Journal of Geophysical Research, 39, L03105.

Tokar, R. L., R. J. Wilson, R. E. Johnson, M. G. Henderson, M. F. Thomas, M. M. Cowee, E. C. Sittler, Jr., D. T. Young, H. J. McAndrews, H. T. Smith, (2008), Cassini Detection of Water - group pick - up ions in Saturn's torus, Geophysical Research Letters 35, L14202, doi: 10.1029/2008GL034749.

Tucker, O. J., R. E. Johnson, J. I. Deighan, A. N. Volkov, (2013), Diffusion and thermal escape of H2 from Titan’s atmosphere: Monte Carlo simulations, Icarus, 222, 149–158, doi: 10.1016/j.icarus.2012.10.016.

Ulusen, D., J. G. Luhmann, Y. J. Ma, K. Mandt, J. H. Waite, M. K. Dougherty, J.-E. Wahlund, C. T. Russell, T. A. Craven, N. Edberg, K. Agren, (2012), Comparisons of Cassini flybys of the Titan magnetospheric interaction with an MHD model: Evidence for organized behavior at high altitudes, Icarus, 217, 43–54, doi: 10.1016/j.icarus.2011.10.009.

Ulusen, D., J. Luhmann, Y. Ma, S. Ledvina, T. Cravens, K. Mandt, J. H. Waite Jr., J.-E. Wahlund, (2010), Investigation of the force balance in the Titan ionosphere: Cassini T5 flyby model/data comparisons, Icarus, 210, 867–880.

Vervack, R. J. and J. I. Moses, (2015), Saturn’s upper atmosphere during the Voyager era: Reanalysis and modeling of the UVS occultations, Icarus, 258, 135–163, doi: 10.1016/j.icarus.2015.06.007

Vigren, E., M. Galand, R. V. Yelle, A. Wellbrock, A. J. Coates, D. Snowden, J. Cui, P. Lavvas, N. J. T. Edberg, O. Shebanits, J.-E. Wahlund, V. Vuitton, K. Mandt, (2015), Ionization balance in Titan’s nightside ionosphere, Icarus, 248, 539–546, doi: 10.1016/j.icarus.2014.11.012.

Vigren, E., M. Galand, R. V. Yelle, J. Cui, J.-E. Wahlund, K. Ågren, P. P. Lavvas, I. C. F. Müller-Wodarg, D. F. Strobel, V. Vuitton, A. Bazin, (2013), On the thermal electron balance in Titan’s sunlit upper atmosphere, Icarus, vol. 223, pp. 234–251, doi: 10.1016/j.icarus.2012.12.010.

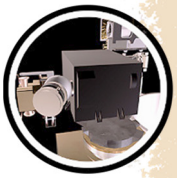

Vuitton, V., P. Lavvas, R. V. Yelle, M. Galand, A. Wellbrock, G. R. Lewis, A. J. Coates, J.-E. Wahlund, (2009), Negative ion chemistry in Titan's upper atmosphere, Planetary and Space Science, 57, 1558–1572.

Vuitton, V., R. V. Yelle, J. Cui, (2008), Formation and distribution of benzene on Titan, Journal of Geophysical Research, doi: 1 0.1029/2007JE002997.

Vuitton, V., R. V. Yelle, M. J. McEwan, (2007), Ion Chemistry and N-containing Molecules in Titan’s Upper Atmosphere, Icarus, doi: 10.1016/j.carus.2007.06.023.

Vuitton, V., R. V. Yelle, V. Anicich, (2006), The Nitrogen Chemistry of Titan’s Upper Atmosphere Revealed, The Astrophysical Journal Letters, vol. 647, no.2, L175-L178

Wahlund, J.-E., M. Galand, I. Meuller-Wodarg, J. Cui, R. V. Yelle, F. J. Crary, K. Mandt, B. Magee, J. H. Waite, Jr., D. T. Young, A. J. Coates, P. Garnier, K. Ågren, M. Andre, A. I. Eriksson, T. E. Cravens, V. Vuitton, D. A. Gurnett, W. S. Kurth, (2009), On the amount of heavy molecular ions in Titan's ionosphere, Planetary and Space Science, 57, 1857–1865.

Waite Jr., J. H., R. Perryman, M. Perry, K. Miller, J. Bell, T. E. Cravens, C. R. Glein, J. Grimes, M. Hedman, J. Cuzzi, T. Brockwell, B. Teolis, L. Moore, D. Mitchell, A. Persoon, W. S. Kurth, J-E. Wahlund, M. Morooka, L. Z. Hadid, S. Chocron, J. Walker, A. Nagy, R. Yelle, S. Ledvina, R. Johnson, W. Tseng, O. J. Tucker, W.-H. Ip, (2018), Chemical Interactions between Saturn’s Atmosphere and its Rings, Science, doi: 10.1126/science.aat2382.

Waite Jr., J. H., C. R. Glein, R. S. Perryman, B. D. Teolis, B. A. Magee, G. Miller, J. Grimes, M. E. Perry, K. E. Miller, A. Bouquet, J. L. Lunine, T. Brockwell, S. J. Bolton, (2017), Cassini finds molecular hydrogen in the Enceladus plume: Evidence for hydrothermal processes, Science, 356, 155–159.

Waite, J. H., J. Bell, R. Lorenz, R. Achterberg, F. M. Flasar, (2013), A model of variability in Titan’s atmospheric structure, Planetary and Space Science, 86, 45–56, doi: 10.1016/j.pss.2013.05.018.

Waite Jr., J. H., W. S. Lewis, B. A. Magee, J. I. Lunine, W. B. McKinnon, C. R. Glein, O. Mousis, D. T. Young, T. Brockwell, J. Westlake, M.-J. Nguyen, B. D. Teolis H. B. Niemann, R. L. McNutt, M. Perry, W.-H. Ip, (2009), Liquid water on Enceladus from observations of ammonia and 40Ar in the plume, Nature, 460, 487–490.

Waite, J. H., D. T. Young, A. J. Coates, F. J. Crary, B. A. Magee, K. E. Mandt, J. H. Westlake, (2008), The source of heavy organics and aerosols in Titan’s atmosphere, Proceedings of the International Astronomical Union, vol. 4, issue S251 (Organic Matter in Space), pp. 321-326, doi: 10.1017/S1743921308021844.

Waite Jr., J. H., D. T. Young, T. E. Cravens, A. J. Coates, F. J. Crary, B. Magee, J. Westlake, (2007), The process of tholin formation in Titan’s upper atmosphere, Science, 316, 870–875.

Waite Jr., J. H., M. Combi, W.-H. Ip, T. E. Cravens, R. L. McNutt, Jr., W. Kasprzak, R. Yelle, J. Luhmann, H. Niemann, D. Gell, B. Magee, G. Fletcher, J. Lunine, W.-L. Tseng, (2006), Cassini Ion and Neutral Mass Spectrometer: Enceladus plume composition and structure, Science, 311, 1419–1422.

- - - - - - - - - - - - - -

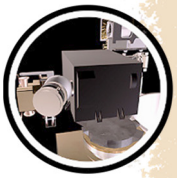

Waite, J. H., H. Niemann, R. V. Yelle, W. T. Kasprzak, T. E. Cravens, J. G. Luhmann, R. L. McNutt, W.-H. Ip, D. Gell, V. de la Haye, I. Müller-Wordag, B. McGee, N. Borggren, S. Ledvina, G. Fletcher, E. Walter, R. Miller, S. Scherer, R. Thorpe, J. Xu, B. Block, K. Arnett, (2005a), Ion Neutral Mass Spectrometer (INMS) results from the first flyby of Titan, Science, 308 (5724), 982–986.

Waite, J. H., T. E. Cravens, W.-H. Ip, W. T. Kasprzak, J. G. Luhmann, R. L. McNutt, H. B. Niemann, R. V. Yelle, I. Müller-Wodarg, S. A. Ledvina, S. Scherer, (2005b), Oxygen ions observed near Saturn's A Ring, Science, 307 (5713), 1260–1262.

Waite Jr., J. H., W. S. Lewis, W. T. Kasprzak, V. G. Anicich, B. P. Block, T. C. Cravens, G. G. Fletcher, W.-H. Ip, J. G. Luhmann, R. L. McNutt, H. B. Niemann, J. K. Parejko, J. E. Richards, R. L. Thorpe, E. M. Walter, R. V. Yelle, (2004), The Cassini Ion and Neutral Mass Spectrometer (INMS) investigation, Space Science Reviews, 114, 113–231.

Walker, J. D., S. Chocron, J. H. Waite, T. Brockwell, (2015), The vaporization threshold: Hypervelocity impacts of ice grains into a titanium Cassini spacecraft instrument chamber, Procedia Engineering, 103, 628–635, doi: 10.1016/j.proeng.2015.04.081.

Wang, H. and M. Frenklach, (1997), A detailed kinetic modeling study of aromatics formation in laminar premixed acetylene and ethylene flames, Combustion and Flame, vol. 110, issues 1–2, pp. 173–221.

Westlake, J. H., J. H. Waite, J. M. Bell, R. Perryman, (2014a), Observed decline in Titan's thermospheric methane due to solar cycle drivers, Journal of Geophysical Research, 119, 8586–8599, doi: 10.1002/2014JA020394.

Westlake, J. H., J. H. Waite, N. Carrasco, M. Richard, T. Cravens, (2014b), The role of ion-molecule reactions in the growth of heavy ions in Titan's ionosphere, Journal of Geophysical Research, 119, 5951–5963, doi: 10.1002/2014JA0202008.

Westlake, J. H., C. P. Paranicas, T. E. Cravens, J. G. Luhmann, K. E. Mandt, H. T. Smith, D. G. Mitchell, A. M. Rymer, M. E. Perry, J. H. Waite Jr., J.-E. Wahlund, (2012a), The observed composition of ions outflowing from Titan, Geophysical Research Letters, 39, L19104, doi: 10.1029/2012GL053079.

Westlake, J. H., J. H. Waite Jr., K. E. Mandt, N. Carrasco, J. M. Bell, B. A. Magee, J.-E. Wahlund, (2012b), Titan's ionospheric composition and structure: Photochemical modeling of Cassini INMS data, Journal of Geophysical Research, 117, E01003, 21, doi: 10.1029/2011JE003883.

Westlake, J. H., J. Bell, J. H. Waite, Jr., R. E. Johnson, J. G. Luhmann, K. E. Mandt, B. A. Magee, A. M. Rymer, (2011), Titan's thermospheric response to various plasma and solar environments, Journal of Geophysical Research, 116, A03318.

Wilson, E. H., S. K. Atreya, A. Coustenis, (2003), Mechanisms for the formation of benzene in the atmosphere of Titan, Journal of Geophysical Research: Planets, vol. 108, Issue E2, doi: 10.1029/2002JE001896.

Yelle, R. V., J. Serigano, T. T. Koskinen, S. M. Hörst, M. E. Perry, R. S. Perryman, J. H. Waite Jr., (2018), Thermal Structure and Composition of Saturn's Upper Atmosphere From

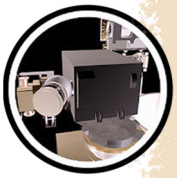

Cassini/Ion Neutral Mass Spectrometer Measurements, Geophysical Research Letters 45, no. 20, pp. 10951–10958, doi: 10.1029/2018GL078454.

Yelle, R. V., V. Vuitton, P. Lavvas, S. J. Klippenstein, M. A. Smith, S. M. Hörst, J. Cui, (2010), Formation of NH 3 and CH 2 NH in Titan's upper atmosphere, Faraday Discussions 147, pp. 31–49. doi: 10.1039/C004787M.

Yelle, R.V., J. Cui, I.C.F. Müller-Wodarg, (2008), Methane Escape from Titan's Atmosphere, Journal of Geophysical Research, vol. 113, Issue E10, doi: 10.1029/2007JE003031.

Yelle, R. V., N. Borggren, V. De La Haye, W. T. Kasprzak, H. B. Niemann, I. Müller-Wodarg, J. H. Waite Jr., (2006), The vertical structure of Titan's upper atmosphere from Cassini ion neutral mass spectrometer measurements, Icarus, 182, 567–576.

Yeoh, S. K., T. A. Chapman, D. B. Goldstein, P. L. Varghese, L. M. Trafton, (2015), On understanding the physics of the Enceladus south polar plume via numerical simulation, Icarus, 253, 205–222

Young, D. T., J. J. Berthelier, M. Blanc, J. L. Burch, A. J. Coates, R. Goldstein, M. Grande, T. W. Hill, R. E. Johnson, V. Kelha, D. J. McComas, , E. C. Sittler, K. R. Svenes, K. Szegö, P. Tanskanen, K. Ahola, D. Anderson, S. Bakshi, R. A. Baragiola, B. L. Barraclough , R. K. Black, S. Bolton, T. Booker, Bowman, P. Casey, G. Dirks, N. Eaker, J. T. Gosling, H. Hannula, C. Holmlund, H. Huomo, J. M. Illiano, P. Jensen, M. A. Johnson, D. Linder, T. Luntama, S. Mayrice, K. McCabe, B. T. Narheim, J. E. Nordholt, A. Preece , J. Rudzki, A. Ruitberg, K. Smith, S. Szalai, M. F. Thomsen, K. Viherkanto, T. Vollmer, T. E. Wahl, M. Wuest, T. Ylikorpi, C. Zinsmeyer, (2004), Cassini Plasma Spectrometer Investigation, Space Science Review, vol. 114, pp. 1– 112, doi: 10.1007/s11214-004-1406-4.